UILU-ENG-75-2025

CIVIL ENGINEERING STUDIES

STRUCTURAL RESEARCH SERIES NO. 421

MOTION ON THE SURFACE OF A LAYERED ELASTIC HALF SPACE PRODUCED BY A BURIED DISLOCATION PULSE

By

M. SEYYEDIAN-CHOOBI

A. R. ROBINSON

A Technical Report of
Research Sponsored in Part by
THE OFFICE OF NAVAL RESEARCH
DEPARTMENT OF THE NAVY
Contract No. N00014-75-C-0164
Project No. NR 064-183
and in part by
THE NATIONAL SCIENCE FOUNDATION
Contract GK 24294

UNIVERSITY OF ILLINOIS
at URBANA-CHAMPAIGN
URBANA, ILLINOIS
NOVEMBER 1975

MOTION ON THE SURFACE OF A LAYERED ELASTIC HALF SPACE PRODUCED BY A BURIED DISLOCATION PULSE

By

M. Seyyedian-Choobi

A. R. Robinson

A Technical Report of
Research Sponsored in Part by
THE OFFICE OF NAVAL RESEARCH
DEPARTMENT OF THE NAVY
Contract No. N00014-75-C-0164
Project No. NR 064-183
and in part by
THE NATIONAL SCIENCE FOUNDATION
Contract GK 24294

UNIVERSITY OF ILLINOIS
at URBANA-CHAMPAIGN
URBANA, ILLINOIS

November 1975

ACKNOWLEDGMENT

This report was prepared as a doctoral dissertation by Mr. Mirhamid Seyyedian-Choobi and was submitted to the Graduate College of the University of Illinois at Urbana-Champaign in partial fulfillment of the requirements for the degree of Doctor of Philosophy in Civil Engineering. The thesis was done under the supervision of Dr. A. R. Robinson, Professor of Civil Engineering.

The authors wish to thank Dr. L. A. Lopez of the Department of Civil Engineering, for extremely valuable discussions. The investigation was supported in part by the Office of Naval Research under Contracts N00014-67-A-0305-0010 and N00014-75-C-0164 (Numerical and Approximate Methods of Stress Analysis) and in part by the National Science Foundation under Contracts GK 24204 (Prediction of Earthquake Motion) and AEN 75-08456 (Design for Protection Against Natural Hazards).

The numerical results were obtained with the use of the IBM 360-75 computer system of the Computing Services Office of the University of Illinois at Urbana-Champaign.

TABLE OF CONTENTS

LIST OF FIGURES

1. INTRODUCTION

1.1 Object and Scope

In design of earthquake-resistant structures it is common practice to determine the dynamic behavior of structures on the basis of a previously recorded ground motion. It is also customary to conduct laboratory investigations on suitable prototypes of structures which are significant from engineering viewpoints when the model is subjected to a prescribed base motion. Recorded accelerograms used for these purposes may not, however, represent the actual characteristics of probable strong ground motion in the vicinity of the construction site. The more realistic the ground motion is for the site in question, the more meaningful will be the computed response.

To obtain a ground motion input for a structural calculation at a particular site, one method [1]* is to develop a statistical model with the capability of predicting what can be expected in the way of destructive seismic waves. This, in turn, requires a large amount of recorded data. However, at present the number of available strong-motion accelerograms is quite limited and the accumulation of strong-motion seismic records is, fortunately, a very slow process.

Another alternative to fill this gap in information is the development of analytical models which can simulate the surface motion when the mechanism of wave generation at the focus and the geological configuration at the observation point are well defined. The seismic profile of the near-surface layer considered in the analytic models has a profound influence on

---

* Number in brackets refer to entries in the List of References.

the ground motion. For example, the spectrum of the motion recorded in Mexico City [2] on the very soft ground that was formerly the bed of a lake has a pronounced peak at a period of approximately 2.5 seconds. According to Housner [3], this coincides with the computed period of the fundamental mode of vibration of the lake bed as a "bowl of jelly".

In attempting to predict the general features of the motion using a physically based model, two different problems are encountered:

i) Choosing an appropriate mechanism which describes the processes of wave generation at the focus of earthquake; and

ii) Calculating the dynamic response of a point at the free surface on the basis of this mechanism.

The first problem is mainly concerned with the conditions on the focus and information about the source mechanism. The overwhelming majority of seismologists in the United States agree on Reid's elastic rebound theory [4] which asserts that the processes of occurrence of shallow earthquakes are connected with ruptures of the medium on a fault plane. The validity of this assumption is supported by a quantitative comparison of the field geodetic measurements with those obtained using dislocation theory. For example, Chinnery [5] successfully inferred the static displacements in the vicinity of the San Andreas fault. Also, the results of Knopoff's [6] dislocation model and that of Wyss and Brune [7] were found in good agreement with the recorded data of the 1906 San Francisco and 1964 Alaskan earthquakes.

Investigations of seismic wave kinematics have convinced seismologists that a mechanism other than a propagating fracture on a fault is most likely the case for deep-focus earthquakes. Examining a large amount

of recorded seismic data, Japanese seismologists [8,9] came to a conclusion that the focus could be represented in the form of a sphere of a small radius on the surface of which the distributed radial forces are specified. In this study we are primarily concerned with shallow earthquakes and, therefore, the focus is represented by a propagating shear fault.

The emphasis in the present work is placed on the second problem, i.e., development of a mathematical scheme which describes the motion on the surface in terms of the geological parameters of the source (orientation of the fault plane and direction of the movement) and in terms of the seismic profile of the medium. The time history of the ground displacements is of primary interest because of the direct relationship between them and the motions to which large structures such as dams or nuclear power plants might be subjected.*

The main problem treated in this investigation is the wave propagation in an elastic solid comprised of a single layer which overlies a homogeneous half space. The seismic disturbances will be assumed to radiate from an arbitrarily oriented shear fault in the half space. The occurrence of a sudden discontinuity in displacements on the fault surface gives rise to waves which after reflection and refraction from the surfaces of discontinuity, produce motion on the free surface.

As is usually the case in elastic wave propagation, the principal difficulty that arises is the interaction of the dilatational and distortional waves at a bounding surface. The complexity of the problem can be judged by the fact that it is necessary to satisfy boundary conditions on three surfaces:

---

* The interaction of the structure with the motion in its vicinity is ignored in this study.

on the inclined fault plane, on the surface of discontinuity, and on the free surface.

The method of self-similar potentials in conjunction with a new concept which is developed in this study, and is referred to as the concept of auxiliary complex domain, is found to be an effective analytical technique in solving certain dislocation problems. This method was applied to the problem of dip-slip and strike-slip faulting in a layered media.

1.2 Previous Studies

Several methods have been used in the past to solve dislocation problems in a homogeneous or layered half space. Haskell [10] investigated seismic displacements in the near-field of a vertical, uniformly propagating fault with strike-slip motion using the de Hoop [11] elastodynamic representation theorem. His model does not include presence of the free surface and, consequently, surface waves are not present [12]. Aki [13] has also considered the near-field displacements created by a propagating fault. He takes the Fourier transforms of integrals derived by Maruyama [14] and then carries out a numerical integration over the fault plane to obtain the displacement spectrum. Finally a numerical inverse Fourier transform is used to return to the time domain.

To include the influence of the free surface in the simulated records, Burridge and Knopoff [15,16] proposed the concept of the point source equivalent to an impulsive dislocation. The fault plane is divided into a number of small areas each one of which has associated with it a concentrated multipole of forces. Although the method permits the consideration

of the surface waves in the computation of the ground notion, a numerical integration over the fault plane requires formidable computational effort. The models described above have been refined by some researchers in recent years. In 1964, Knopoff [17] developed a matrix method for the solution of the wave propagation in the layered media. Abramovici [18] solved similar problems using a Laplace transformation technique.

The method of self-similar potentials which was originally developed by V. I. Smirnov and S. L. Sobolev, turns out to be a relatively simple and extremely powerful alternative technique for solving two-dimensional dislocation problems. Kostrov [19,20] applied the method to the problems of propagation of shear and tension cracks in an infinite elastic medium. The entire solution involves at most one quadrature in the complex plane. The present study uses the same method with significant modification to account for a free surface and an inclined fault plane.

The advantages of the method of self-similar potentials over other approaches described above are twofold:

1) The Green's function solution which has been used in previous models applies to an elastic full space problem. The solution for a propagating dislocation by the Smirnov-Sobolev method involves no more complication than using it to find the Green's function for the half space or layered half space.* The final integration necessary in Haskell's [10] approach, the source of most of the computational effort, is then totally eliminated.

---

* Farewell's [31] results are identical with the Green's function solution.

2) The method considered here can be applied not only for the problems of spreading dislocation, but also to a mechanism of stick-slip fault motion.* The starting and stopping character of the crack propagation can also be described in a precise manner.

1.3 Method of Solution

In this study, the Smirnov-Sobolev technique is extended to permit the solution of two-dimensional dislocation problems when the effect of layering and free surface are included in the analysis. The key to this extension is the introduction of an auxiliary complex plane such that boundary conditions on both free surface and fault plane can be simultaneously satisfied.

The solution for two two-dimensional problems, one plane strain and the other antiplane, when combined properly, leads to an appropriate expressions for the displacement fields on the surface. The solution for the former corresponds to dip-slip faulting whereas the latter represents strike-slip faulting.

The work is organized in the following manner. Chapter 2 provides a brief review of the method of self-similar potentials in order to give a basis for the developments in succeeding sections. The displacement fields produced by an inclined shear fault within an infinite elastic medium are presented in Chapter 3. The effect of the free surface and the concept of auxiliary complex domain is discussed in detail in Chapter 4. The numerical

---

* The occurrence of stick-slip motion has been observed in laboratory experiments with geologic materials. See Ref. [21,22].

integration techniques employed in the computation of displacements are examined and illustrative examples are provided. Chapter 5 treats the effect of layering in the surface motions. Calculated records obtained in this study are compared with the observed strong motion records of Pacoima Dam. Finally, Chapter 6 summarizes the developments in this study and provides some suggestion for the application of the results to earthquake models. In addition, some further problems which might be solved by the method of self-similar potentials using the newly developed concept of auxiliary complex domain are described.

1.4 Notations

The symbols used in this study are defined in the text when they first appear. Those symbols most frequently used are listed below.

a	speed of the P wave $(\sqrt{\frac{\lambda + 2\mu}{\rho}})$
a_1	speed of the P wave in medium 1 (Chapter 5)
a_2	speed of the P wave in medium 2 (Chapter 5)
b	speed of the S wave $(\sqrt{\frac{\mu}{\rho}})$
b_1	speed of the S wave in medium 1 (Chapter 5)
b_2	speed of the S wave in medium 2 (Chapter 5)
c	speed of the Rayleigh wave
c_1	same as a

c_2	same as b
d	thickness of the near-surface soil layer
D	y-coordinate of the observation point on the free surface
D_x	dislocation amplitude for dip-slip fault
D_z	dislocation amplitude for strike-slip fault
R_{D_x}, L_{D_x}	dislocation amplitudes for dip-slip unilateral fault propagating along the positive and negative x-axis, respectively
R_{D_z}, L_{D_z}	dislocation amplitudes for strike-slip unilateral fault propagating along the positive and negative x-axis, respectively
$E_1(\eta), E_2(\eta)$	see Eqs. 5.23
f	angle of incidence
H(t)	heaviside step function
h_1, h_2	see Eqs. 5.6a
i	$\sqrt{-1}$
K_1, K_2	see Eqs. 5.6a
M_v, M_h	moments of vertical and horizontal double-force, respectively
n_1, n_2	see Eqs. 5.6a
p_i	see Eq. 2.6a
$R(\theta^2)$	Rayleigh function

r_o	$\sqrt{x_o^2 + D^2}$
t	time coordinate
$\bar{\bar{t}}$	see Eq. 5.27
Δt	increment of time
t_o	arrival time of the incident disturbance
T^o_{yz}, T^o_{zx}	complex tangential tractions for the self-similar antiplane problem
u_x, u_y	components of the displacement field for plane strain problems
u_z	displacement field for the antiplane problem
u_x^*, u_y^*, u_z^*	complex displacements associated with u_x, u_y and u_z
U_x, U_y, U_z	components of the displacement field for the problem subjected to the homogeneous tractions of degree -1
U_x^*, U_y^*, U_z^*	complex displacements associated with U_x, U_y and U_z
$U_x^{(1)}, U_y^{(1)}, U_z^{(1)}$	components of the displacement field in medium 1 (Chapter 5)
$U_x^{(2)}, U_y^{(2)}, U_z^{(2)}$	components of the displacement field in medium 2 (Chapter 5)
U_x^P, U_y^P	P-wave displacement components
U_x^S, U_y^S	S-wave displacement components
U_x^H, U_y^H	Head wave displacement components

U_x^{SS}, U_y^{SS}	displacement components corresponding to the reflected S wave
$R_{U_x}^*, R_{U_y}^*, R_{U_z}^*$	complex displacements corresponding to the unilateral fault propagating along the positive x-axis
$L_{U_x}^*, L_{U_y}^*, L_{U_z}^*$	complex displacements corresponding to the unilateral fault propagating along the negative x-axis
$e_{U_x}^*, e_{U_y}^*, e_{U_z}^*$	see Eqs. 3.18
V_{22}	displacement for the antiplane problem in medium 2 of Chapter 5
W, W_2, W_{22}	displacement for the antiplane problem, incident waves and reflected waves, respectively
x, y, z	Cartesian space coordinates
X_o	distance of the point of crack initiation from the free surface
x_o	distance of the point of crack initiation from the interface between two dissimilar media
α	speed of rupture propagation
β	see Eq. 4.5
γ	angle of the fault plane inclination
$\gamma_{11}, \gamma_{21}, \gamma_{111}$	scalar dilatational potentials for medium 2 of Chapter 5

$\Gamma_{11}, \Gamma_{21}, \Gamma_{111}$	complex dilatational potentials associated with γ_{11}, γ_{21}, and γ_{111}, respectively
δ_1, δ_2	see Eqs. 2.6a, 4.13 and 4.22
δ_{21}, δ_{22}	see Eqs. 4.22 and 5.10a
δ_{11}, δ_{12}	see Eqs. 4.12 and 5.2a
Δ_{11}, Δ_{12}	see Eqs. 5.2b
Δ_{22}, Δ_{21}	see Eqs. 5.10b
Δ_{111}, Δ_{112}	see Eqs. 5.24
η_1, η_2	see Eqs. 2.21 and 4.10
η_{11}, η_{12}	see Eqs. 4.15 and 4.13
η_{22}, η_{21}	see Eqs. 22
$\bar{\eta}$	see Eq. 4.2a
η_o	see Eq. 4.35
θ_1, θ_2	see Eqs. 2.10
λ, μ	Lame' constants of elasticity
$(\lambda_1, \mu_1), (\lambda_2, \mu_2)$	Lame' constants of elasticity for media 1 and 2, respectively
μ	μ_1/μ_2 in Chapter 5
ξ_{11}, ξ_{12}	see Eqs. 5.2b

ξ_1^o	see Eq. 5.4
ξ_{22}, ξ_{21}	see Eqs. 5.10b
ξ_2^o	see Eq. 5.12
ξ_{111}, ξ_{112}	see Eqs. 5.24
ξ_{111}^o	see Eq. 5.26
$\bar{\xi}_{111}$	see Eqs. 5.27
ρ	mass density of the elastic solid
$\sigma_x^*, \sigma_y^*, \sigma_z^*, \tau_{xy}^*$	complex components of the stress field for the plane strain problem
$\sum_x^o$, $\sum_y^o$, T_{xy}^o	complex self-similar stresses for plane problem
$\sum_x^*$, $\sum_y^*$, T_{xy}^*	complex homogeneous tractions of degree -1 (plane problem)
$\phi, \phi_1, \phi_{11}, \phi_{21}$	scalar dilatational potentials
$\Phi, \Phi_1, \Phi_{11}, \Phi_{21}$	complex dilatational potentials associated with ϕ, ϕ_1, ϕ_{11}, ϕ_{21}
ψ_z, ψ_{12}, ψ_{22}	scalar distortional potentials
Ψ_z, Ψ_{12}, Ψ_{22}	complex distortional potentials associated with ψ_z, ψ_{12}, ψ_{22}
ω_{12}, ω_{22}, ω_{112}	scalar distortional potentials for medium 2 of Chapter 5

Ω_{12}, Ω_{22}, Ω_{112}	complex distortional potentials associated with ω_{12}, ω_{22} and ω_{112}, respectively

2. DETERMINATION OF THE STRESS AND DISPLACEMENT FIELDS BY THE METHOD OF SELF-SIMILAR POTENTIALS

2.1 General Equations

The equations of motion of small amplitude for a homogeneous, isotropic solid which has elastic properties defined by the Lamé constants λ and μ, can be expressed in terms of the displacements as follows,

$$\begin{aligned}
(\lambda + \mu)\frac{\partial \Delta}{\partial x} + \mu\nabla^2 u_x &= \rho\frac{\partial^2 u_x}{\partial t^2} \\
(\lambda + \mu)\frac{\partial \Delta}{\partial y} + \mu\nabla^2 u_y &= \rho\frac{\partial^2 u_y}{\partial t^2} \\
(\lambda + \mu)\frac{\partial \Delta}{\partial z} + \mu\nabla^2 u_z &= \rho\frac{\partial^2 u_z}{\partial t^2}
\end{aligned} \tag{2.1}$$

where (x,y,z) are cartesian coordinates, ρ is the mass density of the solid, u_x, u_y, u_z are the components of the displacement vector $\bar{u}$, and t is the time. The dilation Δ and the Laplacian operator ∇^2 are defined by:

$$\begin{aligned}
\Delta &= \frac{\partial u_x}{\partial x} + \frac{\partial u_y}{\partial y} + \frac{\partial u_z}{\partial z} \\
\nabla^2 &= \frac{\partial^2}{\partial x^2} + \frac{\partial^2}{\partial y^2} + \frac{\partial^2}{\partial z^2}
\end{aligned} \tag{2.2}$$

It is customary to apply the Helmholtz theorem [23] to the displacement vector $\bar{u}$, thereby, representing it as the sum of the gradient of a scalar potential, ϕ, and the curl of a vector potential, $\bar{\psi}$. That is,

$$\bar{u} = \text{grad}\ \phi + \text{curl}\ \bar{\psi} \tag{2.3}$$

where $\bar{\psi}$ satisfies the condition div $\bar{\psi} = 0$. The scalar potential determines the irrotational (P) portion of the displacements; the vector potential, the equivoluminal (S) portion.

For the equations of motion to be satisfied, it is both a necessary and a sufficent condition that the potentials satisfy the wave equations [24],

$$(\nabla^2 - \frac{1}{a^2}\frac{\partial^2}{\partial t^2})\,\phi = 0$$
$$(\nabla^2 - \frac{1}{b^2}\frac{\partial^2}{\partial t^2})\,\psi_i = 0 \qquad (2.4)$$

where $a = \sqrt{\frac{\bar{\lambda} + 2\bar{\mu}}{\rho}}$ and $b = \sqrt{\frac{\bar{\mu}}{\rho}}$ are the speeds of the irrotational and equivoluminal waves, respectively. In what follows, the customary geophysical designation of P and S wave will be used instead of the terms "irrotational" and "equivoluminal." For the case of plane strain in which the displacements are zero in the z-direction, the x and y components of $\bar{\psi}$ are zero. The Helmholtz decomposition again leads to

$$(\nabla^2 - \frac{1}{a^2}\frac{\partial^2}{\partial t^2})\phi = 0$$
$$(\nabla^2 - \frac{1}{b^2}\frac{\partial^2}{\partial t^2})\,\psi_z = 0 \qquad (2.5)$$

Another plane problem of interest in this study is one of the anti-plane type for which the displacement vector is $(0,0,u_z)$ and is a function of x, y, and t only. The equations of motion reduce to a single one.

$$(\nabla^2 - \frac{1}{b^2}\frac{\partial^2}{\partial t^2}) u_z = 0 \qquad (2.6)$$

As will be demonstrated in the succeeding chapters, a plane strain and an antiplane problem when combined, yields the solution for a shear dislocation problem in which the Burgers vector [25] lies in the fault plane.

2.2 The Method of Self-Similar Potentials

The method of self-similar potentials is an extremely efficient technique which provides the solution to the two-dimensional wave propagation problems without formidable mathematical manipulation. The method applies to the problems where the boundary and initial conditions are homogeneous functions of the spatial variables and time--those which are commonly referred to as self similar problems.

This approach to wave propagation problems was first developed by two Soviet mathematicians, V. I. Smirnov and S. L. Sobolev [26] more than forty years ago. In 1969 Thompson and Robinson [27,28,29], with the emphasis on presenting a motivation and bibliography of the method, applied the method to various dynamic contact problems which involve an arbitrarily shaped rigid die and a linearly elastic half space. Later, Johnson and Robinson [30] explored the application of the method in conjunction with rotational superposition to solve three-dimensional problems involving a single force parallel to the surface of an elastic half space. More recently, Farewell and Robinson [31] extended the previous problem to the one in which a couple with different orientation is applied at a point beneath the surface. A brief summary of the procedure and some elements of the Smirnov-Sobolev technique which

are essential to the developments in this study are presented in the following section. For additional details, the reader is referred to the references given above.

2.2.1 General Remarks

The homogeneous boundary and initial conditions which characterize the self similar problems make it possible to reduce the number of independent variables necessary to describe the motion of the body, e.g., (x,y,t) becomes (x/t,y/t). This reduction is accomplished by introducing a complex variable, θ_i, which is defined implicitly by the equation

$$t - \theta_i x - y\sqrt{c_i^{-2} - \theta_i^2} + p_i(\theta_i) = 0 \qquad (2.6a)$$

The parameter c_i and the complex function $p_i(\theta_i)$ will be discussed in detail in the next section. It has been shown that [27] θ_i or any sufficiently smooth function of θ_i, say, $f(\theta_i)$ provides a solution to the differential equation of motion. The plane strain and antiplane problems uncouple. The solution to the former is in terms of a dilatational (P) wave and a vertically polarized distortional (SV) wave while the latter is in terms of a horizontally polarized distortional (SH) wave. These plane problems will be briefly treated in the following sections.

2.2.2 Solution of a Plane Strain Problem of Self-Similar Potentials

Solution to the plane strain problem can be obtained in terms of the self similar potential function, ϕ and ψ_z, henceforth denoted ψ, derived in Section 2.1. The functions ϕ and ψ are real parts of corresponding

complex potentials Φ and Ψ. That is,

$$\phi = \text{Re } \Phi(\theta_1)$$
$$\psi = \text{Re } \Psi(\theta_2) \tag{2.7}$$

where θ_1 and θ_2 are complex variables which parametrize the characteristic surfaces of the wave equation. The following implicit function defines the variables θ_1 and θ_2,

$$\delta_i \equiv t - \theta_i x - y\sqrt{c_i^{-2} - \theta_i^2} + p_i(\theta_i) = 0 \tag{2.8}$$
$$i = 1, 2$$

where $c_1 = a$, $c_2 = b$ and $p_i(\theta_i)$ is any analytic function of θ_i. For the problems in which the loading is applied initially at the origin of the (x, y,t) space, only the characteristic surfaces through the origin are of interest and $p_i(\theta_i) = 0$. For subsurface loadings considered in subsequent sections $p_i(\theta_i) \neq 0$. Consider the particular case when $p_i(\theta_i) = 0$. In this case the Eq. 2.8 has the form:

$$\delta_i \equiv t - \theta_i x - y\sqrt{c_i^{-2} - \theta_i^2} = 0 \tag{2.9}$$

These surfaces are planes tangent to the cone $x^2 + y^2 = c_i^2 t^2$. Figure 1 shows the trace of several of these planes in the (x/t, y/t) plane. As indicated previously, any sufficiently smooth function of θ_i, in this case, ϕ and ψ, will automatically satisfy the wave equation.

Solution of Eq. 2.9 provides the values of the θ_i variables and defines a mapping of the (x,y,t) space into the complex θ_i plane. For

$x^2 + y^2 < c_i^2 t^2$,

$$\theta_i = \frac{1}{r^2}\left(tx + iy(t^2 - r^2 c_i^{-2})^{1/2}\right) \tag{2.10a}$$

and for $x^2 + y^2 > c_i^2 t^2$,

$$\theta_i = \frac{1}{r^2}\left[tx + \varepsilon y(r^2 c_i^{-2} - t^2)^{1/2}\right] \tag{2.10b}$$

where $r^2 = x^2 + y^2$, $\varepsilon = +1$ for $x < 0$ and $\varepsilon = -1$ for $x > 0$. It is seen that the variable θ_i is real beyond the wave front and complex behind it. The value of θ_i is constant on a characteristic plane and $\theta_1 = \theta_2$ at points on the $y = 0$ surface where the characteristic plane intersects the boundary. The fact that θ_1 and θ_2 possess equal values on the $y = 0$ surface facilitates the solution to the initial value problems in which $y = 0$ is the boundary.

The mapping defined by Eqs. 2.10 transforms the half space $y \geq 0$ into the upper half θ_i plane. Figure 2 shows some features of the mapping. Briefly, the surface $y = 0$ together with the region outside and on the wave front map onto the real θ_i axis and the region inside the wave front maps into the region off the real θ_i axis. The $y = 0$ surface maps into the real θ_i axis independently of c_i, a fact essential to the solution that follows. The complex displacements can be written in terms of the complex self similar potentials as:

$$u_x^* = \frac{\partial \Phi(\theta_1)}{\partial x} + \frac{\partial \Psi(\theta_2)}{\partial y}$$

$$u_y^* = \frac{\partial \Phi(\theta_1)}{\partial y} - \frac{\partial \Psi(\theta_2)}{\partial x} \tag{2.11}$$

$$u_z^* = 0$$

It should be observed that only the real parts of u_x^* and u_y^* have physical significance and represents the real displacements. The derivatives of θ_i are found from Eq. 2.9 to be

$$\frac{\partial \theta_i}{\partial x} = \frac{\theta_i}{\delta_i'}$$

$$\frac{\partial \theta_i}{\partial y} = \frac{\sqrt{c_i^{-2} - \theta_i^2}}{\delta_i'} \tag{2.12a}$$

$$\frac{\partial \theta_i}{\partial t} = -\frac{1}{\delta_i'}$$

where

$$\delta_i' = -x + \frac{y\theta_i}{\sqrt{c_i^{-2} - \theta_i^2}} \tag{2.12b}$$

$$= \frac{i\sqrt{t^2 - c_i^{-2}(x^2 + y^2)}}{\sqrt{c_i^{-2} - \theta_i^2}}$$

Hence,

$$u_x^* = \Phi'(\theta_1)\frac{\theta_1}{\delta_1'} + \Psi'(\theta_2)\frac{\sqrt{b^{-2} - \theta_2^2}}{\delta_2'}$$

$$u_y^* = \Phi'(\theta_1)\frac{\sqrt{a^{-2} - \theta_1^2}}{\delta_1'} - \Psi'(\theta_2)\frac{\theta_2}{\delta_2'} \tag{2.13a}$$

where

$$\Phi' = \frac{\partial\Phi}{\partial\theta_1} \quad \text{and} \quad \Psi' = \frac{\partial\Psi}{\partial\theta_2} \tag{2.13b}$$

Employing the Leibniz rule for differentiation of an integral and considering the derivatives of θ_i defined by Eqs. 2.12a, one can write the displacements of Eqs. 2.13a in a slightly different but more convenient form as:

$$u_x^* = \frac{\partial}{\partial t}\left[-\int_0^{\theta_1} \theta\Phi'(\theta)d\theta - \int_0^{\theta_2} \sqrt{b^{-2} - \theta^2}\,\Psi'(\theta)d\theta\right]$$

$$u_y^* = \frac{\partial}{\partial t}\left[-\int_0^{\theta_1} \sqrt{a^{-2} - \theta^2}\,\Phi'(\theta)d\theta + \int_0^{\theta_2} \theta\Psi'(\theta)d\theta\right] \tag{2.14}$$

The complex stresses are then:

$$\frac{\sigma_y^*}{\mu} = \frac{\partial^2}{\partial t^2}\left[\int_0^{\theta_1} (b^{-2} - 2\theta^2)\Phi'(\theta)d\theta - \int_0^{\theta_2} 2\theta\sqrt{b^{-2} - \theta^2}\,\Psi'(\theta)d\theta\right]$$

$$\frac{\sigma_x^*}{\mu} = \frac{\partial^2}{\partial t^2}\left[\int_0^{\theta_1} (b^{-2} + 2\theta^2 - 2a^{-2})\Phi'(\theta)d\theta + \int_0^{\theta_2} 2\theta\sqrt{b^{-2} - \theta^2}\,\Psi'(\theta)d\theta\right]$$

$$\frac{\tau^*_{xy}}{\mu} = \frac{\partial^2}{\partial t^2}\left[\int_0^{\theta_1} 2\theta\sqrt{a^{-2} - \theta^2}\,\Phi'(\theta)d\theta + \int_0^{\theta_2}(b^{-2} - 2\theta^2)\Psi'(\theta)d\theta\right]$$

$$\frac{\sigma^*_z}{\mu} = \frac{\partial^2}{\partial t^2}\left[\int_0^{\theta_1}(b^{-2} - 2a^{-2})\,\Phi'(\theta)d\theta\right] \qquad (2.15)$$

where θ is dummy variable of integration.

Any loading that is homogeneous in spatial and time coordinates can be represented by an appropriate integration or differentiation of Eqs. 2.14 depending on the degree of homogeneity.* For example, consider the case in which an elastic solid is subjected to a homogeneous boundary tractions of degree zero. The expressions for the complex stresses and displacements are as follows,

$$\sum_x^o = \int_o^t \int_o^\tau \sigma^*_x \, d\tau_1 d\tau$$

$$\sum_y^o = \int_o^t \int_o^\tau \sigma^*_y \, d\tau_1 d\tau \qquad (2.16)$$

$$T^o_{xy} = \int_o^t \int_o^\tau \tau^*_{xy} \, d\tau_1 d\tau$$

Substituting for σ^*_x, σ^*_y and τ^*_{xy} from Eqs. 2.15, the stresses are found to be

*Thompson and Robinson have discussed the generalization of the method of self similar potential and its application to the problems in which boundary tractions (or displacements) are homogeneous of degree n. See Ref. [27] for additional details.

$$\frac{\sum_x^o}{\mu} = \int_o^{\theta_1} (b^{-2} + 2\theta^2 - 2a^{-2})\Phi'(\theta)d\theta + \int_o^{\theta_2} 2\theta\sqrt{b^{-2} - \theta^2}\,\Psi'(\theta)d\theta$$

$$\frac{\sum_y^o}{\mu} = \int_o^{\theta_1} (b^{-2} - 2\theta^2)\Phi'(\theta)d\theta - \int_o^{\theta_2} 2\theta\sqrt{b^{-2} - \theta^2}\,\Psi'(\theta)d\theta \qquad (2.17a)$$

$$\frac{T_{xy}^o}{\mu} = \int_o^{\theta_1} 2\theta\sqrt{a^{-2} - \theta^2}\,\Phi'(\theta)d\theta + \int_o^{\theta_2} (b^{-2} - 2\theta^2)\,\Psi'(\theta)d\theta$$

Similar expressions for the complex displacements are:

$$U_x^o = \int_o^t - \{\int_o^{\theta_1} \theta\Phi'(\theta)d\theta + \int_o^{\theta_2} \sqrt{b^{-2} - \theta^2}\,\Psi'(\theta)d\theta\}\,d\tau \qquad (2.17b)$$

$$U_y^o = \int_o^t - \{\int_o^{\theta_1} \sqrt{a^{-2} - \theta^2}\,\Phi'(\theta)d\theta - \int_o^{\theta_2} \Psi'(\theta)d\theta\}\,d\tau$$

On the surface $y = o$, $\theta_1 = \theta_2 = \bar{\theta} = \frac{t}{x}$. Equations 2.17a and 2.17b become:

$$\frac{\sum_x^o}{\mu} = \int_o^{\bar{\theta}} [(b^{-2} + 2\theta^2 - 2a^{-2})\Phi'(\theta) + 2\theta\sqrt{b^{-2} - \theta^2}\,\Psi'(\theta)]d\theta$$

$$\frac{\sum_y^o}{\mu} = \int_o^{\bar{\theta}} [(b^{-2} - 2\theta^2)\Phi'(\theta) - 2\theta\sqrt{b^{-2} - \theta^2}\,\Psi'(\theta)]d\theta \qquad (2.18a)$$

$$\frac{T^o_{xy}}{\mu} = \int_o^{\overline{\theta}} [2\theta\sqrt{a^{-2} - \theta^2}\,\Phi'(\theta) + (b^{-2} - 2\theta^2)\,\Psi'(\theta)]\,d\theta$$

and,

$$U^o_x = \int_o^t - \{\int_o^{\overline{\theta}} [\theta\Phi'(\theta) + \sqrt{b^{-2} - \theta^2}\,\Psi'(\theta)]d\theta\}\,d\tau \qquad (2.18b)$$

$$U^o_y = \int_o^t - \{\int_o^{\overline{\theta}} [\sqrt{a^{-2} - \theta^2}\,\Phi'(\theta) - \theta\Psi'(\theta)]d\theta\}\,d\tau$$

Assuming that the normal and tangential tractions are defined on the boundary, one can obtain the complex potentials Φ' and Ψ' in the following manner: differentiate the last two of Eqs. 2.18a with respect to θ and solve the resulting simultaneous equations for Φ' and Ψ'. The following expressions can be easily verified.

$$\Phi'(\theta_1) = \frac{1}{\mu}\,\frac{(b^{-2} - 2\theta_1)\,\sum_y^{o'}(\theta_1) + 2\theta_1\sqrt{b^{-2} - \theta_1^2}\;T^{o'}_{xy}(\theta_1)}{R(\theta_1^2)} \qquad (2.19a)$$

$$\Psi'(\theta_2) = \frac{1}{\mu}\,\frac{(b^{-2} - 2\theta_2^2)\,T^{o'}_{xy}(\theta_2) - 2\theta_2\sqrt{a^{-2} - \theta_2^2}\;\sum_y^{o'}(\theta_2)}{R(\theta_2^2)}$$

where

$$\sum_y^{o'}(\theta_i) = \frac{d\,\sum_y^o(\theta_i)}{d\theta_i} \qquad T^{o'}_{xy}(\theta_i) = \frac{d\,T^o_{xy}(\theta_i)}{d\theta_i} \qquad (2.18b)$$

and

$$R(\theta_i^2) = (b^{-2} - 2\theta_i^2)^2 + 4\theta_i^2\sqrt{a^{-2} - \theta_i^2}\sqrt{b^{-2} - \theta_i^2} \qquad (2.19c)$$

is the Rayleigh function.

A complete description of the method, as it applies to the self-similar traction problems can be summarized as:

1. Given the real boundary tractions, $\sum_y = \text{Re}\ \sum_y^o$ and $T_{xy} = \text{Re}\ T_{xy}^o$ on the surface $y = 0$, determine the complex stresses by applying the Cauchy integral theorem [32] for the half plane. The resulting functions can be expressed in terms of $\bar{\theta} = t/x$ on the boundary.
2. Find Φ' and Ψ' from Eqs. 2.19a by substituting for $\sum_y^{o'}$ and $T_{xy}^{o'}$ obtained in step 1.
3. Substitute the expressions into Eqs. 2.18. The real part of the results after carrying out the necessary integrations give the stress and displacement fields within the half space.

2.2.3 Solution of the Antiplane Problem

The antiplane problem is treated in a similar manner as the plane strain problem. The major difference is that the solution for the antiplane case is found in terms of a displacement function rather than a potential function. The displacement function, w, is the real part of the complex function $W(\theta_2)$. That is,

$$w = \text{Re}\ W(\theta_2)$$

The complex variable θ_2 is defined by Eqs. 2.10.

For a problem with homogeneous tractions of degree zero, the displacements and stresses are found in a manner analogous to Sec. 2.2.2. The results are:

$$U_z^o = \int_o^t \left[\int_o^{\theta_2} W'(\theta) d\theta \right] d\tau$$

$$\frac{T_{yz}^o}{\mu} = -\int_o^{\theta_2} \sqrt{b^{-2} - \theta^2}\, W'(\theta) d\theta \qquad (2.20)$$

$$\frac{T_{zx}^o}{\mu} = -\int_o^{\theta_2} \theta W'(\theta) d\theta$$

The general approach of Sec. 2.2.2 applies equally well to the antiplane problem and similar steps should be taken.

2.3 Extension of the Method of Self-Similar Potentials to Boundary Value Problems Involving Non-Parallel Boundaries

As mentioned in the proceeding section, the fact that θ_1 and θ_2 possess equal values on the surface $y = 0$ is essential to the solution of plane strain problems. This requirement can be easily maintained for problems with a single plane boundary. In fact, the equation of the characteristic plane is defined in a manner that this condition is automatically satisfied. However, there exists a class of problems in elastodynamic theory which involve more than one boundary. For example, the problem of an impulsive line source acting inside an elastic and isotropic quarter

plane, three-quarter plane, or two "welded" quarter plane with stress-free surfaces are typical geophysical problems.

In particular, the problem of great interest in the study of models of earthquakes is the one in which a fault of arbitrary dip in an elastic half space experiences sudden discontinuity in the displacement across the fault surface, thus, radiating elastic waves to the surface. It will be demonstrated in the subsequent chapters that the method of the self-similar potentials is applicable to this two-dimensional dislocation problem and an exact solution can be obtained in a fairly straightforward manner.

For example, in the case of a vertical fault plane which is located in an elastic half-space the expression for incident potentials in the θ-plane can be easily obtained by using the Cauchy integral theorem together with the prescribed boundary conditions on the fault surface. Two other potentials, namely, reflected P and S-wave potentials are found by introducing a new complex variable, η_i, such that

$$\eta_i = \sqrt{c_i^{-2} - \theta_i^2} \tag{2.21}$$

The equation of the characteristic plane in terms of η_i becomes:

$$\delta_i \equiv t - x\sqrt{c_i^{-2} - \eta_i^2} - y\eta_i = 0 \tag{2.22}$$

It is apparent that η_1 and η_2 have equal values on the $x = 0$ surface--the condition that permits determination of the reflected potentials. For the case of an inclined fault plane, transformation (2.21) is of more general form; however, the η_i's retain the previous property. Further details along with numerical examples will be provided in Chapter 4.

3. RADIATION OF ELASTIC WAVES FROM A DISLOCATION SOURCE

3.1 General Remarks

It was indicated in Chapter 1 that, according to seismological evidence, shallow-focus earthquakes occur as a result of sudden tangential motion of Earth material across a pre-existing fault plane. The mechanical energy released by this sudden slippage is carried away from the source region in the form of seismic waves and produces disturbance at the interior points of the medium. A kinematic model can be developed such that it retains the major physical features of the faulting process and describes the motion at any point inside an infinite elastic solid.

Several researchers have investigated faulting models adopting different approaches. Steketee [33] used Volterra's formula to derive analytical expressions for the displacement fields as an integral over the fault plane involving nuclei of strain which he interpreted as being due to the action of systems of point forces. Later, Maruyama [34] extended Steketee's work to include different type of point sources. Geller [35] developed analytic solutions for a two-dimensional dislocation problem. He integrated the Green's function solution for a shear fault along the direction of infinite length, thus, reducing the surface integral over the fault area to a line integral over the depth of the fault. Knopoff and Gilbert [36] used the "Knopoff-de Hoop representation theorems" to obtain first motions of body waves from a propagating fault. They have shown that the radiation pattern of a shear fault coincides with that of two double-force with opposite moments in an unfaulted solid.

The models mentioned above, have failed to consider several physical features which are associated with the processes of crack propagation. For example, it has been shown that the rupture velocity is in general less than the speed of P wave [37], whereas Geller's model is based upon the assumption that the dislocation front travels with infinite speed, the phenomenon which cannot be justified in the physical sense. It is also agreed by many seismologists that because of high tangential friction on the fault surface, the dislocation front may cease for a short period of time and then begin to propagate at some slightly later time. This factor too is not included in the existing models.

This chapter treats dislocation problems in an unbounded medium using the method of self-similar potentials. In spite of the apparent simplicity of the method, the model allows for consideration of the phenomena neglected in the previous models and some important features of the source mechanism are exhibited in the radiation pattern. The variation of rupture velocity in different strata can also be taken into account. This is of particular interest in dealing with problems in which the geological property of the medium contained between the focus and the observation point changes considerably. Finally, application of the method of self similar potentials to the faulting models makes it possible to define the starting and stopping position of the dislocation front in an arbitrary fashion in a proper time and spatial domain.

In the subsequent sections two different types of faulting will be considered:

1. Rupture starts at a point on the fault and propagates in two opposite directions (bilateral fault) and;

2. Faulting starts at a point and propagates only in one direction.

The solution for these two problems, when combined properly, results in the expressions for displacement fields corresponding to a fault with infinite length and finite depth. It is assumed that the dislocation amplitude varies as a step function in time. The extension to any other time dependence is not difficult.

3.2 Elastic Waves Radiated from a Bilaterally Propagating Shear Fault

Consider a fault plane located in an elastic, homogeneous, and isotropic medium extending to infinity in all directions. At some initial time two opposite sides of the fault suddenly acquire a relative displacement tangential to the fault plane along a segment with infinite length and infinitesimal depth. The dislocation front then, propagates bilaterally at right angles to itself, sweeping out a rectangular area. Thus, the fault plane can be visualized as a geometrical discontinuity across which a sudden slip takes place in an arbitrary direction. Figure 3 shows the fault model. As mentioned before, the general solution for a two-dimensional dislocation problem can be decomposed to a plane and antiplane problem. The former corresponds to the slip in the x-direction (dip-slip), and the latter results from the slip in the z-direction (strike-slip). Both cases will be examined in detail and expressions for displacement fields will be derived.

The following assumptions have been made throughout this study:

1. No geometrical nor functional dependence exists in the z-direction, i.e., all planes perpendicular to the z-axis are exactly identical at any given time.
2. The velocity of propagation is uniform for any single dislocation pulse.
3. The dislocation is uniform.
4. The effect of medium nonlinearity or inelasticity is ignored.

3.2.1 Solution to the Plane Strain Problem

The boundary conditions on the fault surface are defined by the following equations.

$$U_x\Big|_{y=0^-} = -\frac{D_x}{2}\,[H(t+t') - H(t-t')]$$

$$U_x\Big|_{y=0^+} = +\frac{D_x}{2}\,[H(t+t') - H(t-t')]\ ; \quad t' = \frac{|x|}{\alpha} \tag{3.1a}$$

and

$$\Sigma_y = 0 \quad \text{for all} \quad |x| \quad \text{(see Appendix A)} \tag{3.1b}$$

where, D_x is the relative displacement of two opposite surface of the fault plane, α the velocity of crack propagation, and H the Heaviside step function.

The problem under consideration is completely determined by a prescribed tangential movement on the boundary which is a homogeneous function of degree zero. Therefore, all displacements are homogeneous of degree zero. That is,

$$U_x\,(kx, ky, kt) = U_x\,(x, y, t)$$
$$U_y\,(kx, ky, kt) = U_y\,(x, y, t) \qquad (3.2a)$$

It follows that stresses are homogeneous functions of degree -1, i.e.,

$$\sum_x\,(kx, ky, kt) = k^{-1} \sum_x\,(x, y, t)$$
$$\sum_y\,(kx, ky, kt) = k^{-1} \sum_y\,(x, y, t) \qquad (3.2b)$$

Equations 2.14 and 2.15 of Sec. 2.2.2 when integrated once in the time domain, gives stress and displacement fields for a problem in which boundary tractions are homogeneous functions of degree -1 (see Sec. 2.8 in Ref. [27]). The results are:

$$U_x^* = \int_0^t u_x^*\, d\tau \quad ; \qquad U_y^* = \int_0^t u_y^*\, d\tau \qquad (3.2c)$$

and

$$\sum_x^* = \int_0^t \sigma_x^*\, d\tau \quad ; \qquad \sum_y^* = \int_0^t \sigma_y^*\, d\tau \qquad (3.2d)$$

The following relationships hold between the complex stresses and displacements and their real parts

$$U_x = \text{Re}\, U_x^* \quad ; \qquad U_y = \text{Re}\, U_y^* \qquad (3.2e)$$

$$\sum_x = \text{Re} \sum_x^* \quad ; \qquad \sum_y = \text{Re} \sum_y^* \qquad (3.2f)$$

Substituting for u_x^*, u_y^*, σ_x^*, and σ_y^* from Eqs. 2.13a and 2.13b, we have the following expressions,

$$U_x^* = -\int_0^{\theta_1} \theta\Phi'(\theta)d\theta - \int_0^{\theta_2} \sqrt{b^{-2} - \theta^2}\,\Psi'(\theta)d\theta$$

$$U_y^* = -\int_0^{\theta_1} \theta\Phi'(\theta)d\theta + \int_0^{\theta_2} \theta\Psi'(\theta)d\theta \qquad (3.3a)$$

and,

$$\frac{\sum_y^*}{\mu} = \frac{\partial}{\partial t}\left[\int_0^{\theta_1} (b^{-2} - 2\theta^2)\,\Phi'(\theta)d\theta - \int_0^{\theta_2} 2\theta\sqrt{b^{-2} - \theta^2}\,\Psi'(\theta)d\theta\right]$$

(3.3b)

$$\frac{\sum_x^*}{\mu} = \frac{\partial}{\partial t}\left[\int_0^{\theta_1} (b^{-2} + 2\theta^2 - 2a^{-2})\Phi'(\theta)d\theta + \int_0^{\theta_2} 2\theta\sqrt{b^{-2} - \theta^2}\,\Psi'(\theta)d\theta\right]$$

$$\frac{T_{xy}^*}{\mu} = \frac{\partial}{\partial t}\left[\int_0^{\theta_1} 2\theta\sqrt{a^{-2} - \theta^2}\,\Phi'(\theta)d\theta + \int_0^{\theta_2} (b^{-2} - 2\theta^2)\Psi'(\theta)d\theta\right]$$

The complex variables θ_1 and θ_2 are defined by Eqs. 2.9 and θ is the dummy variable of integration.

To obtain the self similar potentials Φ' and Ψ' which solve the two-dimensional dislocation problem, it is necessary to express the stresses and displacements in the complex θ-plane. This can be accomplished using the Cauchy integral theorem together with the boundary values expressed by Eqs. 3.1. The results are:

$$U_x^*(\bar{\theta}) = -\frac{1}{i\pi}\int_{-\infty}^{+\infty} \frac{D_x\,[H(\xi + \alpha t) - H(\xi - \alpha t)]}{\xi - x}\,d\xi$$

$$= -\frac{D_x}{2i\pi}\,\ln\frac{1 + \alpha\bar{\theta}}{1 - \alpha\bar{\theta}} \qquad (3.4a)$$

and

$$\sum_y^*(\bar{\theta}) = 0 \tag{3.4b}$$

where, $\bar{\theta} = t/x$ on the $y = 0^+$ surface, and α is the rupture velocity.

Equations 3.4 when combined with the first and third of Eqs. 3.3, yield the complex potentials Φ' and Ψ'. Their values can be computed from the following equations:

$$\Phi'(\bar{\theta}) = -\frac{2D_x\alpha b^2}{i\pi} \cdot \frac{\bar{\theta}}{1 - \alpha^2\bar{\theta}^2}$$

$$\Psi'(\bar{\theta}) = -\frac{D_x\alpha b^2}{i\pi} \cdot \frac{b^{-2} - 2\bar{\theta}^2}{(1 - \alpha^2\bar{\theta}^2)\sqrt{b^{-2} - \bar{\theta}^2}} \tag{3.5}$$

Since the $y = 0$ plane maps into the real axes in the complex θ_1 and θ_2-plane, the potentials $\Phi'(\bar{\theta})$ and $\Psi'(\bar{\theta})$ must be the boundary values of Φ' and Ψ' in the same complex domains, respectively. It has been shown [32] that $\Phi'(\theta_1)$ and $\Psi'(\theta_2)$ can be determined at any point off the real axis in the complex domain by replacing $\bar{\theta}$ in the first and second of Eqs. 3.5 with θ_1 and θ_2, respectively. That is,

$$\Phi'(\theta_1) = -\frac{2D_x\alpha b^2}{i\pi} \cdot \frac{\theta_1}{1 - \alpha^2\theta_1^2} \qquad \text{for } y \geq 0^+ \tag{3.6}$$

$$\Psi'(\theta_2) = -\frac{D_x\alpha b^2}{i\pi} \cdot \frac{b^{-2} - 2\theta_2^2}{(1 - \alpha^2\theta_2^2)\sqrt{b^{-2} - \theta_2^2}}$$

The problem is now completely determined. The motion can be described at any point of the medium* by simply substituting for the complex potentials in Eqs. 3.3a, i.e.,

$$U_x^* = \frac{2D_x\alpha b^2}{i\pi}\left[\int_0^{\theta_1} \frac{\theta^2}{1-\alpha^2\theta^2}\,d\theta + \int_0^{\theta_2} \frac{b^{-2}-2\theta^2}{2(1-\alpha^2\theta^2)}\,d\theta\right] \tag{3.7}$$

$$U_y^* = \frac{2D_x\alpha b^2}{i\pi}\left[\int_0^{\theta_1} \frac{\theta\sqrt{a^{-2}-\theta^2}}{1-\alpha^2\theta^2}\,d\theta - \int_0^{\theta_2} \frac{\theta(b^{-2}-2\theta^2)}{2(1-\alpha^2\theta^2)\sqrt{b^{-2}-\theta^2}}\,d\theta\right]$$

Obviously, only the real portion of U_x^* and U_y^* represent the physical disturbance in the body.

The integrals on the right side of Eqs. 3.7 when evaluated, lead to the following explicit expressions for the displacements:

---

*If a cut is made between $-b^{-1}$ and $+b^{-1}$ in θ_2-plane such that the radical $\sqrt{b^{-2}-\theta^2}$ become single-valued at every point, the potentials defined by Eqs. 3.6 will also solve the $y \leq 0^-$ half space problem whose boundary conditions are defined by Eqs. 3.1.

$$U_x^* = \frac{2D_x b^2}{i\pi}\left[\frac{\theta_2 - \theta_1}{\alpha} + \frac{1}{2\alpha^2}\ln\frac{\alpha\theta_1 + 1}{\alpha\theta_1 - 1} + \frac{1}{4b^2}\ln\frac{1 + \alpha\theta_2}{1 - \alpha\theta_2}\right.$$

$$\left. - \frac{1}{2\alpha^2}\ln\frac{\alpha\theta_2 + 1}{\alpha\theta_2 - 1}\right]$$

$$U_y^* = \frac{2D_x b^2}{i\pi\alpha}\left[\sqrt{\alpha^{-2} - a^{-2}}\ \tan^{-1}\left(\frac{\sqrt{a^{-2} - \theta_1^2}}{\sqrt{\alpha^{-2} - a^{-2}}}\right)\right.$$

$$+ \frac{\alpha^2 - 2b^2}{2\alpha b\sqrt{b^2 - \alpha^2}}\ \tan^{-1}\left(\frac{\alpha b\sqrt{b^{-2} - \theta_2^2}}{\sqrt{b^2 - \alpha^2}}\right)$$

$$- \sqrt{\alpha^{-2} - a^{-2}}\ \tan^{-1}\left(\frac{1}{a\sqrt{\alpha^{-2} - a^{-2}}}\right)$$

$$+ \frac{2b^2 - \alpha^2}{2\alpha b\sqrt{b^2 - \alpha^2}}\ \tan^{-1}\left(\frac{\alpha}{\sqrt{b^2 - \alpha^2}}\right) - \sqrt{a^{-2} - \theta_1^2}$$

$$\left. + \sqrt{b^{-2} - \theta_2^2} + a^{-1} - b^{-1}\right] \qquad (3.7a)$$

The investigation of Eqs. 3.7 reveals that the irrotational as well as equivoluminal components of the displacements are zero, as expected, beyond the front of the P and S-wave. The denominator of the integrands are zero at points $\theta = \pm\alpha^{-1}$. However, since $\alpha^{-1} > b^{-1} > a^{-1}$, the path of integration does not include any of these simple poles and the integrands are all analytic functions of θ in the region of interest. As a result, the displacements are finite and continuous for all $t > 0$. The case in which $\alpha >$ b,

although not justifiable in the physical sense, can be treated without any difficulty.

3.2.2 Solution to the Antiplane Problem

Solution for the SH-wave component of the displacement is found in an even simpler manner than that described in the previous section. In this case the upper half plane ($y \leq 0^-$) has a permanent tangential displacement in the z-direction relative to the lower half-plane ($y \geq 0^+$) adjacent to it. The boundary condition on the fault plane when expressed in terms of the variable θ, is found to be

$$U_z^*(\theta) = -\frac{D_z}{2i\pi} \ln \frac{1 - \alpha\theta}{1 + \alpha\theta} \tag{3.8}$$

where

$$D_z = U_z\Big|_{y=0^+} - U_z\Big|_{y=0^-} \quad \text{and} \quad U_z = \text{Re } U_z^* \tag{3.9}$$

The derivative of the complex displacement potential is defined by the equation

$$W'(\theta_2) = \frac{\alpha D_z}{i\pi} \frac{1}{1 - \alpha^2\theta_2^2} \tag{3.10}$$

Equation 3.10 describes an incident SH-wave potential. Corresponding displacement field is determined from the equation

$$U_z^* = \frac{\alpha D_z}{i\pi} \int_0^{\theta_2} \frac{1}{1 - \alpha^2\theta^2}\, d\theta \qquad (3.11)$$

$$= \frac{D_z}{2i\pi} \cdot \ln \frac{\alpha^{-1} - \theta_2}{\alpha^{-1} - \theta_2}$$

Equation 3.7 together with Eq. 3.11 determines the complete solution for a two-dimensional dislocation problem in which cracking propagates at both directions and displacement discontinuity on the fault plane has a step function time dependence.

3.3 Elastic Waves Radiated from a "Unilateral" Shear Fault

The solution for a problem in which slip starts at a point on the fault plane and propagates unilaterally along the x-axis is found in much the same fashion as that for the bilaterally spreading fault. The only difference arises from the fact that an appropriate time and coordinate shift has to be considered in defining the new complex variables* θ_i^R and θ_i^L. In what follows the superscripts R and L will be used to designate the displacements for two different problems in which the dislocation front propagates in the positive and negative x-direction, respectively. The fault models are shown in Fig. 4. The analysis in this section parallels that of Sec. 3.2 and reiteration of the procedures is not necessary. For a dip-slip fault propagating in the positive x-axis, the following fields can be easily verified.**

*The notation θ_i will be used whenever a condition applies to both the θ_1 and θ_2 plane.

**The expressions for the incident P and S-wave potentials which correspond to a unilaterally propagating shear fault are derived in Appendix B.

$$R_{U_x}^* = \frac{D_x^R \alpha b^2}{i\pi} \left[\int_0^{\theta_1^R} \frac{\theta^2}{1 - \alpha\theta}\, d\theta + \int_0^{\theta_2^R} \frac{b^{-2} - 2\theta^2}{2(1 - \alpha\theta)}\, d\theta\right] \tag{3.12}$$

$$R_{U_y}^* = \frac{D_x^R \alpha b^2}{i\pi} \left[\int_0^{\theta_1^R} \frac{\theta\sqrt{a^{-2} - \theta^2}}{1 - \alpha\theta}\, d\theta - \int_0^{\theta_2^R} \frac{\theta(b^{-2} - 2\theta^2)}{2(1 - \alpha\theta)\sqrt{b^{-2} - \theta^2}}\, d\theta\right]$$

Performing integrations* of Eqs. 3.12, we have

$$R_{U_x}^* = \frac{D_x^R b^2}{i\pi\alpha^2} \left[\frac{1}{2}(1 - \alpha\theta_1^R)^2 - \frac{1}{2}(1 - \alpha\theta_2^R)^2 + 2\alpha(\theta_1^R - \theta_2^R)\right.$$

$$\left. + \ln(1 - \alpha\theta_1^R) + \left(\frac{\alpha^2}{2b^2} - 1\right) \ln(1 - \alpha\theta_2^R)\right] \tag{3.12a}$$

---

*It may be more convenient to evaluate the integrals numerically. The explicit form of the displacements derived here is useful in finding the residual displacements.

$$R_{U_y}^{*} = \frac{D_x^R b^2}{i\pi\alpha^2}\left[\frac{\alpha^2 - 2a^2}{2a^2}\cdot\sin^{-1}(a\theta_1^R) - \frac{\sqrt{a^2-\alpha^2}}{a}\cdot\sin^{-1}\left(\frac{\alpha a^{-1} - a\theta_1^R}{1-\alpha\theta_1^R}\right)\right.$$

$$+ \sin^{-1}(b\theta_2^R) + \frac{2b^2-\alpha^2}{2b\sqrt{b^2-\alpha^2}}\cdot\sin^{-1}\left(\frac{\alpha b^{-1} - b\theta_2^R}{1-\alpha\theta_2^R}\right)$$

$$+ \alpha\left(\sqrt{a^{-2} - \theta_1^{R^2}} - \sqrt{b^{-2} - \theta_2^{R^2}}\right) + \frac{\alpha^2}{2}\left(\theta_1^R\sqrt{a^{-2} - \theta_1^{R^2}}\right.$$

$$\left.\left. - \theta_2^R\sqrt{b^{-2} - \theta_2^{R^2}}\right) + \frac{\sqrt{a^2-\alpha^2}}{a}\sin^{-1}\left(\frac{\alpha}{a}\right)\right.$$

$$\left. - \frac{2b^2-\alpha^2}{2b\sqrt{b^2-\alpha^2}}\sin^{-1}\left(\frac{\alpha}{b}\right) - \left(\frac{\alpha}{a} - \frac{\alpha}{b}\right)\right]$$

Similar results are obtained for a unilaterally propagating strik-slip fault as shown below

$$R_{U_z}^{*} = \frac{D_z^R\alpha}{2i\pi}\int_0^{\theta_2^R}\frac{d\theta}{1-\alpha\theta} \tag{3.13a}$$

or

$$R_{U_z}^{*} = -\frac{D_z^R}{2i\pi}\ln(1-\alpha\theta_2^R) \tag{3.13b}$$

The complex variable θ_i^R is defined by the equation

$$\theta_i^R = \frac{t'(x - x_o^R) + iy\sqrt{t'^2 - c_i^{-2}\,(y^2 + (x - x_o^R)^2)}}{y^2 + (x - x_o^R)^2} \qquad (3.14)$$

where, x_o^R denotes the x-coordinate of the point at which cracking started initially (see Fig. 4), $c_1 = a$, $c_2 = b$, and $t' = t - \frac{|x_o^R|}{\alpha}$.

Except for a minor change in Eq. 3.14, the problem in which faulting spreads in the negative x-axis is determined in a similar manner. The results for both the dip-slip and strike-slip faulting are as follows

i) dip-slip fault:

$$L_{U_x^*} = \frac{D_x^L \alpha b^2}{i\pi}\left[\int_0^{\theta_1^L} \frac{\theta^2}{1 + \alpha\theta}\, d\theta + \int_0^{\theta_2^L} \frac{b^{-2} - 2\theta^2}{2(1 + \alpha\theta)}\, d\theta\right] \qquad (3.15a)$$

$$L_{U_y^*} = \frac{D_x^L \alpha b^2}{i\pi}\left[\int_0^{\theta_1^L} \frac{\theta\sqrt{a^{-2} - \theta^2}}{1 + \alpha\theta}\, d\theta - \int_0^{\theta_2^L} \frac{\theta(b^{-2} - 2\theta^2)}{2(1 + \alpha\theta)\sqrt{b^{-2} - \theta^2}}\, d\theta\right]$$

or,

$$L_{U_x^*} = -\frac{D_x^L b^2}{i\pi\alpha^2}\left[\frac{1}{2}(1 + \alpha\theta_1^L)^2 - \frac{1}{2}(1 + \alpha\theta_2^L) + 2\alpha(\theta_2^L - \theta_1^L)\right.$$

$$\left. + \frac{1}{2}\alpha^2 b^{-2} \ln(1 + \alpha\theta_2^L) + \ln\left(\frac{1 + \alpha\theta_1^L}{1 + \alpha\theta_2^L}\right)\right]$$

$$L_{U_y}^{*} = \frac{D_x^L b^2}{i\pi\alpha^2} \left[\left(1 - \frac{1}{2} a^{-2}\alpha^2\right) \sin^{-1}\left(a\theta_1^L\right) \right.$$

$$- \sin^{-1}\left(b\theta_2^L\right) - \sqrt{1 - \alpha^2 a^{-2}} \sin^{-1}\left(\frac{\alpha a^{-1} + a\theta_1^L}{1 + \alpha\theta_1^L}\right)$$

$$+ \frac{2 - \alpha^2 b^{-2}}{2\sqrt{1 - \alpha^2 b^{-2}}} \sin^{-1}\left(\frac{\alpha b^{-1} + b\theta_2^L}{1 + \alpha\theta_2^L}\right) + \sqrt{1 - \alpha^2 a^{-2}} \sin^{-1}\left(\alpha a^{-1}\right)$$

$$- \frac{2 - \alpha^2 b^{-2}}{2\sqrt{1 - \alpha^2 b^{-2}}} \sin^{-1}\left(\alpha b^{-1}\right) - \frac{1}{2}\alpha^2 \left(\theta_1^L \sqrt{a^{-2} - \theta_1^{L^2}}\right.$$

$$\left. - \theta_2^L \sqrt{b^{-2} - \theta_2^{L^2}}\right) + \alpha\left(\sqrt{a^{-2} - \theta_1^{L^2}} - \sqrt{b^{-2} - \theta_2^{L^2}}\right)$$

$$\left. - \alpha a^{-1} + \alpha b^{-1}\right] \qquad (3.15b)$$

ii) strike-slip fault:

$$L_{U_z}^{*} = \frac{D_z \alpha}{2i\pi} \int_0^{\theta_2^L} \frac{d\theta}{1 + \alpha\theta} \qquad (3.16a)$$

or

$$L_{U_z}^{*} = \frac{D_z}{2i\pi} \ln\left(1 + \alpha\theta_2^L\right) \qquad (3.16b)$$

where,

$$\theta_i^L = \frac{t'(x + x_o^L) + iy\sqrt{t'^2 - c_i^{-2}(y^2 + (x + x_o^L)^2)}}{y^2 + (x + x_o^L)^2} \qquad (3.17)$$

The parameter x_o^L is shown in Fig. 4; and $t' = t - \frac{|x_o^L|}{\alpha}$.

It will be shown in the subsequent section that superposition of the responses of different dislocation problems obtained in Secs. 3.2 and 3.3, determines displacements corresponding to a single dislocation pulse.

3.4 The Mechanics of Intermittent Faulting

The analyses described in the proceeding sections are based upon the assumption that the fault-slip dependence on time is a Heaviside step function so that, nonuniform frictional effects and jerky stick-type motion are neglected. Also, it was assumed that the dislocation front propagates with constant velocity in either one or two directions.

However, it is generally agreed [37] that a reasonably large portion of a fault plane, centered roughly about the epicenter, fails first. This triggers other portions of the fault plane at the ends of the initial failure. The sequential cracking continues until, finally, the entire or the large portion of the fault which generates the earthquake has failed.

One way to simulate this phenomenon is to discretize the fault plane into elementary segments along the fault depth [38]. These segments which are usually referred to as primary slips are shown in Fig. 5. The distribution of these elementary sources in time and space domain can be found from a simple stochastic model. The parameters which describe the model, and are closely associated with the aftershock events, require thorough investigation and could be the subject of future research.

The process of simulation of the strong ground motion necessitates solutions for the seismic sources in which the dislocation fronts stop at certain points. This can be accomplished by a suitable superposition of the results obtained in Secs. 3.2 and 3.3. A bilateral fault with initial slip in a given direction is the first source of motion. Upon this are superposed, at a later time, two separate unilateral faults of the same type but with initial slips in the opposite direction. Figure 6 shows schematically the superposition of the fault sources described earlier. For a single dislocation pulse with finite depth which is located in an infinite elastic medium, the displacement fields are defined by the equations

$$\begin{aligned} {}^{e}U_x^* &= U_x^* - {}^{R}U_x^* - {}^{L}U_x^* \\ {}^{e}U_y^* &= U_y^* - {}^{R}U_y^* - {}^{L}U_y^* \end{aligned} \tag{3.18a}$$

and

$${}^{e}U_z^* = U_z^* - {}^{R}U_z^* - {}^{L}U_z^* \tag{3.18b}$$

The superscript "e" denotes motion corresponding to an elementary dislocation pulse. Substitution for the quantities on the right-hand side from Eqs. 3.7a, 3.12a and 3.15b, yields the response of a primary slip at a given point. The complete time history of displacements is obtained when the responses of a sequence of elementary sources are properly combined in time domain.

The advantage of the method of self similar potentials over the existing standard procedures can be judged in the ease of choosing the

proper fundamental problem for analysis and carrying the analysis to the point of numerical calculations.

3.5 Variation of the Residual Deformations with Distance from the Fault

The investigation of the earthquake source mechanism often requires that the depth and dimensions of the seismic source be inferred from measurements of the residual displacements at various distances from the fault plane. The appropriate mechanism for each earthquake is then selected by comparing the geodetic observations that have been made around the fault with those predicted from the solution of the dislocation models. Chinnery [5], among others, studied static changes that accompany faulting within the earth and developed a mathematical model based upon the dislocation theory. Results of the study were successfully compared with those actually recorded along the San Andreas fault. Since the fault is very long (nearly 300 kms) and quite shallow (estimated depth of 6 kms), it is reasonable to compare the observed displacements with the predictions for a fault of infinite length.

The permanent deformation associated with a particular dislocation pulse can be evaluated from Eqs. 3.18 when t approaches infinity. After somewhat lengthy calculations and tedious mathematical manipulations, the following expressions can be verified.

$$e_{U_x}(x,y,t=\infty) = \frac{D_x b^2}{2\pi} \{b^{-2} [\tan^{-1} (\frac{x_o - x}{y}) + \tan^{-1} (\frac{x_o + x}{y})]$$

$$- y(b^{-2} - a^{-2})[\frac{x + x_o}{y^2 + (x + x_o)^2} - \frac{x - x_o}{y^2 + (x - x_o)^2}]\}$$

$$e_{U_y}(x,y,t=\infty) = 0 \tag{3.19}$$

$$e_{U_z}(x,y,t=\infty) = \frac{D_z}{2\pi}\left\{\tan^{-1}\left(\frac{x_o - x}{y}\right) + \tan^{-1}\left(\frac{x_o + x}{y}\right)\right\}$$

where, $D_x = D_x^R = D_x^L$, $D_z = D_z^R = D_z^L$, $x_o = |x_o^R| = |x_o^L|$, $e_{U_x} = \mathrm{Re}\ e_{U_x}^*$, and so forth.

It is seen from Eqs. 3.19 that the speed with which cracking propagates has no influence on the residual displacement. It depends only upon the fault width x_o, the x and y coordinates of the point under consideration, and the elastic property of the material ($\frac{a^2}{b^2} = \frac{\mu}{\lambda + 2\mu}$). Equations 3.19 can be further simplified by considering points which are located on the y-axis (x = 0). The results are as follows

$$e_{U_x}(0,y,t=\infty) = \frac{D_x b^2}{\pi}\left\{b^{-2}\tan^{-1}\left(\frac{x_o}{y}\right) - (b^{-2} - a^{-2})\frac{x_o y}{x^2 + y^2}\right\}$$

$$e_{U_y}(0,y,t=\infty) = 0 \tag{3.20}$$

$$e_{U_z}(0,y,t=\infty) = \frac{D_z}{\pi}\tan^{-1}\left(\frac{x_o}{y}\right)$$

In the limit when $y \to 0^+$, Eqs. 3.20 reduce to

$$e_{U_x}(0,0^+,t=\infty) = \frac{D_x}{2}$$

$$e_{U_y}(0,0^+,t=\infty) = 0 \tag{3.21}$$

and

$$^{e}U_z(0,0^+,t=\infty) = \frac{D_z}{2}$$

which are the prescribed displacement discontinuities on the fault plane.

The variation of the residual deformations with distance from the fault surface is illustrated in Fig. 7. It is observed that both components of the displacements decrease rapidly (like $\frac{1}{y}$) at intermediate distances, and vanish at points far from the source (large y).

3.6 The Point Dislocation

Consider a displacement dislocation model in which a sudden fracture occurs over an infinitisimal area of the fault plane at time t = 0 and remains constant thereafter. This simply implies that the area over which the faulting takes place has been shrunk in the limit to the origin. Depending on the direction of the relative movement on the fault surface, the waves generated by this elementary source can be either P-SV wave (plane problem), or SH-wave (antiplane problem). Only the waves of the first type will be considered here. The analysis of the SH-wave does not introduce any difficulty.

The self-similar potentials which solve the plane problem can be obtained directly from Eq. 3.6 by replacing $(2D_x\alpha)$ by Δ_x, the amplitude of the point dislocation, and letting $\alpha \to 0$. This simply means that the "intensity" of the dislocation is held constant as the speed of cracking approaches zero. Therefore, the source of elastic waves is a point dislocation. It follows that

$$\Phi' = -\frac{\Delta_x b^2}{i\pi}\,\theta_1 \quad ; \qquad \Psi' = -\frac{\Delta_x b^2}{2i\pi}\,\frac{b^{-2} - 2\theta_2^2}{\sqrt{b^{-2} - \theta_2^2}} \tag{3.22}$$

Substituting for Φ' and Ψ' in Eqs. 2.13a, the response of a point dislocation is found to be

$$u_x^* = -\frac{\Delta_x b^2}{i\pi}\left[\frac{\theta_1^2}{\delta_1'} + \frac{b^{-2} - 2\theta_2^2}{2\delta_2'}\right]$$

$$u_y^* = -\frac{\Delta_x b^2}{i\pi}\left[\frac{\theta_1\sqrt{a^{-2} - \theta_1^2}}{\delta_1'} - \frac{\theta_2(b^{-2} - 2\theta_2^2)}{2\delta_2'\sqrt{b^{-2} - \theta_2^2}}\right] \tag{3.23}$$

where, δ_i' is defined by Eq. 2.12b.

Comparison of the results with Eqs. C.3 of Appendix C and the observation that* $M = \mu\Delta_x$ [39] reveals that the response of a nonpropagating fault is identical with that of a suddenly applied pair of double forces with opposite moments. The static displacements are found by substituting for θ_i and δ_i' in Eqs. 3.23 in terms of x, y, and t and letting t approach to infinity. It can be easily verified that

$$u_x(x,y,t=\infty) = -\frac{\Delta_x b^2}{\pi}\left\{\frac{x^2 y}{r^4}(b^{-2} - a^{-2}) + \frac{ya^{-2}}{2r^2}\right\}$$

$$u_y(x,y,t=\infty) = -\frac{\Delta_x b^2}{\pi}\left\{\frac{xy^2}{r^4}(b^{-2} - a^{-2}) + \frac{xa^{-2}}{2r^2}\right\} \tag{3.24}$$

where, $r^2 = x^2 + y^2$ and (u_x, u_y) are the real parts of the complex displacements u_x^* and u_y^*.

---

*M is the moment of two concentrated forces acting at a point on the fault plane.

Expressions similar to those represented by Eqs. 3.24 and in a slightly different form have been derived by Love [40]. This indicates that an impulsive dislocation source can be replaced by a suitable system of point forces such that the response at any point remains unchanged.

4. EFFECT OF THE FREE SURFACE ON THE RADIATION PATTERN

4.1 General Remarks

The previous analysis of the elastic waves radiating from a seismic source was based upon the assumption that the elastic medium extends to infinity in all directions, so that the displacement fields were uninfluenced by the presence of any plane boundary. This chapter is devoted to the calculation of the seismic motions on the surface of an elastic half space when a uniformly propagating shear fault, with an arbitrary dip, experiences a sudden discontinuity in displacement on the fault plane. The relative movement of the opposite sides of the fault is also arbitrarily oriented; that is, both dip-slip and strike-slip motions will be considered.

To take the effect of the free surface into account, two different approaches have been adopted by seismologists. One method [41] is to replace the fault plane by a finite number of elementary point dislocations the responses of which are equivalent to that of the multipoles of forces. The seismic waves radiating from each individual source are resolved into P, SV, and SH components along each ray path and then multiplied by the reflection coefficient at the surface appropriate to these components. This method requires lengthy numerical integrations over the fault surface. The second approach is to simply double the computed displacements, as suggested by Haskell [10] and practically used by AKi [13] and Kanamori [42]. This correction, although appropriate for the SH-wave component, is not justifiable for the waves of SV and P types. In particular, the Rayleigh wave will be missed altogether.

The phenomena which arise at a free surface due to incident disturbances are often of a totally different character from the incident disturbance. The interaction of P and SV disturbances to form surface waves and the development of a head wave are the most obvious of such differences. The method to be used in this study permits ready identification of these effects and does so with a minimum of calculation.

In what follows, the amplitude of dislocation is considered as a step function in time, which permits a simple extension to any time or space variation of the amplitude. Illustrative examples will be provided at the end of this chapter.

4.2 Reflection of the Seismic Waves from the Free Surface

When a disturbance generated by a seismic source within an elastic half space reaches the free surface, certain conditions must be satisfied which results in the creation of the reflected potentials. Prior to the arrival of the incident waves, the motions of the body are not affected by the presence of the free surface and, therefore, displacements at any interior point are determined entirely by the incident potentials. The solution for this problem, with the emphasis on the method of analysis, was found in Chapter 3. This section deals with the case in which reflection occurs at the boundary and, therefore, both incident as well as reflected potentials contribute to the motion at a given point.

The phenomenon of reflection in the study of the seismic waves requires solutions for the three uncoupled two-dimensional problems as described below:

1. The reflected SH wave due to an incident SH wave;
2. The reflected P and SV waves due to an incident SV wave;
3. The reflected P and SV waves due to an incident P wave.

The incident SH wave radiates from a strike-slip shear fault, whereas P and SV disturbances result from a dip-slip faulting mechanism.

Before proceeding with the analysis of the reflected potentials, it should be emphasized that the complete solution for a dislocation source in an elastic half space requires satisfying certain conditions on the following non-parallel plane boundaries:

1. The fault plane on which a displacement discontinuity is prescribed and normal stress is set to zero; and
2. The actual free surface on which normal and tangential tractions are set to zero.

The complex variable $\theta_i(x/t, y/t)$, which is defined implicitly by the equation

$$t - \theta_i x - y\sqrt{c_i^{-2} - \theta_i^2} = 0 \qquad (4.1)$$

maps the fault plane (the surface $y = 0$) into the real axis in the complex θ_i-plane. Moreover, it is apparent from Eq. 4.1 that θ_i's retain equal values on the $y = 0$ surface, i.e.,

$$\theta_1 = \theta_2 = t/x \qquad \text{for } y = 0 \qquad (4.2)$$

These conditions which are essential in the determination of the incident self-similar potentials, cannot be maintained for planes other than the $y = 0$ surface. The mapping described above transforms points on different planes

in the (x,y,t) space into curves in complex θ_i-plane which do not necessarily coincide with the real θ-axis and, consequently, the θ_i's will no longer be equal.

It is implicit in the Smirnov-Sobolev technique that all the potentials for solving a reflection problem must have identical values at any point of the reflecting boundary. Indeed, it is convenient to treat reflections of the incident P and SV waves separately even though they come from the same source. This observation suggests that a new complex variable, say, η_i be introduced such that (1) it retains equal values for both direct and reflected waves on the free surface, just as θ_i on the fault plane, and (2) there exists a one-to-one correspondence between θ_i and η_i which permits obtaining one from the other by a simple transformation. The incident potentials Φ' and Ψ' which are developed as a result of satisfying certain conditions on the fault plane and are expressed in terms of θ_i, can be easily transformed into the η_i-plane. The problem is then virtually reduced to the one with a single plane boundary, namely, the surface of the half space. The stress and displacement fields can be obtained in the complex η_i domain, utilizing the method of self similar potentials.

In the subsequent section, the transformation just described will be developed in detail and the mapping of the (x,y,t) space into the complex η_i-plane will be illustrated.

4.3 An Auxiliary Complex Domain (η_i-plane)

Consider a shear fault with an arbitrary dip confined to an elastic, homogeneous half space shown in Fig. 8. A coordinate system (x,y) is attached

to the fault plane such that its origin coincides with the point of crack initiation and the fault surface is represented by the y = 0 plane. Define a new set of coordinates (x_1,y_1) having the same origin as the previous ones, ox and oy, and forming an angle γ with the y-axis (oy_1 is parallel to the surface of the half space). The two sets of coordinates are related by

$$\begin{aligned} x &= - x_1 \sin\gamma + y_1 \cos\gamma \\ y &= - x_1 \cos\gamma - y_1 \sin\gamma \end{aligned} \tag{4.3}$$

Substituting for x and y in Eq. 4.1, the equation of the characteristic plane in the (x_1,y_1,t) space becomes

$$t - x_1(-\theta_i \sin\gamma - \sqrt{c_i^{-2} - \theta_i^2} \cos\gamma) - y_1(\theta_i \cos\gamma - \sqrt{c_i^{-2} - \theta_i^2} \sin\gamma) = 0 \tag{4.4}$$

It is convenient to set

$$\theta_i = + c_i^{-1} \cos\beta \quad \text{and} \quad \sqrt{c_i^{-2} - \theta_i^2} = - c_i^{-1} \sin\beta \tag{4.5}$$

so that Eq. 4.4 can be rewritten in a more convenient form as

$$t - x_1[c_i^{-1} \sin(\beta - \gamma)] - y_1[c_i^{-1} \cos(\beta - \gamma)] = 0 \tag{4.6}$$

where, β is the complex variable defined by Eq. 4.5. Further simplification is made by letting

$$\cos(\beta - \gamma) = c_i \eta_i$$

and (4.7)

$$\sin(\beta - \gamma) = c_i \sqrt{c_i^{-2} - \eta_i^2}$$

where, η_i is a new complex variable which parametrizes the characteristic planes in the (x_1, y_1, t) space. Substituting for $\cos(\beta - \gamma)$ and $\sin(\beta - \gamma)$ into Eq. 4.6, the equation of the characteristic surfaces which are tangent to the wave front becomes:

$$t - x_1 \sqrt{c_i^{-2} - \eta_i^2} - y_1 \eta_i = 0 \tag{4.8}$$

Equations 4.7 can be solved for $\cos\beta$ and $\sin\beta$. Direct substitution of the results into Eqs. 4.5 leads to the following relations between θ_i and η_i:

$$\theta_i = \eta_i \cos\gamma - \sqrt{c_i^{-2} - \eta_i^2} \sin\gamma$$

$$\sqrt{c_i^{-2} - \theta_i^2} = -(\eta_i \sin\gamma + \sqrt{c_i^{-2} - \eta_i^2} \cos\gamma) \tag{4.9}$$

If a cut is made between $-c_i^{-1}$ and c_i^{+1} in each η_i plane in order that the radical $\sqrt{c_i^{-2} - \eta_i^2}$ be single-valued at every point,* its counterpart in the θ_i-plane, $\sqrt{c_i^{-2} - \theta_i^2}$, becomes automatically single-valued (in accordance with the transformation (4.9)). Equation 4.8 when solved for η_i, yields

$$\eta_i = \frac{t y_1 \pm i x_1 \sqrt{t^2 - \dfrac{x_1^2 + y_1^2}{c_i^{-2}}}}{x_1^2 + y_1^2} \tag{4.10}$$

*The radical $\sqrt{c_i^{-2} - \eta_i^2}$ is defined to be negative for η_i positive and imaginary, with a cut on the real η axis from $-c_i^{-1}$ to $+c_i^{-1}$.

Because of the previous definition of θ_i and the correspondence between θ_i and η_i, and considering the fact that θ_i is a single-valued complex variable, only the negative sign in Eq. 4.10 is acceptable, i.e.,

$$\eta_i = \frac{ty_1 - ix_1\sqrt{t^2 - \frac{x_1^2 + y_1^2}{c_i^{-2}}}}{x_1^2 + y_1^2} \tag{4.11}$$

It will become apparent in the subsequent analysis that the η_i's are identical on any x_1 = constant plane specifically on the surface of the half space. This is the condition which makes it possible to calculate the displacement fields and stresses in an elastic half-space and in layered solids. All calculations in the remaining sections will be performed in the complex η_i domain, instead of the θ_i-plane. Also the components of the displacements will be expressed in the (X,Y) coordinate system (see Fig. 8).

The reflection of the incident P and SV wave on the surface of the body and the resulting motions will be treated in the following two sections.

4.4 Incident P Wave

Generally, a P wave incident on a free surface generates both dilatational and distortional disturbances. The geophysical designation of these reflected phases are PP and PS, respectively. For instance, PS corresponds to a wave which is of P type before the reflection and of S type afterwards. Although the reflection problem is not strictly self-similar, Smirnov-Sobolev potentials still lead to the proper solution [43].

4.4.1 Method of Analysis

The solution for the present problem is found in terms of the incident potential ϕ_1 and reflected potentials ϕ_{11} and ψ_{12} where

$$\phi_1 = \text{Re}\ \Phi_1(\eta_i) \tag{4.12a}$$

and

$$\phi_{11} = \text{Re}\ \Phi_{11}(\eta_{11}) \tag{4.12b}$$

$$\psi_{12} = \text{Re}\ \Psi_{12}(\eta_{12})$$

The complex variables η_1, η_{11}, and η_{12} are defined implicitly as

$$\delta_1 = t - (X - X_o)\sqrt{a^{-2} - \eta_1^2} - Y\eta_1 = 0$$

$$\delta_{11} = t + (X + X_o)\sqrt{a^{-2} - \eta_{11}^2} - Y\eta_{11} = 0 \tag{4.13}$$

$$\delta_{12} = t + X\sqrt{b^{-2} - \eta_{12}^2} + X_o\sqrt{a^{-2} - \eta_{12}^2} - Y\eta_{12} = 0$$

where X_o is the x-coordinate of the point of crack initiation shown in Fig. 8.

The first and second of Eqs. 4.13 when solved for η_1 and η_{11} yield

---

*The subscripts "12" and "21" used by Johnson and Robinson [30] have been interchanged in this study to provide direct correspondence with the geophysical terms PS and SP, respectively.

$$\eta_1 = \frac{tY - i(X - X_o)\sqrt{t^2 - \dfrac{y^2 + (X - X_o)^2}{a^2}}}{Y^2 + (X - X_o)^2} \qquad (4.14)$$

$$Y^2 + (X - X_o)^2 \leq a^2 t^2$$

and

$$\eta_{11} = \frac{tY + i(X + X_o)\sqrt{t^2 - \dfrac{Y^2 + (X + X_o)^2}{a^2}}}{Y^2 + (X + X_o)^2} \qquad (4.15)$$

$$Y^2 + (X + X_o)^2 \leq a^2 t^2$$

Further investigation of the Eqs. 4.13 reveals that:

1. The complex variables η_1, η_{11}, and η_{12} are identical on the X = 0 surface.
2. η_1 and η_{11} parametrize the characteristic surfaces through the point $(X_o,0)$ and its image $(-X_o,0)$, respectively.

The form of η_{12} defined by the last equation of 4.13 is developed by seeking a common value for the η's on the X = 0 surface. It is apparent that η_{12} represents a disturbance which travels into the medium at speed b, the distortional wave speed.

Figure 9 shows typical wave fronts for the P, PP, and PS waves. In the case of P and PP waves, the fronts are circular cylinders with their centers at $X = X_o$ and $X = -X_o$, respectively. The front of PS wave is also a cylinder, however, to find its coordinates the following two non-linear, simultaneous equations must be solved [44]:

$$\delta_{12} = t + X\sqrt{b^{-2} - \eta_{12}^2} + X_o\sqrt{a^{-2} - \eta_{12}^2} - Y\eta_{12} = 0$$

$$\delta'_{12} = -\frac{X\eta_{12}}{\sqrt{b^{-2} - \eta_{12}^2}} - \frac{X_o\eta_{12}}{\sqrt{a^{-2} - \eta_{12}^2}} - Y = 0 \qquad (4.16)$$

where

$$\delta'_{12} = \frac{\partial\delta_{12}}{\partial\eta_{12}}$$

A numerical technique used to solve Eqs. 4.16 has been discussed in Ref. [30].

Equations 4.13 define the mapping of the (X,Y,t) space into the complex η_1, η_{11}, and η_{12} planes. All points on the surface of the half-space are mapped into the points on the curve c_o in the complex planes. The regions of interest and the mapping of several typical points are illustrated in Figs. 10, 11 and 12.

4.4.2 Determination of the Stresses and Displacement Fields

The stresses and displacements at any point in the half-space are found in a manner precisely similar to that of Sec. 3.2.1. Since the arrival of incident P wave at the free surface gives rise to the reflection of PP and PS potentials, the motion at any point is described by the superposition of three different fields, namely, incident potential Φ'_1 and reflected potentials Φ'_{11} and Ψ'_{12}. Taking into account appropriate changes in the δ_i's and their derivatives, the following expressions can be easily verified*

---

*The superscript "P" is used to designate the P-wave component of the displacements.

$$U_X^P = \mathrm{Re}\ \{ - \int_0^{\eta_1} \Phi_1'(\eta)\sqrt{a^{-2} - \eta^2}\, d\eta + \int_0^{\eta_{11}} \Phi_{11}'(\eta)\sqrt{a^{-2} - \eta^2}\, d\eta$$

$$- \int_0^{\eta_{12}} \eta\Psi_{12}'(\eta)\, d\eta \ \} \qquad (4.17a)$$

$$U_Y^P = \mathrm{Re}\ \{ - \int_0^{\eta_1} \eta\Phi_1'(\eta)\, d\eta - \int_0^{\eta_{11}} \eta\Phi_{11}'(\eta)\, d\eta$$

$$- \int_0^{\eta_{12}} \sqrt{b^{-2} - \eta^2}\ \Psi_{12}'(\eta)\, d\eta \ \}$$

and

$$\frac{\sum_x^P}{\mu} = \mathrm{Re}\ \{\frac{\partial}{\partial t}\ [\int_0^{\eta_1} (b^{-2} - 2\eta^2)\ \Phi_1'(\eta)\, d\eta + \int_0^{\eta_{11}} (b^{-2} - 2\eta^2)\Phi_{11}'(\eta)d\eta$$

$$- \int_0^{\eta_{12}} 2\eta\sqrt{b^{-2} - \eta^2}\ \Psi_{12}'(\eta)\, d\eta] \ \}$$

$$\frac{\sum_y^P}{\mu} = \mathrm{Re}\ \{\frac{\partial}{\partial t}\ [\int_0^{\eta_1} (b^{-2} - 2a^{-2} + 2\eta^2)\ \Phi_1'(\eta)\, d\eta$$

$$+ \int_0^{\eta_{11}} (b^{-2} - 2a^{-2} + 2\eta^2)\Phi_{11}'(\eta)d\eta + \int_0^{\eta_{12}} 2\eta\sqrt{b^{-2} - \eta^2}\ \Psi_{12}'(\eta)d\eta]\}$$

$$\frac{T^{P}_{XY}}{\mu} = \mathrm{Re}\left\{\frac{\partial}{\partial t}\left[\int_{0}^{\eta_1} 2\eta\sqrt{a^{-2}-\eta^2}\,\Phi_1'(\eta)d\eta - \int_{0}^{\eta_{11}} 2\eta\sqrt{a^{-2}-\eta^2}\,\Phi_{11}'(\eta)d\eta\right.\right.$$

$$\left.\left. + \int_{0}^{\eta_{12}} (2\eta^2 - b^{-2})\,\Psi_{12}'(\eta)d\eta\right]\right\} \qquad (4.17b)$$

On the surface of the half space (the X = 0 plane) the upper limits of the integrals have a common value η_o. That is,

$$\eta_1 = \eta_{11} = \eta_{12} = \eta_o \qquad \text{for } X = 0$$

The first and third equations of 4.17b when set equal to zero (the normal and tangential tractions are zero on the free surface), yield two simultaneous equations which can be solved for the derivatives of the reflected potentials, Φ_1' and Ψ_{12}'. The results are:

$$\Phi_{11}' = -\frac{(b^{-2} - 2\eta_o^2)^2 - 4\eta_o^2\sqrt{a^{-2}-\eta_o^2}\,\sqrt{b^{-2}-\eta_o^2}}{R(\eta_o^2)}\,\Phi_1'(\upsilon_o)$$

$$\Psi_{12}' = \frac{4\eta_o(b^{-2} - 2\eta_o^2)\sqrt{a^{-2}-\eta_o^2}}{R(\eta_o^2)}\,\Phi_1'(\eta_o) \qquad (4.18)$$

where, $R(\eta_o^2)$ is the Rayleigh function defined by

$$R(\eta_o^2) = (b^{-2} - 2\eta_o^2)^2 + 4\eta_o^2\sqrt{a^{-2}-\eta_o^2}\,\sqrt{b^{-2}-\eta_o^2} \qquad (4.19)$$

The values of Φ_{11}' and Ψ_{12}' are uniquely determined in the region of

interest in the complex η-plane when their values are specified along the curve c_o which is the image of the free surface in the complex η plane. This is accomplished by replacing η_o in Eqs. 4.18 with η_{11} and η_{12}, respectively. It follows that

$$\Phi_{11}'(\eta_{11}) = -\frac{(b^{-2} - 2\eta_{11}^2)^2 - 4\eta_{11}^2\sqrt{a^{-2} - \eta_{11}^2}\ \sqrt{b^{-2} - \eta_{11}^2}}{R(\eta_{11}^2)}\ \Phi_1'(\eta_{11})$$

$$\Psi_{12}'(\eta_{12}) = \frac{4\eta_{12}(b^{-2} - 2\eta_{12}^2)\sqrt{a^{-2} - \eta_{12}^2}}{R(\eta_{12}^2)}\ \Phi_1'(\eta_{12}) \tag{4.19}$$

The primary object of this study is the investigation of the displacement fields on the surface of the medium on which all η's retain equal values. This significant feature of the complex variables (η's) results in a considerable simplification of the analysis. Equations 4.17a are rewritten in a more condensed form as shown below

$$U_X^P = \mathrm{Re}\int_0^{\eta_o} \frac{-2b^{-2}(b^{-2} - 2\eta^2)\sqrt{a^{-2} - \eta^2}}{R(\eta^2)}\ \Phi_1'(\eta)d\eta$$

$$U_Y^P = \mathrm{Re}\int_0^{\eta_o} \frac{-4b^{-2}\eta\sqrt{a^{-2} - \eta^2}\ \sqrt{b^{-2} - \eta^2}}{R(\eta^2)}\ \Phi_1'(\eta)d\eta \tag{4.20}$$

where,

$$\eta_o = \frac{tY + iX_o\sqrt{t^2 - \dfrac{X_o^2 + Y^2}{a^2}}}{X_o^2 + Y^2} \tag{4.21}$$

and η is the dummy variable of the integration.

The numerical scheme used in the calculation of the integrals in Eqs. 4.20 will be explained later. For a shear fault propagating with constant velocity in both directions, $\Phi_1'(\theta)$ is defined by the first of Eqs. 3.5. Given any point in the complex η domain, one can find the corresponding θ value from the first of Eqs. 4.9. Direct substitution of θ into Eqs. 3.5 gives the proper value of $\Phi_1'(\eta)$. Thus, the integrands of Eqs. 4.20 can be evaluated at any point along the path of the integration. The curve along which integrations are performed in described in Sec. 4.8.1.

Notice that θ_i and η_i are both single-valued variables and, therefore, Φ_1' is uniquely defined in both complex regions.

4.5 Incident SV Wave

When an incident SV wave reaches a free surface, both dilatational and distortional disturbances are generated, as was the case with the incident P-wave. The major difference in the two instances is that the incident SV-wave is usually associated with the creation of head waves and surface components of the reflected P wave. The geophysical notations, SP and SS, are used to distinguish the reflected irrotational and equivoluminal potentials, respectively.

4.5.1 Method of Analysis

The solution is sought in terms of the reflected potentials ϕ_{21} and ψ_{22} where

$$\phi_{21} = \text{Re}\ \Phi_{21}(\eta_{21})$$

$$\psi_{22} = \text{Re}\ \Psi_{22}(\eta_{22}) \tag{4.21}$$

The equations of the characteristic planes in the (X,Y,t) space for the incident and reflected potentials are defined as follows

$$\delta_2 = t - (X - X_o)\sqrt{b^{-2} - \eta_2^2} - Y\eta_2 = 0$$

$$\delta_{21} = t + X\sqrt{a^{-2} - \eta_{21}^2} + X_o\sqrt{b^{-2} - \eta_{21}^2} - Y\eta_{21} = 0$$

$$\delta_{22} = t + (X + X_o)\sqrt{b^{-2} - \eta_{22}^2} - Y\eta_{22} = 0 \tag{4.22}$$

An implicit expression for η_2 and η_{22} can be found by solving the first and third of Eqs. 4.22 for η_2 and η_{22}. It follows that

$$\eta_2 = \frac{tY - i(X - X_o)\sqrt{t^2 - \dfrac{Y^2 + (X - X_o)^2}{b^2}}}{Y^2 + (X - X_o)^2} \tag{4.23}$$

$$Y^2 + (X - X_o)^2 \leq b^2 t^2$$

and

$$\eta_{22} = \frac{tY + i(X + X_o)\sqrt{t^2 - \dfrac{Y^2 + (X + X_o)^2}{b^2}}}{Y^2 + (X + X_o)^2} \tag{4.24}$$

$$Y^2 + (X + X_o)^2 \leq b^2 t^2$$

It can be observed that

1. The complex variables η_2, η_{21}, and η_{22} are identical on the $X = 0$ surface.
2. η_2 and η_{22} parametrize the characteristic planes through the points $(+X_0,0)$ and $(-X_0,0)$, respectively.

The equation of the characteristic plane for the reflected SP wave is developed such that the η's for both incident and reflected potentials have a common value on the $X = 0$ surface.

The angle of incidence of the S-wave with the free surface, f, is of great importance in the study of the wave fronts of the reflected SP and SS potentials. For f less than $\cos^{-1}(b/a)$, head wave will be formed and the reflected SP wave will become a surface phenomenon [45], propagating in the horizontal direction. The case in which f is greater than $\cos^{-1}(b/a)$ is different from the previous one in that no head wave will be formed and the effects of the S, SS, and SP waves on the surface of the half-space are as in Sec. 4.4.2. The forms of the wave fronts in the two cases are depicted in Figs. 13 and 14.

The mapping of the (X,Y,t) space into the complex η_2, η_{21} and η_{22} planes is given by Eqs. 4.22. Prior to the arrival of the S wave at the surface, η_{21} and η_{22} are not considered and only the η_2 plane is considered. After reflection, all complex planes will be considered. The two cases discussed above possess important characteristics in the complex domain. Assuming that $\bar{\eta}$ corresponds to the intersection of the S-wave front with the free surface, and noting that $\bar{\eta}$ is a real quantity, the following inequalities can be easily verified.

$$|\tilde{\eta}| < a^{-1} \qquad \text{for} \qquad f > \cos^{-1}(b/a)$$

$$|\tilde{\eta}| > a^{-1} \qquad \text{for} \qquad f < \cos^{-1}(b/a)$$

$$|\tilde{\eta}| = a^{-1} \qquad \text{for} \qquad f = \cos^{-1}(b/a)$$

Figures 15 through 20 show the wave fronts and their counterparts on the complex η-plane in both cases ($f \lesseqgtr \cos^{-1}(b/a)$). It should be observed that the surface of the half-space is mapped into the curve c_o in the complex plane. This curve limits the region of interest in the η-plane, the region corresponding to the points in the body which have been set into motion by the arrival of the wave fronts.

4.5.2 Determination of the Plane Displacement Fields

The reflected potentials, Φ'_{21} and Ψ'_{22}, are found when the conditions of zero tractions on the free surface (the X = 0 plane) are satisfied. Before applying these conditions, appropriate expressions for the stresses and displacement fields must be developed. It is not difficult to show that

$$U_X^S = \text{Re}\left\{ -\int_0^{\eta_2} \eta\Psi'_2(\eta)d\eta - \int_0^{\eta_{22}} \eta\Psi'_{22}(\eta)d\eta + \int_0^{\eta_{21}} \sqrt{a^{-2} - \eta^2}\ \Phi'_{21}(\eta)d\eta \right\} \tag{4.25}$$

$$U_Y^S = \mathrm{Re}\left\{\int_0^{\eta_2} \sqrt{b^{-2} - \eta^2}\ \Psi_2'(\eta)d\eta - \int_0^{\eta_{22}} \sqrt{b^{-2} - \eta^2}\ \Psi_{22}'(\eta)d\eta \right.$$

$$\left. - \int_0^{\eta_{21}} \eta\Phi_{21}'(\eta)d\eta \right\}$$

and

$$\frac{\sum_X^S}{\mu} = \mathrm{Re}\left\{\frac{\partial}{\partial t}\left[\int_0^{\eta_2} 2\eta\sqrt{b^{-2} - \eta^2}\ \Psi_2'(\eta)d\eta - \int_0^{\eta_{22}} 2\eta\sqrt{b^{-2} - \eta^2}\ \Psi_{22}'(\eta)d\eta \right.\right.$$

$$\left.\left. + \int_0^{\eta_{21}} (b^{-2} - 2\eta^2)\ \Phi_{21}'(\eta)d\eta\right]\right\}$$

$$\frac{\sum_Y^S}{\mu} = \mathrm{Re}\left\{\frac{\partial}{\partial t}\left[-\int_0^{\eta_2} 2\eta\sqrt{b^{-2} - \eta^2}\ \Psi_2'(\eta)d\eta \right.\right. \qquad (4.26)$$

$$\left.\left. + \int_0^{\eta_{22}} 2\eta\sqrt{b^{-2} - \eta^2}\ \Psi_{22}'(\eta)d\eta + \int_0^{\eta_{21}} (b^{-2} - 2a^{-2} + 2\eta^2)\Phi_{21}'(\eta)d\eta\right]\right\}$$

$$\frac{T_{XY}^S}{\mu} = \mathrm{Re}\left\{\frac{\partial}{\partial t}\left[\int_0^{\eta_2} (2\eta^2 - b^{-2})\ \Psi_2'(\eta)d\eta \right.\right.$$

$$\left.\left. + \int_0^{\eta_{22}} (2\eta^2 - b^{-2})\ \Psi_{22}'(\eta)d\eta - \int_0^{\eta_{21}} 2\eta\sqrt{a^{-2} - \eta^2}\ \Phi_{21}'(\eta)d\eta\right]\right\}$$

The superscript "S" designates the stresses and displacements generated from the interaction of incident S-wave with the free surface. Taking into account that $\eta_2 = \eta_{21} = \eta_{22} = \tilde{\eta}$ for $X = 0$, and applying the condition $\Sigma_X^S\Big|_{X=0} = T_{XY}^S\Big|_{X=0} = 0$, we have the general form of the reflected potentials:

$$\Psi_{22}'(\eta_{22}) = -\frac{(b^{-2} - 2\eta^2)^2 - 4\eta^2\sqrt{a^{-2} - \eta^2}\,\sqrt{b^{-2} - \eta^2}}{R(\eta_{22}^2)}\,\Psi_2'(\eta_{22})$$

$$\Phi_{21}'(\eta_{21}) = \frac{-4\eta_{21}(b^{-2} - 2\eta_{21}^2)\sqrt{b^{-2} - \eta_{21}^2}}{R(\eta_{21}^2)}\,\Psi_2'(\eta_{21}) \qquad (4.27)$$

where $R(\eta^2)$ is the Rayleigh function.

Back substitution of Ψ_{22}' and Φ_{21}' into Eqs. 4.25 and 4.26 gives integral expressions for displacements and stresses at every point inside the body in terms of the incident distortional potentials. Specifically, for the points on the free surface which are not influenced by the head wave disturbance, Eqs. 4.25 can be written in a more convenient form as follows.

$$U_X^S = \mathrm{Re}\left\{\int_0^{\tilde{\eta}} \frac{-4b^{-2}\eta\sqrt{a^{-2} - \eta^2}\,\sqrt{b^{-2} - \eta^2}}{R(\eta^2)}\,\Psi_2'(\eta)d\eta\right\}$$

$$U_Y^S = \mathrm{Re}\left\{\int_0^{\tilde{\eta}} \frac{2b^{-2}(b^{-2} - 2\eta^2)\sqrt{b^{-2} - \eta^2}}{R(\eta^2)}\,\Psi_2'(\eta)d\eta\right\} \qquad (4.28)$$

where,

$$\tilde{\eta} = \frac{tY + iX_o\sqrt{t^2 - \frac{X_o^2 + Y^2}{b^2}}}{X_o^2 + Y^2} \tag{4.29}$$

and η is the dummy variable of integration. For a shear fault propagating with constant velocity in both directions, $\Psi_2'(\eta)$ is obtained from the second of Eqs. 3.5 together with Eqs. 4.9. As before, the integration is carried out numerically in the complex η-plane.

If a head wave passes through the point being considered, it will do so before the arrival of the incident S wave front. As a result, the incident S wave component will not contribute to the displacements. The surface motion is, then, described by the last two terms (corresponding to the SS and SP wave) of Eqs. 4.25. Due to the singularities in the derivatives of the integrands at $\eta = a^{-1}$, standard procedures of numerical integration are not applicable, and the computation of the surface motions requires a special integration scheme which will be used in the subsequent sections. After the incident distortional disturbance has reached the point of interest, all components of the reflected and incident waves will be present and Eqs. 4.28 define the displacement fields.

Figures 21 and 22 illustrate the response of an inclined dip-slip dislocation pulse at two sites A and B, respectively. The fronts of the incident S-wave and reflected SS and SP-wave arrive simultaneously at point A and, therefore, the motion is not affected by the formation of head wave. For site B which is located relatively far from the fault plane the reflected SP-wave becomes a surface phenomenon and the wave front reaches the observation point prior to the arrival of the incident S-wave.

4.6 Incident SH Wave

The SH wave component of the surface displacements can be treated in a much simpler fashion than the other two cases described before. Only one reflected wave of SH type is involved. The incident potential, w_2, and the reflected potential, w_{22}, are defined by the equations

$$\begin{aligned} w_2 &= \text{Re } W_2(\eta_2) \\ w_{22} &= \text{Re } W_{22}(\eta_{22}) \end{aligned} \tag{4.30}$$

where, η_2 and η_{22} are defined by Eqs. 4.23 and 4.24. No head wave exists in this case. The reflected displacement potential, w_{22}, is found by setting the tangential stress on the surface equal to zero. The displacement and stresses are then found to be

$$U_Z = \text{Re}\left[\int_0^{\eta_2} W_2'(\eta)d\eta + \int_0^{\eta_{22}} W_{22}'(\eta)d\eta\right] \tag{4.31a}$$

$$\frac{T_{XZ}}{\mu} = \text{Re}\left\{\frac{\partial}{\partial t}\left[-\int_0^{\eta_2}\sqrt{b^{-2}-\eta^2}\, W_2'(\eta)d\eta + \int_0^{\eta_{22}}\sqrt{b^{-2}-\eta^2}\, W_{22}'(\eta)d\eta\right]\right\} \tag{4.31b}$$

where $W'(\eta) = \dfrac{dW(\eta)}{d\eta}$

Since $T_{XZ}\Big|_{X=0} = 0$, it can be observed from Eq. 4.31b that for the antiplane problem both incident and reflected potentials are identical. That is,

$$W'_{22}(\eta_{22}) = + W'_2(\eta_2) \tag{4.32}$$

The antiplane displacement on the X = 0 surface is given by

$$U_Z = 2\{\mathrm{Re}\,[\int_0^{\tilde{\eta}} W'_2(\eta)d\eta]\} \tag{4.33}$$

$\tilde{\eta}$ is the common value of the complex variables η_2 and η_{22} on the X = 0 plane. For a strike-slip fault propagating in two opposite directions, Eq. 3.10 together with the first of Eq. 4.9 determines the complex displacement function, $W'_2(\eta)$. To obtain displacement fields corresponding to a given dislocation pulse, the response of two unilateral strike-slip faults must be superposed on the results of Eq. 4.33.

Equation 4.33 indicates that the antiplane displacement of any point on the surface of an elastic half space is twice that of the full-space at the same point. This conclusion does not hold for the plane problem (dip-slip faulting).

4.7 The Numerical Integration Techniques

The numerical integration scheme used in this study in the evaluation of the displacements on the free surface will be described below. The numerical analysis of the motions generated by the incident P and SV waves are identical except for the head wave disturbance which requires a somewhat different approach. The computations are carried out in the complex η-plane;

however, only real portions of the final results describe the actual motions and have physical significance.

4.7.1 The P-Wave Disturbance

The components of the surface motion generated by an incident P-wave are defined by the equations

$$U_X^P(0,Y,t) = \mathrm{Re}\left\{\int_0^{\eta_0} \frac{-2b^{-2}(b^{-2} - 2\eta^2)\sqrt{a^{-2} - \eta^2}}{R(\eta^2)}\,\Phi_1'(\eta)d\eta\right\} \tag{4.34}$$

$$U_Y^P(o,Y,t) = \mathrm{Re}\left\{\int_0^{\eta_0} \frac{-4b^{-2}\eta\sqrt{a^{-2} - \eta^2}\,\sqrt{b^{-2} - \eta^2}}{R(\eta^2)}\,\Phi_1'(\eta)d\eta\right.$$

Only the U_X^P component will be considered here. The method applies for the U_Y^P component as well.

The time history of U_X^P at any given point $P(0,D)^*$ is obtained when the first equation of 4.34 is integrated along a contour which is traced out in the complex η plane as η_0 varies with time. Suppose that t_0 denotes the arrival time of the P-wave front. That portion of the contour which corresponds to $0 < t < t_0$ will lie along the real axis between $\eta_0 = 0$ and $\eta_0 = \frac{D}{r_0} a^{-1}$, where $r_0^2 = X_0^2 + D^2$. For $t > t_0$ the path is described by the equation

$$\eta_0 = \frac{D}{r_0 a} \cdot \frac{t}{t_0} + \frac{iX_0\sqrt{2(t - t_0)/t_0 + (t - t_0)^2/t_0^2}}{ar_0} \tag{4.35}$$

*For convenience D is taken as a positive quantity.

where

$$t_o = \frac{r_o}{a}$$

It is apparent that for $t > t_o$ and $D > 0$ the curve defined by Eq. 4.35 lies entirely on the upper half-plane as illustrated in Fig. 24.

Assuming that the dislocation fronts do not propagate faster than the distortional wave velocity ($\alpha < b < a$), and noting that the real root of the Rayleigh function, c, is less than b ($c^{-1} > b^{-1} > a^{-1}$), the integrands in Eqs. 4.34 are all analytic functions in the region of interest. Hence, the path of the integration between each pair of successive points, η_o^J and η_o^{J+1}, can be accurately approximated by a quadratic function. Simpson's one-third rule is used to compute U_X^P numerically. It is convenient for computational purposes to write the first of Eqs. 4.34 in the form

$$U_X^P(0,D,t) = \mathrm{Re}\int_0^{\eta_o(t_o)} I_1(\eta)d\eta + \mathrm{Re}\int_{\eta_o(t_o)}^{\eta_o(t)} I_1(\eta)d\eta \qquad (4.36)$$

where,

$$I_1(\eta) = \frac{-2b^{-2}(b^{-2} - 2\eta^2)\sqrt{a^{-2} - \eta^2}}{R(\eta^2)}\,\Phi_1'(\eta) \qquad (4.36a)$$

and

$$\eta_o(t_o) = \frac{D}{r_o}\,a^{-1}$$

For η in the range of $0 < \eta < D/r_o\,a^{-1}$, the function $I_1(\eta)$ is real-valued except for the coefficient $\frac{1}{2\pi i}$ of $\Phi_1'(\eta)$ (see Eqs. 3.5), and consequently, the result of the integration would be a pure imaginary quantity with the real part being zero. It follows that

$$U_X^P(0,D,t) = 0$$

$$\text{for } 0 < t < t_o \tag{4.37}$$

$$U_Y^P(0,D,t) = 0$$

In other words, there would be no motion before the arrival of the wave front, as expected. For t greater than t_o, Eq. 4.36 is reduced to the following expression

$$U_X^P(0,D,t) = \text{Re} \int_{\eta_o(t_o)}^{\eta_o(t)} I_1(\eta)d\eta \tag{4.38}$$

In order to compute the value of U_X^P at times $t_o + n\Delta t$, Eq. 4.38 is rewritten as follows:

$$U_X^P(0,D,t_o+n\Delta t) = \sum_{j=0}^{j=n-1} \text{Re} \int_{\eta_o^j}^{\eta_o^{j+1}} I_1(\eta)d\eta \tag{4.39}$$

where Δt is a positive increment of time, n is an integer, and η_o^J is defined by the equation

$$\eta_o^J(0,D,t_o+n\Delta t) = \frac{D}{ar_o}\left(1 + J\frac{\Delta t}{t_o}\right) + \frac{iX_o}{ar_o}\left[2\frac{J\Delta t}{t_o} + \left(\frac{J\Delta t}{t_o}\right)^2\right]^{1/2} \tag{4.40}$$

For J = 0, 1, 2, . . ., the points $P_o^J(0,D,t_o+J\Delta t)$ in the (X,Y,t) space are mapped onto their image in the complex η-plane in accordance with Eq. 4.40. These image points lie on a curve which is defined by Eq. 4.35 and is depicted in Fig. 24.

As indicated previously, the function $I_1(\eta)$ is analytic between each

pair of points η_o^J and η_o^{J+1} so that Simpson's rule is applicable. Equation 4.3a then becomes:

$$U_X^P(0,D,t_o+n\Delta t) \simeq \mathrm{Re} \sum_{j=0}^{j=n-1} \left[I_1(\eta_o^J) + 4I_1\left(\frac{\eta_o^J + \eta_o^{J+1}}{2}\right) + I_1(\eta_o^{J+1}) \right] \frac{\eta_o^{J+1} - \eta_o^J}{6} \qquad (4.42)$$

$$J = 0, 1, 2, \ldots$$

Hence, the time variation of U_X^P can be computed from Eq. 4.42 by a simple step-by-step operation.

Briefly, any point on the surface of the half-space is set into motion upon the arrival of the wave front. To obtain the time history of the U_X^P in the interval $(t_o + J\Delta t)$ and $(t_o + (J + 1)\Delta t)$, one can determine corresponding η_o values from Eq. 4.40. Back substitution of η_o's into Eq. 4.36a and use of Eq. 4.42, result in an appropriate value for U_X^P at each time step.

4.7.2 The S-Wave Disturbance

By a method completely analogous to that used in the previous section, the S-wave component of the displacements along the X-axis, U_X^S, is found to be

$$U_X^S(0,D,t) = \mathrm{Re} \int_o^{\tilde{\eta}(t_o)} I_2(\eta)d\eta = 0 \quad \text{for} \quad t < t_o = \frac{(X_o^2 + D^2)^{1/2}}{b} \qquad (4.43)$$

$$U_X^S(0,D,t) = \mathrm{Re} \int_{\tilde{\eta}(t_o)}^{\tilde{\eta}(t)} I_2(\eta)d\eta \tag{4.44}$$

$$= \mathrm{Re} \sum_{J=0}^{J=n-1} [I_2(\tilde{\eta}^J) + 4I_2(\frac{\tilde{\eta}^{J+1} + \tilde{\eta}^J}{2})$$

$$+ I_2(\tilde{\eta}^{J+1})] \frac{\tilde{\eta}^{J+1} - \tilde{\eta}^J}{6}$$

where, t_o denotes the time at which the S wave reaches the point $P_o(0,D)$,

$$I_2(\eta) = \frac{-4b^{-2}\eta\sqrt{a^{-2} - \eta^2}\sqrt{b^{-2} - \eta^2}}{R(\eta^2)} \Psi_2'(\eta) \tag{4.45}$$

and

$$\tilde{\eta}^J = \frac{D}{r_o b}[1 + J\frac{\Delta t}{t_o}] + \frac{iX_o}{br_o}[2\frac{J\Delta t}{t_o} + (\frac{J\Delta t}{t_o})^2]^{1/2} \quad \text{for } t > t_o \tag{4.46}$$

As in Sec. 4.8.1, Δt is a positive increment of time and n is any positive integer. The procedure outlined before applies in the present case as well and reiteration of it is not necessary.

4.7.3 The Head-Wave Disturbance

When an incident S-wave reaches the free surface, depending upon the angle of incidence, head wave is formed and points on the surface are set to motion prior to the arrival of the S-wave front. The displacements so generated are usually referred to as the head-wave disturbances and are described by the following equations

$$U_X^H = \mathrm{Re}\left\{\int_0^{\eta_H(t)} \frac{\eta(b^{-2} - 2\eta^2)^2 - 4\eta^3\sqrt{a^{-2} - \eta^2}\cdot\sqrt{b^{-2} - \eta^2}}{R(\eta^2)}\,\Psi_2'(\eta)d\eta\right.$$

$$\left. - \int_0^{\eta_H(t)} \frac{4\eta(b^{-2} - 2\eta^2)\sqrt{a^{-2} - \eta^2}\cdot\sqrt{b^{-2} - \eta^2}}{R(\eta^2)}\,\Psi_2'(\eta)d\eta\right\} \qquad (4.47)$$

$$U_Y^H = \mathrm{Re}\left\{\int_0^{\eta_H(t)} \frac{(b^{-2} - 2\eta^2)^2\sqrt{b^{-2} - \eta^2} - 4\eta^2(b^{-2} - \eta^2)\sqrt{a^{-2} - \eta^2}}{R(\eta^2)}\,\Psi_2'(\eta)d\eta\right.$$

$$\left. + \int_0^{\eta_H(t)} \frac{4\eta^2(b^{-2} - 2\eta^2)\sqrt{b^{-2} - \eta^2}}{R(\eta^2)}\,\Psi_2'(\eta)d\eta\right\}$$

$$\text{for } 0 < t < t_o = \frac{(X_o^2 + D^2)^{1/2}}{b}$$

The variable of the integration, η, is real and its range of variation is $0 < \eta < \frac{D}{r_o} b^{-1}$ (see Fig. 24). Further investigation of the integrands in Eqs. 4.47 reveals that their derivatives are not analytic at $\eta = a^{-1}$ and, therefore, the standard integration techniques are no longer applicable.

As an example, consider the first integral in the right side of Eqs. 4.47 which corresponds to the SS-wave component of the surface motion.

$$U_X^{SS} = \mathrm{Re}\left\{\int_0^{\eta_H(t)} \frac{\eta(b^{-2} - 2\eta^2) - 4\eta^3\sqrt{a^{-2} - \eta^2}\cdot\sqrt{b^{-2} - \eta^2}}{R(\eta^2)}\,\Psi_2'(\eta)d\eta\right\} \qquad (4.48)$$

The path of integration is a straight line just above the real axis extending from $\eta = 0$ to $\eta = \frac{D}{r_o} b^{-1}$. It is apparent from Eq. 4.48 that the integrand

is imaginary and analytic for all $0 < \eta < a^{-1}$. Therefore,

$$U_X^{SS} = \mathrm{Re} \int_0^{\eta_H(t)} I_3(\eta)d\eta = 0 \quad \text{for} \quad 0 < \eta_H(t) < a^{-1} \tag{4.49}$$

where

$$I_3(\eta) = \frac{\eta(b^{-2} - 2\eta^2)^2 - 4\eta^3\sqrt{a^{-2} - \eta^2}\cdot\sqrt{b^{-2} - \eta^2}}{R(\eta^2)}\,\Psi'(\eta) \tag{4.50}$$

For $a^{-1} < \eta_H(t) < \frac{D}{r_o}\, b^{-1}$, $I_3(\eta)$ is complex-valued since $R(\eta^2)$ is complex-valued in this range. It is convenient to separate the real and imaginary portions of $I_3(\eta)$ by multiplying both numerator and denominator by $\overline{R(\eta^2)}$, the conjugate of the Rayleigh function. The result is

$$I_3(\eta) = (\eta - a^{-1})^{1/2}\, I_{31}(\eta) + iI_{32}(\eta) \tag{4.51}$$

where,

$$I_{31}(\eta) = \frac{-8\eta^3(b^{-2} - 2\eta^2)^2\sqrt{b^{-2} - \eta^2}\,\sqrt{a + \eta}}{R(\eta^2)\cdot\overline{R(\eta^2)}}\,\Psi_2'(\eta) \tag{4.52}$$

$$I_{32} = \frac{-\eta[(b^{-2} - 2\eta^2)^4 + 16\eta^4(a^{-2} - \eta^2)(b^{-2} - \eta^2)]}{R(\eta^2)\cdot\overline{R(\eta^2)}}\,\Psi_2'(\eta) \tag{4.53}$$

$$\overline{R(\eta^2)} = (b^{-2} - 2\eta^2)^2 - 4\eta^2\sqrt{a^{-2} - \eta^2}\,\sqrt{b^{-2} - \eta^2} \tag{4.54}$$

and,

$$R(\eta^2) \cdot \overline{R(\eta^2)} = -16\eta^6(b^{-2} - a^{-2}) + b^{-2}(24b^{-2} - 16a^{-2})\eta^4$$

$$- 8b^{-6}\eta^2 + b^{-8}$$

Notice that in decomposing $I_3(\eta)$ into the real and imaginary parts, represented by Eq. 4.51, the coefficient $\frac{1}{2\pi i}$ of $\Psi_2'(\eta)$ becomes real and possess the value $\frac{1}{2\pi}$. Equation 4.48 can be simplified as follows:

$$U_X^{SS} = \int_{a^{-1}}^{\eta_H(t)} (\eta - a^{-1})^{1/2} I_{31}(\eta)d\eta \quad \text{for} \quad a^{-1} < \eta_H(t) < \frac{D}{r_o} b^{-1} \tag{4.55}$$

Since the function $(\eta - a^{-1})^{1/2}$ has infinite slope at $\eta = a^{-1}$ and varies rapidly thereafter, the usual procedures of the numerical integrations will not lead to an accurate result and, therefore, an alternative approach must be adopted. To this end, $I_{31}(\eta)$ which is analytic between a^{-1} and $\frac{D}{r_o} b^{-1}$ can be approximated by a linearly varying function over a sufficiently small increment $\Delta\eta$. As a result, the numerical evaluation of $(\eta - a^{-1})^{1/2} I_{31}(\eta)$ over the interval $\Delta\eta$ is performed by multiplying the values of $I_{31}(\eta)$ at the end points of this interval by weighting factors which take into account the rapid variation of $(\eta - a^{-1})^{1/2}$ near a^{-1} [29].

The approximation described above can be expressed mathematically in the following manner.

$$(\eta - a^{-1})^{1/2} I_{31}(\eta) \approx (\eta - a^{-1})^{1/2}[A + B(\eta - a^{-1})] \tag{4.56}$$

The coefficients A and B are obtained by solving two simultaneous equations

$$I_L = I_{31}(a^{-1} + J\Delta\eta) = A + B(J\Delta\eta)$$

$$I_R = I_{31}(a^{-1} + (J + 1)\Delta\eta) = A + B((J + 1)\Delta\eta) \tag{4.57}$$

The results are:

$$A = (J + 1)I_L - JI_R; \quad B = \frac{I_R - I_L}{\Delta\eta} \tag{4.58}$$

If the interval between a^{-1} and $\frac{D}{r_o} b^{-1}$ is divided into n sufficiently small increments, it can be shown that an accurate approximation of U_X^{SS} at an intermediate point is given by the formula,

$$U_X^{SS}(a^{-1} + m\Delta\eta) = (\Delta\eta)^{3/2} \sum_{J=0}^{J=m-1} \frac{2}{3} A[(J + 1)^{3/2} - J^{3/2}]$$

$$+ \frac{2}{5} B[(J + 1)^{5/2} - J^{5/2}]\Delta\eta \tag{4.59}$$

where, $0 \leq m \leq n$ and $a^{-1} \leq a^{-1} + m\Delta\eta \leq \frac{D}{r_o} b^{-1}$. For a given value of t, the increment $\Delta\eta$ can be evaluated from the expression

$$t - D(a^{-1} + m\Delta\eta) - X_o[b^{-2} - (a^{-1} + m\Delta\eta)^2]^{1/2} = 0 \tag{4.60}$$

This relationship between t and $(m\Delta\eta)$ is developed from the equation

$$t + (X + X_o)\sqrt{b^{-2} - \eta^2} - Y\eta = 0 \tag{4.61}$$

by choosing an appropriate branch of $\sqrt{b^{-2} - \eta^2}$ and setting X equal to zero. Equation 4.60 defines the front of the head wave disturbance in the (X,Y,t)

space which is tangent to the front of the SS-wave and intersects the surface of the half space at $Y = at - X_0\sqrt{a^2b^{-2} - 1}$.

It should be remarked that even if the presence of a head wave had not been foreseen, the straightforward evaluation of the complex integrals would have demonstrated that a region of real η exists with nonzero distortional component ahead of the S-wave front.

4.8 Surface Motion Due to a Unilateral Shear Fault

Another problem of interest relevant to this study is the one in which the elastic waves radiate from a fault plane lengthening on only one side. This type of faulting model is particularly useful in the study of the earthquake source mechanism when the rupture velocity of the material adjacent to the fault plane varies considerably at different levels. The analysis based upon the assumption of the uniform crack propagation does not provide accurate results unless this change in the rupture velocity is taken into account in the formulation of the model. To this end, the motion produced by a unilateral fault source is superposed on the response of a uniform dislocation model such that the effect of the combined sources on the surface motion is approximately equivalent to that of the actual rupture mechanism.

Also, simulation of the intermittent faulting mechanism and computation of the ground motion when the seismic energy is released from an assumed dislocation pulse, necessitates that the solution for a unilateral fault be properly combined with the results obtained in the previous sections.

This change in the cracking pattern (unilateral and bilateral faulting) does not introduce any difficulty in the determination of the displacement

fields and the problem can be treated in precisely the same manner as the original one in which dislocation fronts were moving in both directions. Appropriate expressions for the incident potentials in both cases have been already developed and represented in Chapter 3 and Appendix B. The only difference in the two instances is consideration of a suitable time and coordinate shift in defining the equations of the characteristic planes corresponding to the incident and reflected wave fronts.

Consider a faulting model shown in Fig. 25. The rupture starts at point c and propagates uniformly upward. The position of the characteristic plane corresponding to the incident P-wave can be determined in the (X,Y,t) space from the equation

$$\delta_1 = t' - (X - X_0)\sqrt{a^{-2} - \eta_1^2} - \xi_1\sqrt{a^{-2} - \eta_1^2} - Y\eta_1 + \xi_2\eta_1 = 0 \tag{4.62}$$

where, $\xi_1 = \rho_0 \sin\gamma$, $\xi_2 = \rho_0 \cos\gamma$, and $t' = t - \frac{|\rho_0|}{\alpha}$. The parameters ρ_0 and γ are shown in Fig. 25. Similar expressions can be defined when the fronts of the reflected waves are considered. As indicated before, the computational procedures and the numerical techniques necessary to calculate the displacement fields are identical for both problems and reiteration of them is not essential. Samples of the calculated displacements on the surface of an elastic half space which are produced by dip-slip as well as strike-slip shear fault are illustrated in Figs. 21 through 23. The location of the observation points, the orientation of the fault plane, and the geometry of the source are also depicted.

5. EFFECT OF THE LAYERING ON THE SURFACE MOTION

5.1 General Remarks

It is a well known phenomenon in seismology that the amplitude of the strong ground motion may be significantly affected by the near-surface geological configuration at the recording site. The influence of the soil profile and seismic properties of the medium and their interaction with the surface motion has been studied and reported by several investigators [3, 46,47]. They have come to the conclusion that the effect of the local geology must be taken into account in developing a dislocation model with an adequate predictive capability.

To this end, it is assumed that the medium can be replaced by horizontally stratified layers having constant thicknesses and overlying a homogeneous half space (bedrock). The elastic waves emerge from a seismic source in the isotropic bedrock, interact with the interface between adjacent layers and free surface, producing the final surface motion. Once the soil inhomogeneity is idealized in the manner described above and a suitable mechanism for the creation of the seismic waves is prescribed, the important task is development of a mathematical scheme which permits determination of the dynamic response at a given point.

The solution for the wave propagation problems in a layered elastic half space has been discussed at great detail in the literature. Ewing, Press and Jardetzky [48] solved some simple problems and provided a complete list of the previous studies. Knopoff [17] developed matrix method solution to the problems of elastic wave propagation in multilayered media in which

waves of P, SV, and SH type radiate from a point source in the homogeneous half space. A somewhat different approach was used by Abramovici [18]. He obtained the solution in two steps: first, the operational solution was found using the Laplace transportation technique and then the results were transformed to the time domain. Finally, Zvolinskii [49,50] applied the Smirnov-Sobolev method to a multilayered medium in conjunction with the asymptotic evaluation of the wave fields near the front of reflected and head waves.

In this study, Zvolinskii's work will be extended to the problems in which the waves arise from a dislocation pulse instead of a point source considered in the earlier models. The medium is assumed to consist of an elastic layer lying on the top of a homogeneous bedrock. As before, the amplitude of the dislocation is taken to be a step function in time. It is also assumed that the displacements and stresses depend only upon the x and y coordinates, meaning that the problem is a two-dimensional one.

Before proceeding with the analysis, it is necessary to develop appropriate expressions for the coefficients of the reflection and transmission from the surfaces of discontinuity.* Compared to the problem of single half space, computation of the displacement fields in layered media is much more involved. This complexity is caused by the presence of two or more interfaces which results in multiple reflection and refraction of elastic waves. The arrival of the incident disturbance at the first interface gives rise to both reflected and transmitted potentials. For the motion on the free surface, seismic waves traveling in the upper layer are of primary

*The free surface is also considered as a surface of discontinuity.

interest and, therefore, only the refracted portion of the incident waves are to be evaluated. This newly generated potential arriving at the free surface creates reflected disturbances traveling away from the surface. The arrival of these disturbances at the interface is, again, associated with the generation of a new set of potentials. However, only the reflected part of the latter contributes to the surface motion and is of analytical significance. Figure 28 illustrates the geometrical representation of the model, the position of the dislocation source, and the path along which incident and reflected (or refracted) waves travel.

The following problems, essential for the determination of the motion, are considered in the subsequent sections:

i) Calculation of the potentials transmitted from the interface of two "welded" half spaces when the source of disturbance lies in the lower half space; and

ii) Calculation of the reflected potentials when the waves traveling in the upper medium encounter the surface separating two media.

The effect of the free surface will be examined in Sec. 5.3.

5.2 Reflection and Refraction of Seismic Waves from the Interface of Two "Welded" Half Spaces

Computation of the time history of displacements on the surface of a single-layered half space necessitates solution for the problem of the transmission of plane body waves through the interface of two welded elastic solids. Each one of the solids is specified by its seismic properties, i.e., the velocity of the P and S waves and the density of the medium.

Simple though the problem may appear, it has a wide range of different solutions depending on the relationship between the parameters described above. The form of the wave fronts and the reflection and refraction of the elastic waves in different cases has been discussed in detail by Johnson and Robinson and is reported in Ref. [30]. The case which is consistant with the local geology of most recording sites is the one in which an isotropic, elastic body with low seismic velocity lies on the surface of a hard bedrock.

A diagram of the elastic solids with complete contact is shown in Fig. 26. The lower half space is denoted as medium 1 having material properties λ_1, μ_1, ρ_1, and corresponding P and S wave velocities, a_1 and b_1. Likewise, the upper half space is designated as medium 2 with properties λ_2, μ_2, ρ_2 and wave velocities a_2 and b_2. It is assumed that the inequality $a_1 > b_1 > a_2 > b_2$ holds throughout this study. The seismic energy radiates from a dislocation pulse located in the medium 1 at a distance $x = x_0$ from the interface between two solids. Depending on the nature of the faulting mechanism, incident waves of P, SV, and SH type might arise from the source mentioned above. The P and SV potentials correspond to a dip-slip dislocation pulse whereas, SH waves emerge from a strike-slip fault motion.

The general solution of the problem decomposes into the following three two-dimensional plane and antiplane cases:

i) The reflected and refracted P and SV waves due to an incident P wave;

ii) The reflected and refracted P and SV waves due to an incident SV wave;

iii) The reflected and refracted SH wave due to an incident SH wave.

By the use of the method of self-similar potentials in a manner precisely similar to that of Chapter 4, appropriate expressions for the reflected and transmitted potentials will be derived in the succeeding sections.

5.2.1 Incident P Wave

The incident P-wave potential and the corresponding reflected and refracted disturbances are defined by the equations:

$$\phi_1 = \text{Re } \Phi_1(\eta_1) \qquad \text{(incident P-wave)} \tag{5.1a}$$

$$\phi_{11} = \text{Re } \Phi_{11}(\eta_{11}) \; ; \quad \psi_{12} = \text{Re } \Psi_{12}(\eta_{12}) \qquad \text{(reflected P and SV wave)}$$

and

$$\gamma_{11} = \text{Re } \Gamma_{11}(\xi_{11}); \quad \omega_{12} = \text{Re } \Omega_{12}(\xi_{12}) \qquad \text{(refracted P and SV wave)} \tag{5.1b}$$

where, η_1, η_{11}, η_{12}, ξ_{11}, and ξ_{12} are defined implicitly as follows,

$$\delta_1 = t - x\sqrt{a_1^{-2} - \eta_1^2} + x_o\sqrt{a_1^{-2} - \eta_1^2} - y\eta_1 = 0$$

$$\delta_{11} = t + x\sqrt{a_1^{-2} - \eta_{11}^2} + x_o\sqrt{a_1^{-2} - \eta_{12}^2} - y\eta_{11} = 0 \tag{5.2a}$$

$$\delta_{12} = t + x\sqrt{b_1^{-2} - \eta_{12}^2} + x_o\sqrt{a_1^{-2} - \eta_{12}^2} - y\eta_{12} = 0$$

and

$$\Delta_{11} = t - x\sqrt{a_2^{-2} - \xi_{11}^2} + x_o\sqrt{a_1^{-2} - \xi_{11}^2} - y\xi_1 = 0$$

$$\Delta_{12} = t - x\sqrt{b_2^{-2} - \xi_{12}} + x_o\sqrt{a_1^{-2} - \xi_{12}^2} - y\xi_{12} = 0 \quad (5.2b)$$

On the surface x = 0, Eqs. 5.2a and 5.2b are identical and all complex variables retain a common value such that

$$\eta_1 = \eta_{11} = \eta_{12} = \xi_{11} = \xi_{12} = \xi_1^o \quad \text{for} \quad x = 0 \quad (5.3)$$

and

$$\xi_1^o = \frac{ty + ix_o\sqrt{t^2 - \dfrac{x_o^2 + y^2}{a_1^2}}}{x_o^2 + y^2} \quad (5.4)$$

For points off the x = 0 surface, the variables in Eq. 5.3 are no longer equal and their values are found numerically from Eqs. 5.2a and 5.2b. The wave front pattern for the P wave incident on the interface of two half spaces and those for the reflected and refracted potentials are shown in Fig. 27.

The following expressions for the displacement fields and normal as well as tangential tractions in the upper half space can be easily verified:

$$U_x^{(2)} = \mathrm{Re}\left\{-\int_0^{\xi_{11}} \sqrt{a_2^{-2} - \eta^2}\,\Gamma_{11}'\,d\eta - \int_0^{\xi_{12}} \eta\Omega_{12}'\,d\eta\right\} \quad (5.5a)$$

$$U_y^{(2)} = \mathrm{Re}\left\{-\int_0^{\xi_{11}} \eta\Gamma_{11}'\,d\eta + \int_0^{\xi_{12}} \sqrt{b_2^{-2} - \eta^2}\,\Omega_{12}'\,d\eta\right\}$$

and

$$\frac{\sum_x^{(2)}}{\mu_2} = \mathrm{Re}\{\frac{\partial}{\partial t}[\int_0^{\xi_{11}}(b_2^{-2} - 2\eta^2)\,\Gamma_{11}'d\eta + \int_0^{\xi_{12}} 2\eta\sqrt{b_2^{-2} - \eta^2}\,\Omega_{12}'d\Omega]\} \tag{5.5b}$$

$$\frac{T_{xy}^{(2)}}{\mu_2} = \mathrm{Re}\{\frac{\partial}{\partial t}[\int_0^{\xi_{11}} 2\eta\sqrt{a_2^{-2} - \eta^2}\,\Gamma_{11}'d\eta + \int_0^{\xi_{12}}(2\eta^2 - b_2^2)\,\Omega_{12}'d\eta]\}$$

The motion in the lower half space is described by the incident ϕ_1 and reflected ϕ_{11} and ψ_{12} disturbances. It is not difficult to show that

$$U_x^{(1)} = \mathrm{Re}\{-\int_0^{\eta_1}\sqrt{a_1^{-2} - \eta^2}\,\phi_1'\,d\eta + \int_0^{\eta_{11}}\sqrt{a_1^{-2} - \eta^2}\,\phi_{11}'\,d\eta - \int_0^{\eta_{12}}\eta\psi_{12}'\,d\mu\} \tag{5.5c}$$

$$U_y^{(1)} = \mathrm{Re}\{-\int_0^{\eta_1}\eta\phi_1'\,d\eta - \int_0^{\eta_{11}}\eta\phi_{11}'\,d\eta - \int_0^{\eta_{12}}\sqrt{b_1^{-2} - \eta^2}\,\psi_{12}'d\eta\}$$

and

$$\frac{\sum_x^{(1)}}{\mu_1} = \mathrm{Re}\{\frac{\partial}{\partial t}[\int_0^{\eta_1}(b_1^{-2} - 2\eta^2)\,\phi_1'\,d\eta + \int_0^{\eta_{11}}(b_1^{-2} - 2\eta^2)\,\phi_{11}'\,d\eta - \int_0^{\eta_{12}}2\eta\sqrt{b_1^{-2} - \eta^2}\,\psi_{12}'\,d\eta]\} \tag{5.5d}$$

$$\frac{T_{xy}^{(1)}}{\mu_1} = \mathrm{Re}\{\frac{\partial}{\partial t}[\int_0^{\eta_1} 2\eta\sqrt{a_1^{-2} - \eta^2}\,\phi_1'\,d\eta - \int_0^{\eta_{11}} 2\eta\sqrt{a_1^{-2} - \eta^2}\,\phi_{11}'$$

$$- \int_0^{\eta_{12}} (b_1^{-2} - 2\eta^2)\,\psi_{12}'\,d\eta]\}$$

Since the two half spaces are in complete contact, displacements and tractions must be continuous on the surface of discontinuity (the x = 0 surface). To maintain this condition the following equations should be satisfied:

$$U_x^{(1)}(0,y,t) = U_x^{(2)}(0,y,t); \quad U_y^{(1)}(0,y,t) = U_y^{(2)}(0,y,t)$$

and

$$\sum_x^{(1)}(0,y,t) = \sum_x^{(2)}(0,y,t); \quad T_{xy}^{(1)}(0,y,t) = T_{xy}^{(2)}(0,y,t)$$

Substituting for the displacements and stresses from the Eqs. 5.5, and noting that the upper limits of the integrals are identical on the x = 0 surface, the following simultaneous equations can be verified:

$$\begin{aligned}
&K_1\phi_{11}' - \eta\psi_{12}' + K_2\Gamma_{11}' + \eta\Omega_{12}' = K_1\phi_1' \\
&-\eta\phi_{11}' - h_1\psi_{12}' + \eta\Gamma_{11}' - h_2\Omega_{12}' = \eta\phi_1' \\
&\mu n_1\phi_{11}' - 2\mu h_1\eta\psi_{12}' - n_2\Gamma_{11}' - 2\eta h_2\Omega_{12}' = -\mu n_1\phi_1' \\
&-2\mu\eta K_1\phi_{11}' - \mu n_1\psi_{12}' - 2\eta K_2\Gamma_{11}' + n_2\Omega_{12}' = -2\mu\eta K_1\phi_1'
\end{aligned} \tag{5.6}$$

where,

$$K_1 = \sqrt{a_1^{-2} - \eta^2} \qquad K_2 = \sqrt{a_2^{-2} - \eta^2} \qquad h_1 = \sqrt{b_1^{-2} - \eta^2}$$

$$h_2 = \sqrt{b_2^{-2} - \eta^2} \qquad n_1 = b_1^{-2} - 2\eta^2 \qquad n_2 = b_2^{-2} - 2\eta^2 \tag{5.6a}$$

$$\mu = \frac{\mu_1}{\mu_2}$$

Using Cramer's rule, Eqs. 5.6 are solved in terms of the incident potential ϕ_1'. The expressions for the refracted potentials are found to be:

$$\Gamma_{11}'(\xi_{11}) = \frac{D_1(\xi_{11})}{D(\xi_{11})}\,\Phi_1'(\xi_{11}) \qquad \Omega_{12}'(\xi_{12}) = \frac{D_2(\xi_{12})}{D(\xi_{12})}\,\Phi_1'(\xi_{12}) \tag{5.7}$$

where,

$$D(\eta) = \begin{vmatrix} K_1 & -\eta & K_2 & \eta \\ -\eta & -h_1 & \eta & -h_2 \\ \mu n_1 & -2\mu h_1 \eta & -n_2 & -2\eta h_2 \\ -2\mu\eta K_1 & -\mu n_1 & -2\eta K_2 & n_2 \end{vmatrix}$$

$$= \eta^2(\mu n_1 - n_2)^2 + K_1 h_1[(n_2 + 2\mu\eta^2)^2] + K_2 h_2[(\mu n_1 + 2\eta^2)^2]$$

$$+ K_1 K_2 h_1 h_2[4\eta^2(1 - \mu)^2] + \mu(n_1 + 2\eta^2)(n_2 + 2\eta^2)(h_1 K_2 + h_2 K_1)$$

$$D_1(\eta) = \begin{vmatrix} K_1 & -\eta & K_1 & \eta \\ -\eta & -h_1 & \eta & -h_2 \\ \mu n_1 & -2\mu h_1 \eta & -\mu n_1 & -2\eta h_2 \\ -2\mu\eta K_1 & -\mu n_1 & -2\mu\eta K_1 & n_2 \end{vmatrix}$$

$$= 2\mu K_1 \{ h_1[(n_2 + 2\mu\eta^2)(n_1 + 2\eta^2)] + h_2[(n_1 + 2\eta^2)(\mu n_1 + 2\eta^2)]$$

and

$$D_2(\eta) = \begin{vmatrix} K_1 & -\eta & K_2 & K_1 \\ -\eta & -h_1 & \eta & \eta \\ n_1 & -2\mu h_1 \eta & -n_2 & -\mu n_1 \\ -2\mu\eta K_1 & -\mu n_1 & -2\eta K_2 & -2\eta\mu K_1 \end{vmatrix} \qquad (5.8)$$

$$= 2\mu\eta K_1 (n_1 + 2\eta^2)[2K_2 h_1 (1 - \mu) + (\mu n_1 - n_2)]$$

Similar expressions can be obtained for the potentials reflected from the interface of two solids. As indicated previously, for the motion on the surface only the transmitted part of the incident potential is of primary interest and, therefore, the reflected disturbance is not computed.

5.2.2 Incident SV-Wave

The incident SV-wave potential and the corresponding reflected

and refracted potentials are taken in the form

$$\psi_2 = \text{Re}\ \Psi_2(\eta_2)$$

$$\psi_{22} = \text{Re}\ \Psi_{22}(\eta_2) \qquad \phi_{21} = \Phi_{21}(\eta_{21}) \tag{5.9}$$

$$\gamma_{21} = \text{Re}\ \Gamma_{21}(\xi_{21}) \qquad \omega_{22} = \text{Re}\ \Omega_{22}(\xi_{22})$$

The equations of the characteristic planes which determine the position of the incident, reflected and refracted wave forms in the (x,y,t) space are defined as follows.

$$\delta_2 = t - x\sqrt{b_1^{-2} - \eta_2^2} + x_o\sqrt{b_1^{-2} - \eta_2^2} - y\eta_2 = 0$$

$$\delta_{22} = t + x\sqrt{b_1^{-2} - \eta_{22}^2} + x_o\sqrt{b_1^{-2} - \eta_{22}^2} - y\eta_{22} = 0 \tag{5.10a}$$

$$\delta_{21} = t + x\sqrt{a_1^{-2} - \eta_{21}^2} + x_o\sqrt{b_1^{-2} - \eta_{21}^2} - y\eta_{21} = 0$$

and,

$$\Delta_{22} = t - x\sqrt{b_2^{-2} - \xi_{22}^2} + x_o\sqrt{b_1^{-2} - \xi_{22}^2} - y\xi_{22} = 0$$

$$\Delta_{21} = t - x\sqrt{a_2^{-2} - \xi_{21}^2} + x_o\sqrt{b_1^{-2} - \xi_{21}^2} - y\xi_{21} = 0 \tag{5.10b}$$

The common value of the complex variables on the x = 0 surface is obtained from any one of Eqs. 5.10a or 5.10b by setting x = 0 and solving for either η or ξ. The result is:

$$\eta_2 = \eta_{22} = \eta_{21} = \xi_{22} = \xi_{21} = \xi_2^o \quad \text{for } x = 0 \tag{5.11}$$

and,

$$\xi_2^o = \frac{ty + ix_o\sqrt{t^2 - \frac{x_o^2 + y^2}{b_1^2}}}{x_o^2 + y^2} \tag{5.12}$$

Figure 29 shows the fronts of the incident SV wave together with the reflected and refracted P and SV waves. The displacement and stress fields corresponding to the refracted disturbance in the upper medium have the form:

$$U_x^{(2)} = \mathrm{Re}\{-\int_o^{\xi_{21}} \sqrt{a_2^{-2} - \eta^2}\, \Gamma_{21}'\, d\eta - \int_o^{\xi_{22}} \eta\Omega_{22}'\, d\eta\}$$

$$U_y^{(2)} = \mathrm{Re}\{-\int_o^{\xi_{21}} \eta\Gamma_{21}'\, d\eta + \int_o^{\xi_{22}} \sqrt{b_2^{-2} - \eta^2}\, \Omega_{22}'\, d\eta\} \tag{5.13a}$$

and

$$\frac{\Sigma_x^{(2)}}{\mu_2} = \mathrm{Re}\{\frac{\partial}{\partial t}[\int_o^{\xi_{21}} (b_2^{-2} - 2\eta^2)\Gamma_{21}' d\eta + \int_o^{\xi_{22}} 2\eta\sqrt{b_2^{-2} - \eta^2}\, \Omega_{22}' d\eta] \tag{5.13b}$$

$$\frac{T_{xy}^{(2)}}{\mu_2} = \mathrm{Re}\{\frac{\partial}{\partial t}[\int_o^{\xi_{21}} 2\eta\sqrt{a_2^{-2} - \eta^2}\, \Gamma_{21}'\, d\eta - \int_o^{\xi_{22}} (b_2^{-2} - 2\eta^2)\, \Omega_{22}'\, d\eta]$$

As in the previous case, the continuity of the traction and displacements on the interface of two solids* leads to the appropriate expressions for the

*Computation of the stresses and displacements in the lower half space parallels that of Sec. 5.2.1 and are repeated here. The results were used in deriving Eqs. 5.14.

refracted potentials in terms of the incident SV-wave potential, ψ_2. That is,

$$\Gamma_{21}'(\xi_{21}) = \frac{D_3(\xi_{21})}{D(\xi_{21})} \Psi_2'(\xi_{21})$$
$$\Omega_{22}'(\xi_{22}) = \frac{D_4(\xi_{22})}{D(\xi_{22})} \Psi_2'(\xi_{22}) \tag{5.14}$$

where,

$$D_3(\eta) = -2\mu\eta h_1(n_1 + 2\eta^2)[(\mu n_1 - n_2) + 2K_1 h_2(1 - \mu)]$$
$$D_4(\eta) = 2\mu h_1(n_1 + 2\eta^2)[K_1(n_2 + 2\mu\eta^2) + K_2(\mu n_1 + 2\eta^2)] \tag{5.15}$$

The parameters h_1, h_2, K_1, and K_2 have been defined in Sec. 5.2.1.

Once the reflected potentials are calculated, the displacements and stresses can be computed at any point in the upper half-space by simply substituting for Γ_{21}' and Ω_{22}' in Eqs. 5.13a and 5.13b, and carrying out the necessary integrations. Interaction of the refracted potentials with the free surface bounding the upper half space results in creation of new reflected disturbances which are determined by satisfying the condition of zero tractions on the free surface.

5.2.3 Incident SH-Wave

The case of an incident SH wave is much simpler and thus requires less computations. The simplicity of the problem is mainly due to the fact that the reflected and refracted disturbances arising at the interface are also of SH type.

The incident potentials and resulting reflected and refracted disturbances are defined by the equations

$$\begin{aligned} w_2 &= \text{Re } W_2(\eta_2) && \text{(incident SH-wave)} \\ w_{22} &= \text{Re } W_{22}(\eta_{22}) && \text{(reflected SH-wave)} \\ v_{22} &= \text{Re } V_{22}(\xi_{22}) && \text{(refracted SH-wave)} \end{aligned} \tag{5.16}$$

The characteristic planes which describe the position of the wave fronts in the (x,y,t) space are:

$$\begin{aligned} \delta_2 &= t - (x - x_o)\sqrt{b_1^{-2} - \eta_2^2} - y\eta_2 = 0 \\ \delta_{22} &= t + (x + x_o)\sqrt{b_1^{-2} - \eta_{22}^2} - y\eta_{22} = 0 \end{aligned} \tag{5.17}$$

and,

$$\Delta_{22} = t - x\sqrt{b_2^{-2} - \xi_{22}^2} + x_o\sqrt{b_1^{-2} - \xi_{22}^2} - y\xi_{22} = 0$$

The potentials w_{22} and v_{22} are found in a straightforward manner. The expressions for the displacements and tangential stresses in the lower half space are:

$$U_z^{(1)} = \text{Re}\left\{\int_0^{\eta_2} W_2'(\eta)d\eta + \int_0^{\eta_{22}} W_{22}'(\eta)d\eta\right\} \tag{5.18}$$

$$\frac{T_{xy}^{(1)}}{\mu_1} = \mathrm{Re}\left\{\frac{\partial}{\partial t}\left[-\int_0^{\eta_2}\sqrt{b_1^{-2}-\eta^2}\;\; W_2'(\eta)d\eta\right.\right.$$

$$\left.\left.+\int_0^{\eta_{22}}\sqrt{b_1^{-2}-\eta^2}\;\; W_{22}'(\eta)d\eta\right]\right\}$$

Similar formulations can be derived for the $x < 0$ half space as shown below

$$U_z^{(2)} = \mathrm{Re}\left\{\int_0^{\xi_{22}} V_{22}'(\eta)d\eta\right\} \tag{5.19}$$

and,

$$\frac{T_{xy}^{(2)}}{\mu_2} = \mathrm{Re}\left\{\frac{\partial}{\partial t}\left[-\int_0^{\xi_{22}}\sqrt{b_2^{-2}-\eta^2}\;\; V_{22}'(\eta)d\eta\right]\right.$$

Assuming that no separation takes place along the interface ("welded" contact), the displacements and tractions remain continuous in the process of successive reflections and refractions. This condition together with the fact that the complex variables η_2, η_{22}, and ξ_{22} are identical on the $x = 0$ surface results in the following relations:

$$\begin{aligned} W_{22}'(\eta_{22}) &= D_5(\eta_{22})\, W_2'(\eta_{22}) \\ V_{22}'(\xi_{22}) &= D_6(\xi_{22})\, W_2'(\xi_{22}) \end{aligned} \tag{5.20}$$

where

$$D_5(\eta) = \frac{\mu h_1 - h_2}{\mu h_1 + h_2} \qquad D_6(\eta) = \frac{2\mu h_1}{\mu h_1 + h_2} \tag{5.21}$$

The parameters h_1, h_2, and μ have been defined earlier. Once the potentials are found, calculation of the displacements and stresses in both media is a simple matter.

5.3 Effect of the Reflecting Boundary on the Surface Motion

It was observed in the proceeding sections that the interaction of the incident potentials with a surface separating two "welded" solids results in newly developed disturbances traveling away from the interface. The presence of a free surface gives rise to multiple reflection of the outgoing waves, each one of which contributes to the surface motion in a different manner.

As an example, consider the case in which an elastic layer with thickness "d" overlies a homogeneous bedrock (see Fig. 30). Suppose γ_{11} be a refracted dilational potential traveling inside the layer. Its arrival at the free surface, creates reflected dilational and distortional disturbances designated with γ_{111} and ω_{112}, respectively. It can be shown that,

$$\Gamma'_{111}(\xi_{111}) = \frac{E_1(\xi_{111})}{R(\xi^2_{111})}\ \Gamma'_{11}(\xi_{111})$$

$$\Omega'_{112}(\xi_{112}) = \frac{E_2(\xi_{112})}{R(\xi^2_{112})}\ \Gamma'_{11}(\xi_{112}) \qquad (5.22)$$

where,

$$\gamma_{111}(\xi_{111}) = \text{Re}\ \Gamma_{111}(\xi_{111}) \qquad \omega_{112}(\xi_{112}) = \text{Re}\ \Omega_{112}(\xi_{112}) \qquad (5.23)$$

$$E_1(\eta) = -n_2^2 + 4\eta^2 K_2 h_2 \qquad E_2(\eta) = 4\eta K_2 n_2$$

The parameters n_2, h_2, and K_2 have been defined in Sec. 5.2.1.

The complex variables ξ_{111} and ξ_{112} are expressed implicitly by the equations

$$\begin{aligned}\Delta_{111} &= t + X\sqrt{a_2^{-2} - \xi_{111}^2} + x_o\sqrt{a_1^{-2} - \xi_{112}^2} \\ &\quad + d\sqrt{a_2^{-2} - \xi_{111}^2} - Y\xi_{111} = 0 \\ \Delta_{111} &= t + X\sqrt{b_2^{-2} - \xi_{112}^2} + x_o\sqrt{a_1^{-2} - \xi_{112}^2} \\ &\quad + d\sqrt{a_2^{-2} - \xi_{112}^2} - Y\xi_{112} = 0\end{aligned} \tag{5.24}$$

where, x_o denotes the distance of the point of rupture initiation from the interface of two media. The displacements on the x = 0 surface associated with the reflected fields γ_{111} and ω_{112} are computed as follows:

$$\begin{aligned}U_x &= \mathrm{Re}\left\{\int_0^{\xi_{111}^o} [\sqrt{a_2^{-2} - \eta^2}\ \Gamma'_{111}(\eta) - \eta\Omega'_{112}(\eta)]d\eta\right\} \\ U_y &= \mathrm{Re}\left\{-\int_0^{\xi_{111}^o} [\eta\Gamma'_{111}(\eta) + \sqrt{b_2^{-2} - \eta^2}\ \Omega'_{112}(\eta)]d\eta\right\}\end{aligned} \tag{5.25}$$

where, ξ_{111}^o is defined implicitly by the equation

$$t + x_o\sqrt{a_1^{-2} - \xi_{111}^{o2}} + d\sqrt{a_2^{-2} - \xi_{111}^{o2}} - Y\xi_{111}^o = 0 \tag{5.26}$$

Computation of the time at which the wave fronts corresponding to the potentials

γ_{111} and ω_{112} reach the point under consideration, and the numerical scheme used to evaluate ξ^{0}_{111} is described in Sec. 5.4. Expressions similar to those of Eqs. 5.25 can be developed for the refracted distortional potential ω_{12}.

The motion on the surface is determined when the results of Eqs. 5.25 and those corresponding to the PSP and PSS waves (see Fig. 32) are superposed on the response of the refracted fields γ_{11} and ω_{12}. Interaction of γ_{111} and ω_{112} with the interface, again, results in new disturbances. However, only the reflected portion of them are significant as far as the displacements on the free surface are concerned. Briefly, the response on the surface of a single-layered half space is obtained by superposing a series of solutions each one of which represents certain reflections. This process of successive reflection and transmission continues until the seismic energy dissipates after a few cycles, and the motion on the surface then ceases.

5.4 Determination of the Arrival Time of the Reflected Disturbances

Equations 5.24 define the position of the characteristic planes in the (X,Y,t) space. These planes are tangent to the fronts of the reflected potentials, γ_{111} and ω_{112}, and specify the position of the wave fronts at any given time t. To determine whether the front corresponding to an assumed potential, say, γ_{111} has reached the point (X = 0, Y = D) on the free surface, the procedures outlined below must be followed. A similar approach applies for any other disturbance.

i) Assume a value of time, $t = \bar{t}$, such that the front has not reached the point in question;

ii) Solve the following non-linear simultaneous equations* for $\bar{Y}$ and $\bar{\xi}_{111}$,

$$\bar{t} + x_o\sqrt{a_1^{-2} - \bar{\xi}_{111}^2} + d\sqrt{a_2^{-2} - \bar{\xi}_{111}^2} - \bar{Y}\,\bar{\xi}_{111} = 0$$

$$\frac{x_o\,\bar{\xi}_{111}}{\sqrt{a_1^{-2} - \bar{\xi}_{111}^2}} + \frac{d\,\bar{\xi}_{111}}{\sqrt{a_2^{-2} - \bar{\xi}_{111}^2}} - \bar{Y} = 0 \qquad (5.27)$$

Equations 5.27 can be solved numerically using the Newton-Raphson method [51];

iii) If $\bar{Y} = D$, the front has arrived at the point under consideration. Otherwise, increment $\bar{t}$ by Δt and repeat the previous steps with $t = \bar{t} + \Delta t$. Once the equality $\bar{Y} = D$ is approximately satisfied, the disturbance has reached the point ($X = 0$, $Y = D$) and the arrival time t_o and the corresponding value of the parameter $\bar{\xi}_{111}$ are known.

To compute the integrals in Eqs. 5.25, the complex variable ξ^o_{111}, the upper limit of the integration, is to be evaluated at times $t = t_o + J\Delta t$ ($J = a, 1, 2, \ldots$). This can be accomplished by applying the Newton-Raphson rule to the first of Eqs. 5.27. The iterative processes converge very rapidly, requiring only two or three successive approximations.

As indicated previously, the values of ξ^o_{111} at any given time represents a point in the complex ξ-plane and determination of the contour of integration as well as the method of numerical analysis is exactly parallel to those explained in Chapter 4.

*See the Appendix of Ref. [44].

5.5 Numerical Example

The analysis outlined in the previous sections has been used to compute the time history of the surface motion when an elastic layer with constant thickness d = 4.0 km and seismic parameters a_2 = 3.10 km/sec and b_2 = 1.79 km/sec overlies a homogeneous half space. The speed of the P and S-wave in the bedrock and the ratio of the shear modulus of two media, $\mu = \frac{\mu_1}{\mu_2}$, are taken to be: a_1 = 6.03 km/sec, b_1 = 3.48 km/sec, and μ = 4.18. It is assumed that the motion in the bedrock is caused by an inclined dip-slip dislocation pulse having a depth equal to 2 km with its center located at distance x_o = 12 km from the surface of discontinuity. The angle of the inclination of the fault plane with respect to the horizon is considered to be 80 degrees.

To compare the motion produced by the faulting model described above with the recorded strong ground motion, the integrated displacements from the accelerograms at the Pacioma Dam [52] were reproduced and represented in Fig. 31. The selection of the Pacioma Dam record for the purpose of comparison is quite reasonable since the source mechanism in the San Fernando fault is believed to be dip-slip dislocation. The resemblance of the computed* and recorded motions indicates that fairly simple models such as the one considered here can be developed to determine a design earthquake at a given site under an assumed source mechanism.

Comparison of the calculated displacements on the surface of a homogeneous half space (shown in Figs. 21 and 22) with those of a horizontally

---

*The motion has been calculated at point P(X = 0, Y = 14 km) on the free surface.

stratified model consisting of a single layer above an elastic half space demonstrates the influence of the layering on the surface motion. Particularly, the change in the direction of the particle displacement in the latter portion of the motion which results from the existence of a near-surface low-velocity layer is not present in the homogeneous half space dislocation model.

This oscillatory feature of the surface motion, which is in fairly good agreement with the observed record of the San Fernando 1971 earthquake, indicates that the effect of the local geology must be considered in developing a physically meaningful faulting model. A sequence of motions generated by dislocation in a layered model can be combined to produce a more realistic design earthquake. The frequency content of the actual acceleration is probably influenced by stick-slip motion at the fault, which have not taken into account in the present model. This phenomenon and consideration of both positive and possible negative slips (rebounds) alters the appearance of an accelerogram much more than the displacements picture.

6. CONCLUSIONS AND RECOMMENDATIONS FOR FURTHER STUDY

6.1 Conclusions

In this study the method of self-similar potentials combined with the concept of the auxiliary complex domain has been applied to develop a fairly simple scheme capable of modeling some important physical features of an earthquake focus and of providing the resulting ground motion. Time histories of the displacements on the surface of an elastic bedrock and of a single-layered half space have been evaluated for both dip-slip and strike-slip fault motions. The results of a two-dimensional dislocation pulse in which the rupture front propagates with an assumed speed have been compared with data recorded during the February 1971 San Fernando earthquakes. The consideration of the local geology on the surface motion is found to be absolutely necessary in obtaining reasonable motion.

The method of self-similar potentials has proven to be a direct and useful approach to the solution of two-dimensional dislocation problems involving two or more plane boundaries. In particular, the method allows for consideration of the presence of the free surface without major computational difficulties. The change in the cracking velocity and variation of the seismic properties of the material contained between the focus and the observation point can be simulated in a straight-forward manner.

The advantages of the analytical technique used in this study over the more usual approaches are as follows:

1. The existing procedures to generate theoretical design earthquakes are generally based upon the concept of a multipole of

forces equivalent to a point dislocation. To obtain displacements at a given site, the response of the point source model had to be integrated over the entire fault plane, a very lengthy computation. However, the spreading dislocation is a convenient basic problem when using the present approach, and the integration described above is automatically eliminated. Calculation of the point source dislocation is also a by-product of the analysis.

The computational difficulties inherent in the standard Laplace or Fourier transformation technique are totally absent in the method of self-similar potentials. The expressions for displacements derived in this study are in a particularly convenient form and the resulting integrals can be easily evaluated on the surface of the half space. The computations involve only quadrature in the complex η plane.

2. The method of self-similar potentials makes it possible to investigate the character of different disturbances (P, SV, and SH wave) separately. Contribution of each one of these waves, including the head wave disturbance, to the solution can be easily determined. In fact, the solution process is such that only physically meaningful quantities are involved.

Briefly, the results of this study indicate that the actual complexity of the ground motion can, for at least some earthquakes, be simulated with the help of a fairly simple and physically reasonable source model. The extension of the present method and development of a new concept of auxiliary complex

domain provide tools that are extremely useful in determination of the displacements on the surface of an elastic half space and of a layered half space. A number of important unsolved problems outlined in the next section can also be approached by adopting the present method of analysis.

6.2 Recommendations for Further Study

The method of ground motion calculation presented in this study can be further extended to include the problem of non-uniform rupture propagation. The effect of the cracking velocity and variation of the amplitude of dislocation with time needs to be investigated. As a result of dynamic friction on the surfaces of the fault plane and existence of local anomalies inside the earth, the faulting process might cease for a short period of time until further propagation takes place at a slightly later time. This phenomenon, a stick-slip motion, has been observed in the experimental dislocation models. The method of analysis adopted in this work seems to provide a promising approach to simulation of the stick-slip faulting, allowing computation of the surface motions.

The need for the extension of the present model to the much more difficult case in which the fault plane has a limited length is apparent. The significance of the three-dimensional models becomes obvious in determining the surface motions at points relatively far from the fault plane.

The motion in the bedrock was assumed to be caused by a single dislocation pulse with an arbitrary orientation. A more useful set of earthquake records can be constructed by developing a suitable stochastic model which allows synthesis of the response to dislocations in which length of the pulses,

their timing, and other parameters are taken as random. Finally, determination of the displacements on the surface of a multilayered half space may well be of considerable interest.

LIST OF REFERENCES

1. Hou, S. N., Earthquake simulation models and their applications, M.I.T. Dept. of Civil Eng., Res. Report R68-15 (1968), Cambridge, Mass.

2. Zeevaert, L., Strong ground motions recorded during earthquake of May the 11th and 19th, 1962 in Mexico City, Bull. Seism. Soc. Am., 54 (1964), 209-251.

3. Tsai, N. C. and Housner, G. W., Calculation of surface motion of a layered halfspace, Bull. Seism. Soc. Am., 60 (1970), 1625-1651.

4. Reid, H. F., The elastic rebound theory of earthquakes, Bull. Dep. Geol. Univ. Calif., 6 (1911), 413-444.

5. Chinnery, M. A., The deformation of the ground around surface faults, Bull. Seism. Soc. Am., 51 (1961, 355-372.

6. Knopoff, L., Energy release in earthquakes, Geophys. J., 1 (1958), 44-52.

7. Wyss, M. and Brune, J. N., The Alaska earthquake of 28 March 1964: A complex multiple rupture, Bull. Seism. Soc. Am., 57 (1967), 1017-1023.

8. Honda, H., The mechanism of the earthquakes, Sci. Rep. Tohoku Univ., Ser. 5, Geophys, 9 (1957), Suppl. 46.

9. Honda, H. and Masatsuka, A., On the mechanism of the earthquakes and the stresses producing them in Japan and its vicinity, Sci. Rep. Tohoku Univ. Ser. 5, Geophys., 4 (1952), 42-60.

10. Haskell, N. A., Elastic displacements in the near-field of a propagating fault, Bull. Seism. Soc. Am., 59 (1969), 865-908.

11. DeHoop, A. T., Representation theorems for the displacement in an elastic solid and their application to elastodynamic diffraction theory, Thesis, Technische Hogeschool, Delft, 1958.

12. Trifunac, M. D. and Udwadi, F. E., Parkfield, California, earthquake of June 37, 1966: A three-dimensional moving dislocation, Bull. Seis. Soc. Am., 64 (1974), 511-533.

13. Aki, K., Seismic displacements near a fault, J. Geophys. Res., 73 (1968), 5359-5376.

14. Maruyama, T., On the force equivalents to dynamical elastic dislocations with reference to the earthquake mechanism, Bull. Earthquake Res. Inst., 41 (1963), 687-697.

15. Burridge, R. and Knopoff, L., Body force equivalents for seismic dislocations, Bull. Seism. Soc. Am., 54 (1964), 1875-1888.

16. Burrdige, R., Lapwood, E. R. and Knopoff, L., First motion from seismic sources near a free surface, Bull. Seism. Soc. Am., 54 (1964), 1889-1913.

17. Knopoff, L., A matrix method for elastic wave problems, Bull. Seism. Soc. Am., 54 (1964), 431-438.

18. Abramovici, F., Numerical seismograms for a layered elastic solid, Bull. Seism. Soc. Am., 60 (1970), 1861-1876.

19. Kostrov, B. V., Self similar problems of propagation of shear cracks, PMM, Vol. 28, No. 5 (1964), 889-898.

20. Kostrov, B. V., The axisymmetric problem of propagation of a tension crack, PMM, Vol. 28, No. 4 (1964).

21. Brace, W. F. and Byerlee, J. C., Stick-slip as a mechanism for earthquakes, Science, 153 (1966), 990-992.

22. Byerlee, J. D., The mechanics of stick-slip, Tectonophysics, 9 (1970), 475-486.

23. Schwartz, M., Green, S. and Rutledge, W. A., Vector Analysis with Applications to Geometry and Physics, Harper, New York, 1960.

24. Sternberg, E., On the integration of the equations of motion in the classical theory of elasticity, Arch. Rational Mech. Anal., 6 (1960), 34-50.

25. Steketee, J. A., Some geophysical applications of the elasticity theory of dislocations, Can. J. Phys., 36 (1958), 1168-1197.

26. Smirnov, V. I. and Sobolev, S. L., On the application of a new method of investigation of the elastic vibrations in the space with axial symmetry, Trud. Inst. Seism. Akad. Nauk SSSR, 29 (1933).

27. Thompson, J. C. and Robinson, A. R., Exact Solution of Some Dynamic Problems of Indentation and Transient Loadings of an Elastic Half Space, Civil Engineering Studies, SRS 350, University of Illinois, Urbana, Illinois, September 1969.

28. Robinson, A. R. and Thompson, J. C., Transient stresses in an elastic half space resulting from the frictionless indentation of a rigid axially symmetric conical die, Proc. Camb. Phil. Soc., 76 (1974), 369-379.

29. Robinson, A. R. and Thompson, J. C., Transient stress states in an elastic half space resulting from the frictionless indentation of a rigid wedge-shaped die, Z. Angew. Math. Mech., 54-3 (1974), 139.

30. Johnson, J. J. and Robinson, A. R., Wave Propagation in a Half Space Due to an Interior Point Load Parallel to the Surface, Civil Engineering Studies, SRS 388, University of Illinois, Urbana, Illinois, July 1972.

31. Farewell, T. E. and Robinson, A. R., Wave Propagation in an Elastic Half Space Due to Couples Applied at a Point Beneath the Surface, Civil Engineering Studies, SRS 411, University of Illinois, Urbana, Illinois, August 1974.

32. Churchill, R. J., Complex Variables and Applications, Second Edition, McGraw-Hill, New York, 1960.

33. Steketee, J. A., On Volterras' dislocations in a semi-infinite elastic medium, Can. J. Phys., 36 (1958), 192-205.

34. Maruyama, T., Statical elastic dislocations in an infinite and semi-infinite medium, Bull. Earthquake Res. Inst., Tokyo Univ., 42 (1964), 289-368.

35. Geller, R. J., Representation theorems for an infinite shear fault, Geophys. J. R. astr. Soc., 39 (1974), 123-131.

36. Knopoff, L. and Gilbert, F., Radiation from a strike-slip fault, Bull. Seism. Soc. Am., 49 (1959), 163-178.

37. Heck, N. H., Earthquake, Princeton University Press, Princeton, 1936.

38. Newmark, N. M., Robinson, A. R., Ang. A.H-S., Lopez, L. A., and Hall, W. J., Methods for Determining Site Characteristics, Proc. Int. Conf. on Microzonation, Seattle, Wash., October 1972.

39. Kostrov, B. V., The theory of the focus for tectonic earthquakes, Izv., Earth Physics, 4 (1970), 84-101.

40. Love, A.E.H., A Treatise on the Mathematical Theory of Elasticity, Fourth edition, Dover, New York, 1944.

41. Mikumo, T., Faulting process of San Fernando earthquake of February 9, 1971, Bull. Seism. Soc. Am., 63 (1973), 249-269.

42. Kanamori, H., Seismological evidence for a lithospheric normal faulting--the Sanriku earthquake of 1933, Phys. Earth Planet. Interiors, 4 (1971), 289-300.

43. Smirnov, V. I., A Course of Higher Mathematics, Vol. III, Part 2, Addison-Wesley, Reading, Mass.

44. Sneddon, I. N., Elements of Partial Differential Equations, McGraw-Hill, New York, 1957.

45. Pekeris, C. L. and Lifson, H., Motion of the surface of a uniform half space produced by a buried pulse, J. Acous. Soc. Am., 29 (1957), 1233-1238.

46. Kanai, K., An empirical formula for the spectrum of strong ground motion, Bull. Earthquake Res. Inst., Tokyo Univ., 39 (1961), 85-96.

47. Lastrico, R. M., Duke, C. M. and Ohta, Y., Effects of site and propagation path on recorded strong earthquake motions, Bull. Seism. Soc. Am., 62 (1972), 933-954.

48. Ewing, W. N., Jardetzky, W. S. and Press, F., Elastic Waves in Layered Media, McGraw-Hill, New York, 1962.

49. Zvolinskii, N. V., Reflected and head waves emerging at a plane interface of two elastic media-I, Bulletin of the Academy of Sciences of the U.S.S.R., Geophysics Series, 10 (1957), 1-21.

50. Zvolinskii, N. V., Reflected waves and head waves arising at a plane interface between two elastic media-II, Izv. Geophysics Ser. (1958), 3-16.

51. Conte, S. D. and de Boor, C., Elementary Numerical Analysis, McGraw-Hill, New York, 1972.

52. Trifunac, M. D. and Hudson, D. E., Analysis of the Pacoima Dam Accelerograms, San Fernando, California, Earthquake of 1971, Bull. Seism. Soc. Am., 61 (1971), 1393-1411.

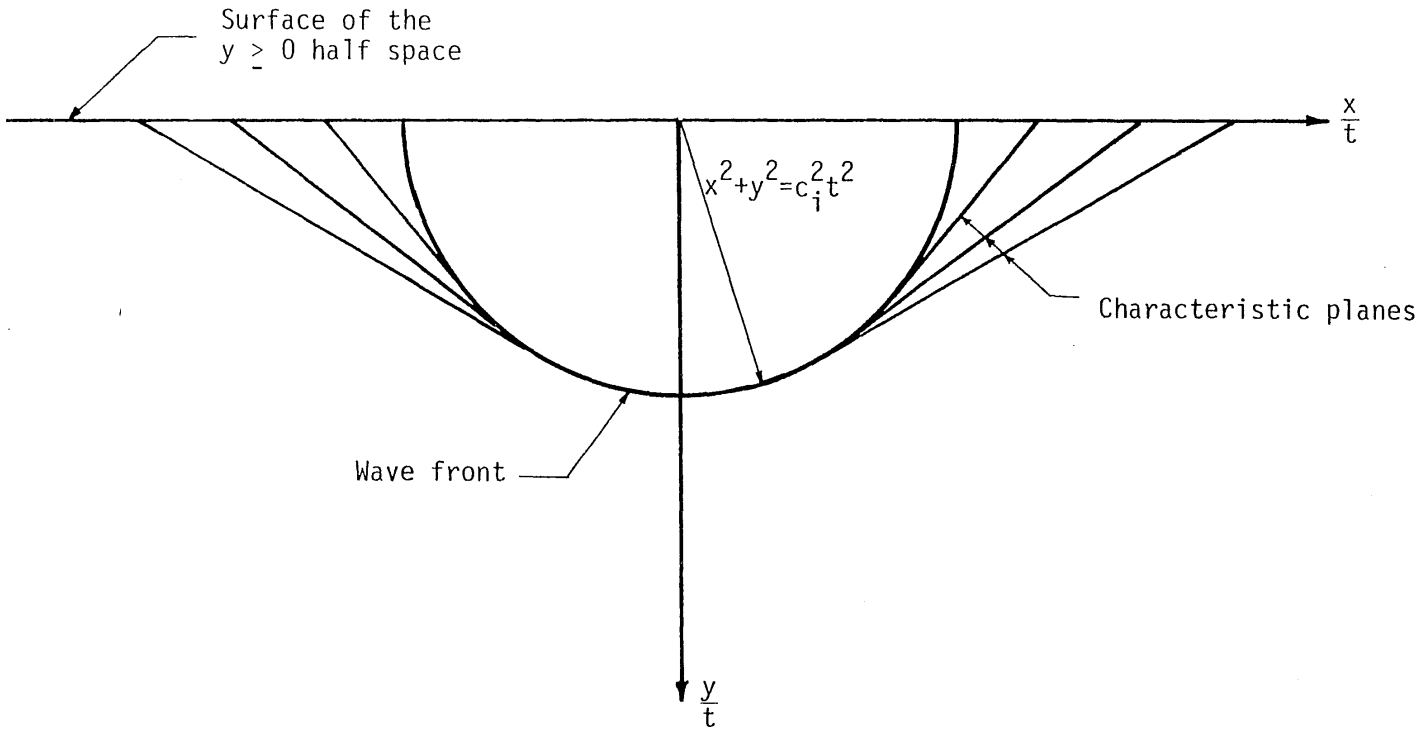

FIG. 1 TYPICAL CHARACTERISTIC PLANES TANGENT TO THE WAVE FRONT

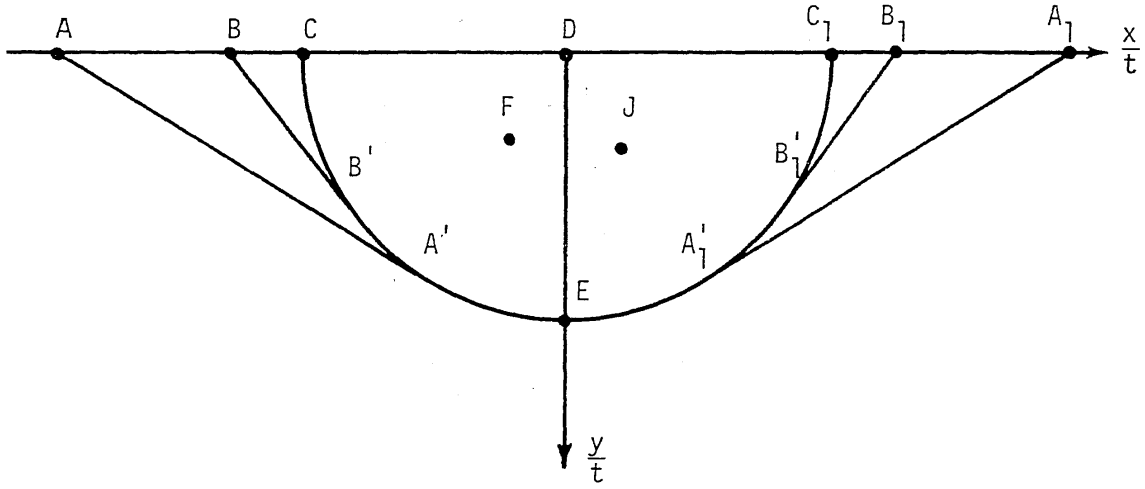

(a) Points in $y \geq o$ half plane

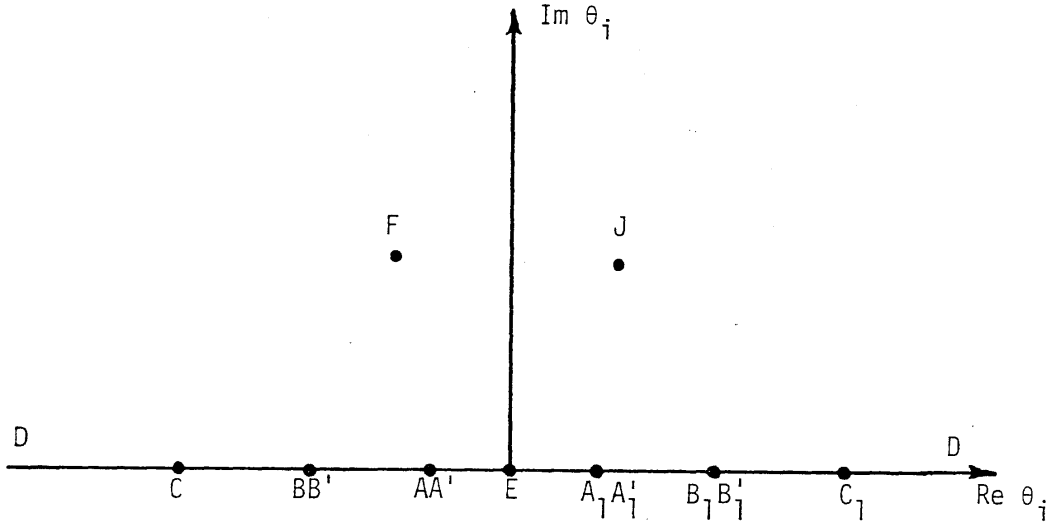

(b) The upper half of the complex θ_i plane

FIG. 2 MAPPING OF THE LOWER HALF SPACE INTO THE COMPLEX θ PLANE

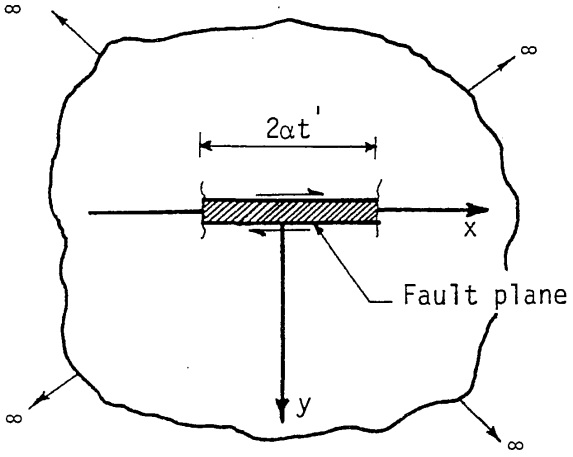

(a) Front view

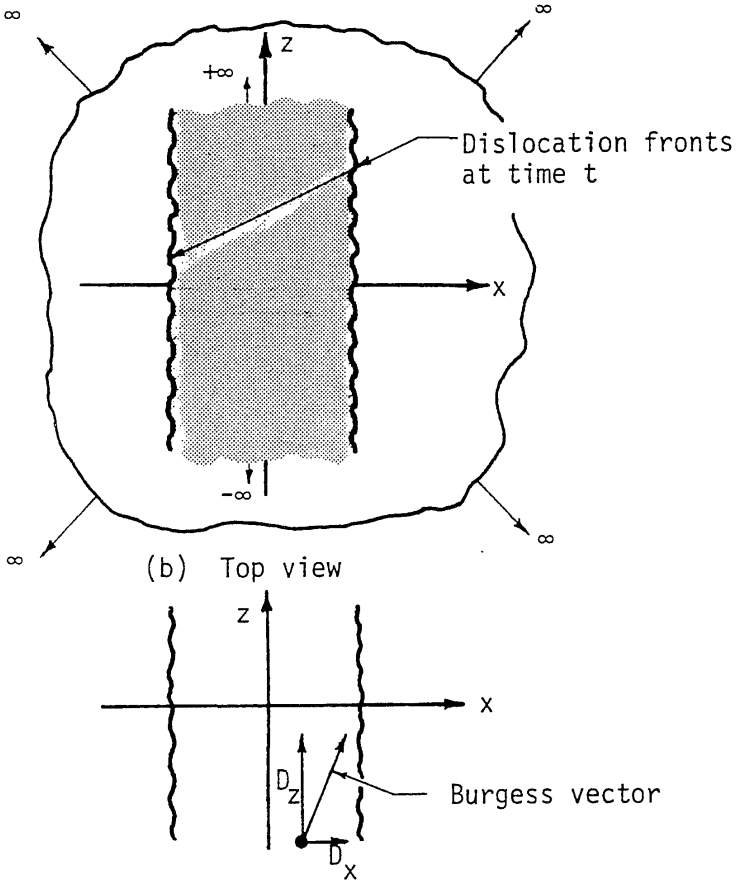

(b) Top view

(c) Dip-slip and strike-slip components of dislocation amplitude

FIG. 3 BILATERALLY PROPAGATING FAULT IN AN INFINITE MEDIUM

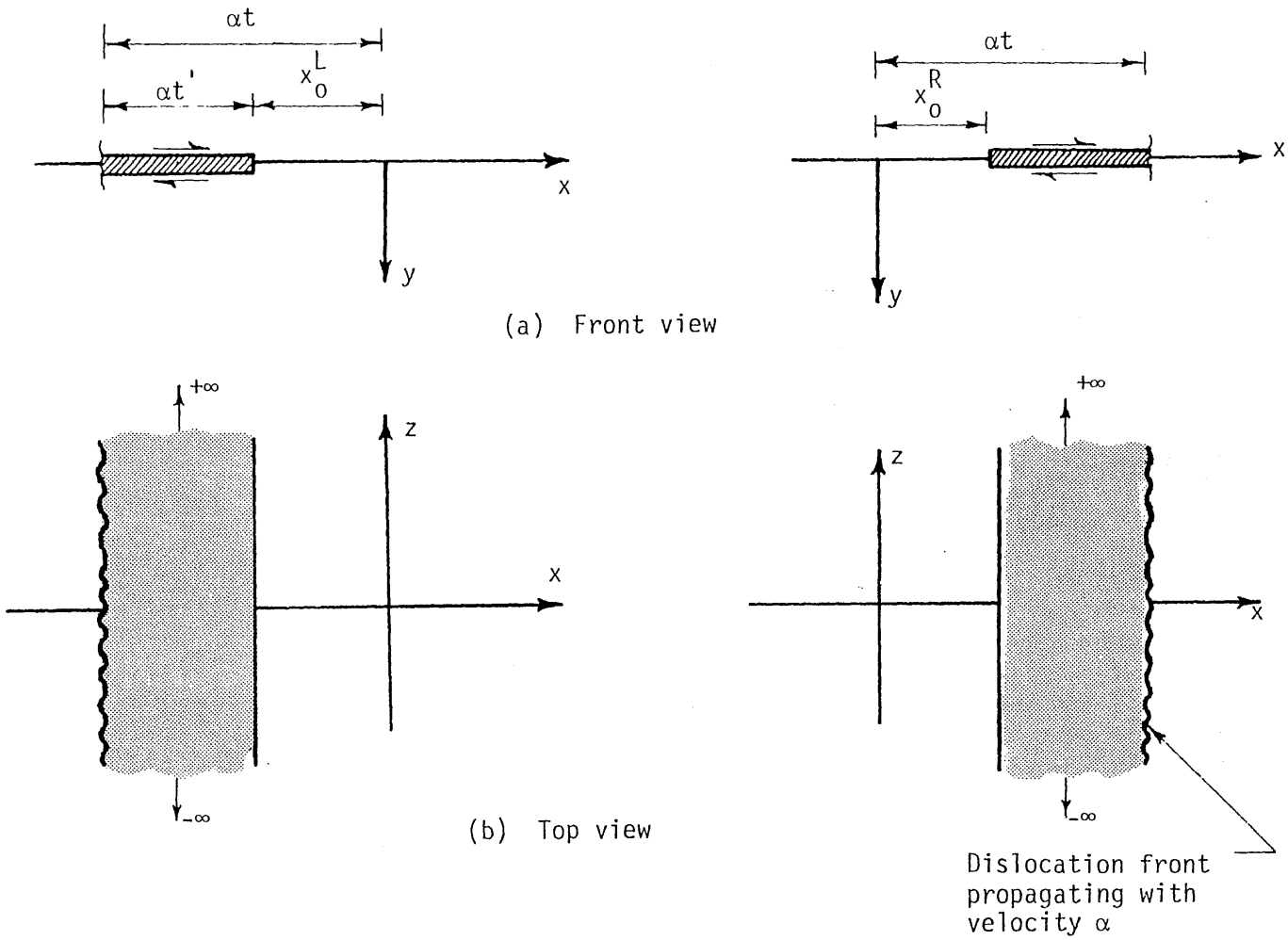

FIG. 4 UNILATERAL SHEAR FAULTS IN AN ELASTIC SOLID

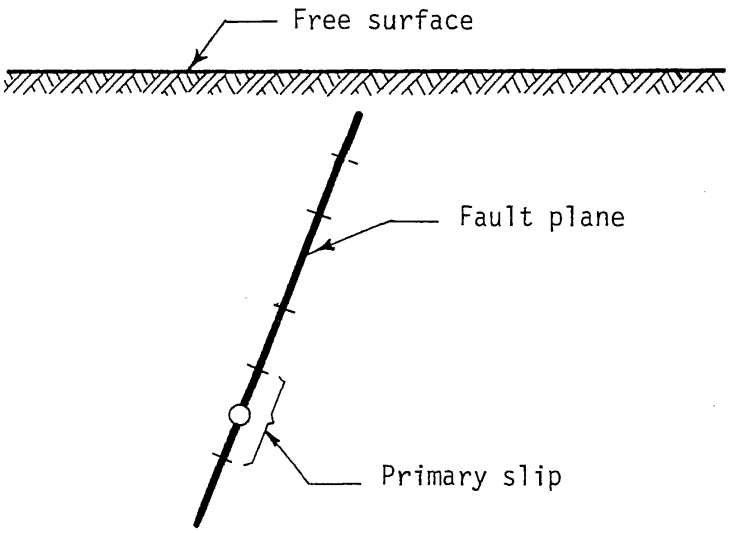

(a) Front view of the fault plane and elementary dislocation pulses

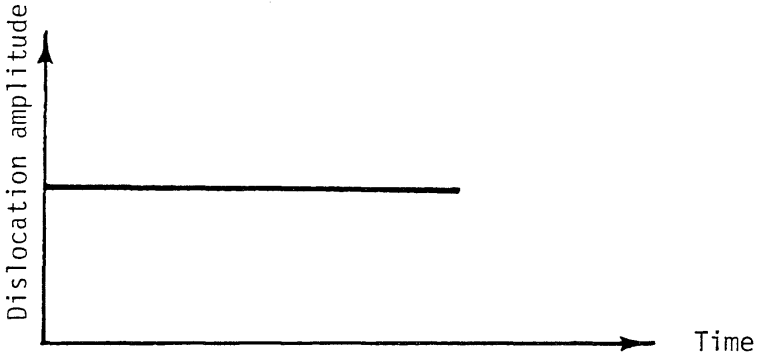

(b) Step dislocation at fault

FIG. 5 TWO-DIMENSIONAL FAULT MODEL CONSISTING OF A NUMBER OF PRIMARY SLIPS

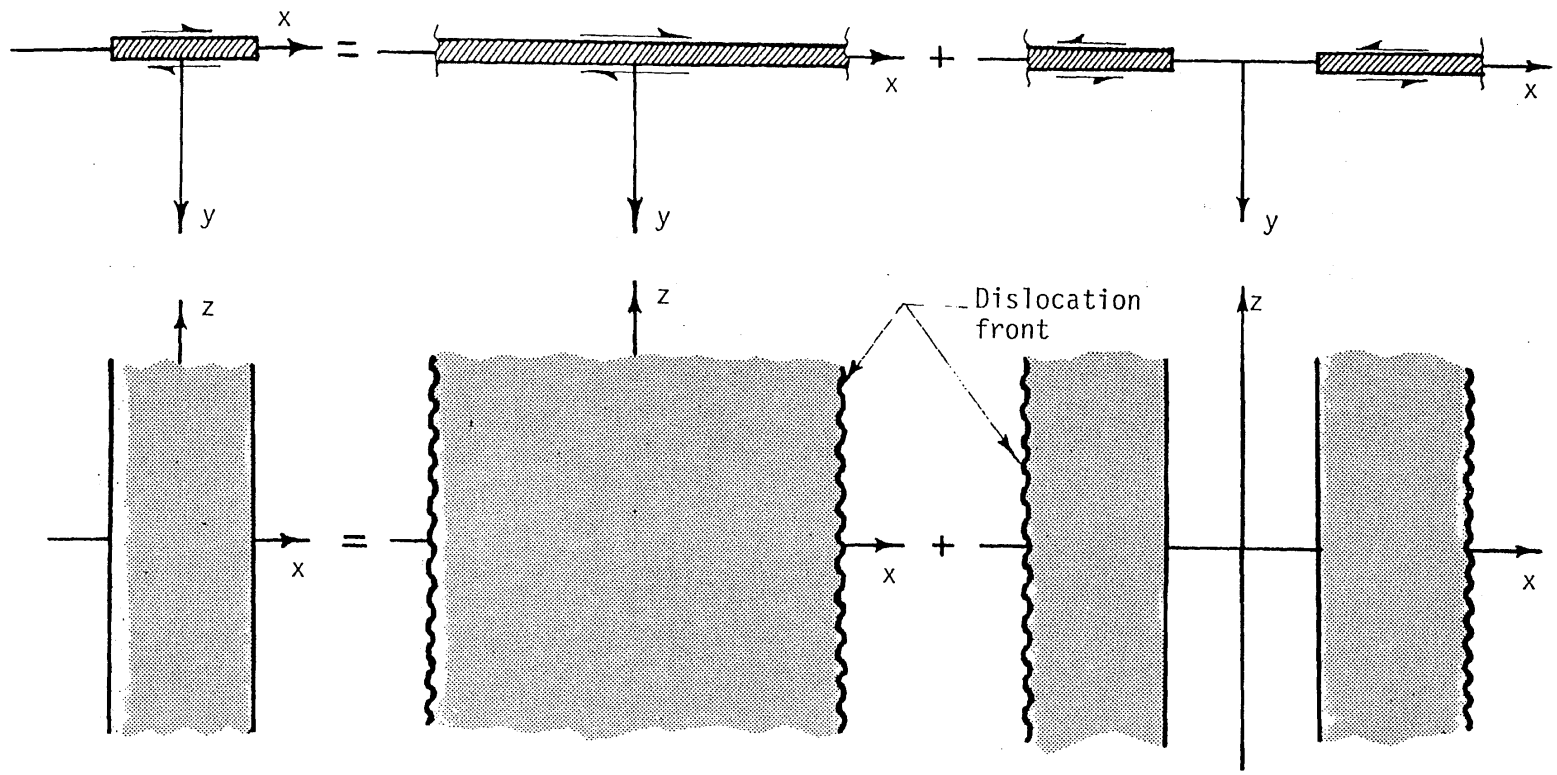

FIG. 6 SUPERPOSITION OF A BILATERAL FAULT (MAIN SOURCE) WITH TWO UNILATERAL DISLOCATIONS

P-wave velocity = 6.0 km/sec

S-wave velocity = 3.50 km/sec

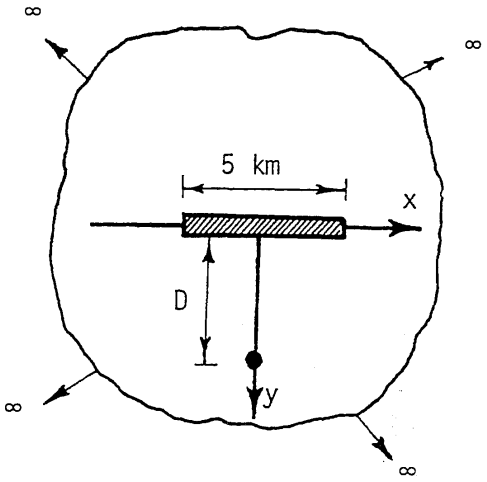

(a) Fault model front view

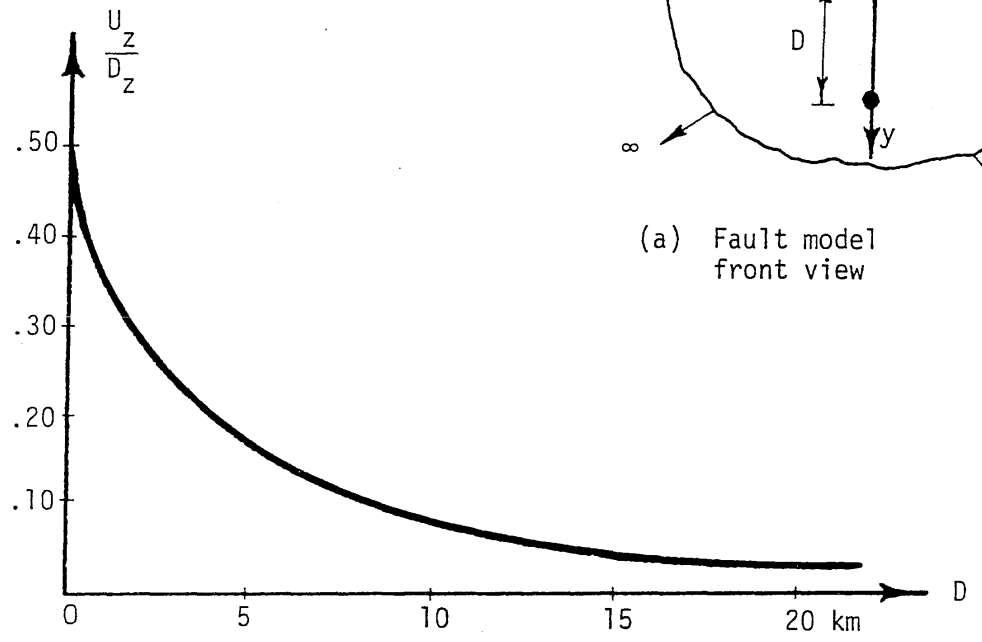

(b) U_z versus D (strike-slip)

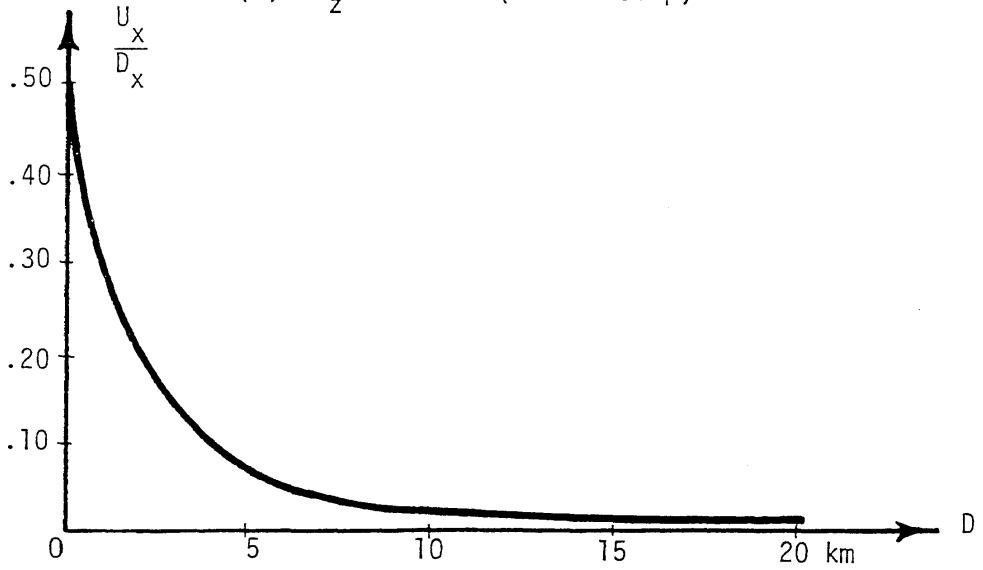

(c) U_x versus D (dip-slip)

FIG. 7 VARIATION OF THE RESIDUAL DEFORMATIONS WITH DISTANCE FROM THE FAULT PLANE

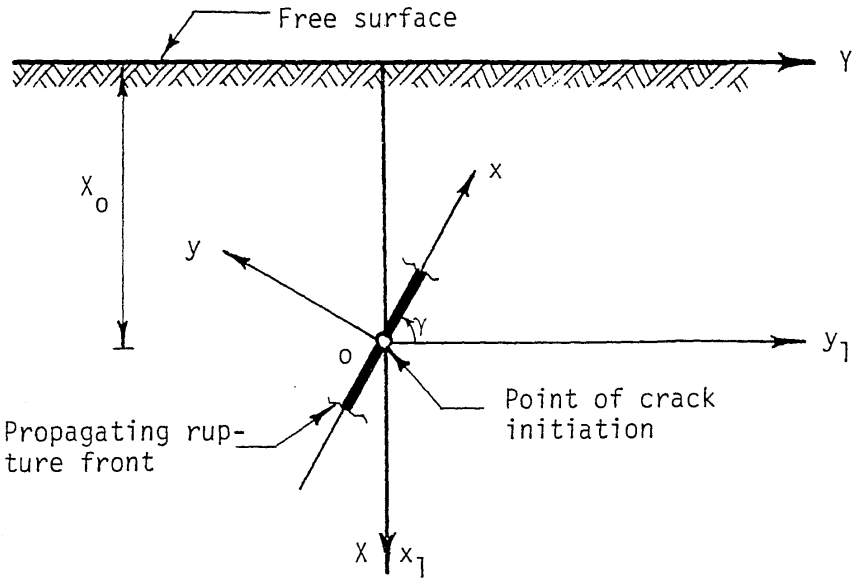

FIG. 8 BILATERAL DISLOCATION FAULT WITH AN ARBITRARY DIP ANGLE γ

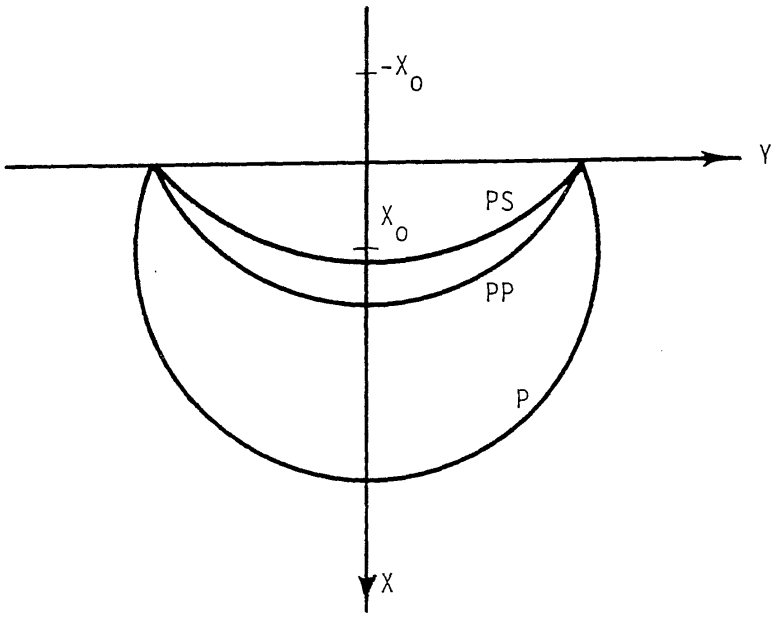

FIG. 9 TYPICAL WAVE FRONTS FOR THE INCIDENT P-WAVE AND REFLECTED PP AND PS WAVES

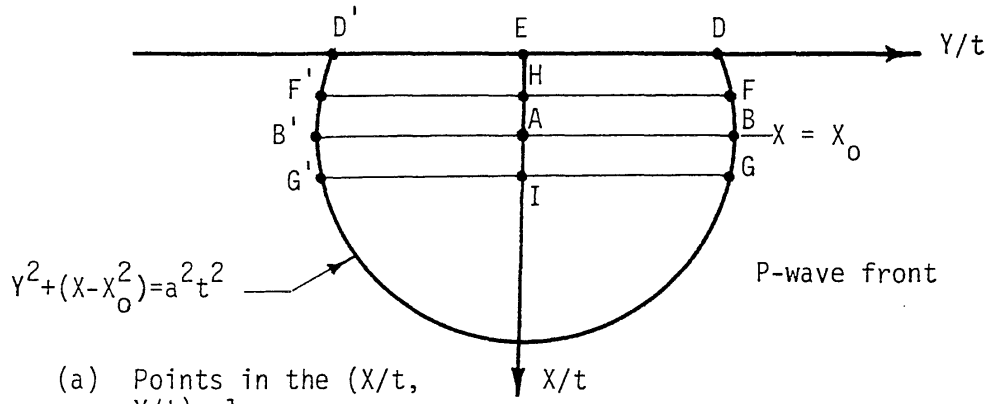

(a) Points in the (X/t, Y/t) plane

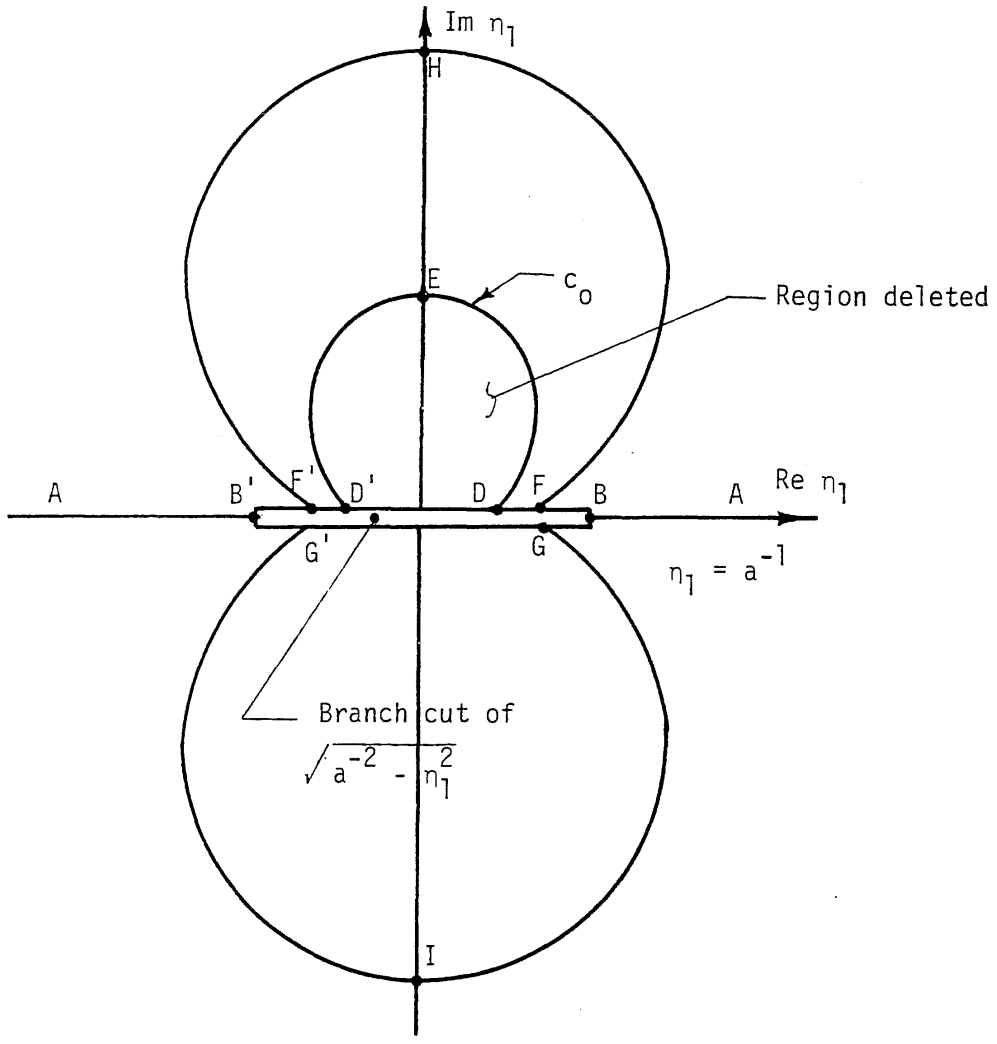

(b) Complex η_1 plane

FIG. 10 MAPPING OF THE $X \geq 0$ HALF PLANE INTO THE COMPLEX η_1 PLANE

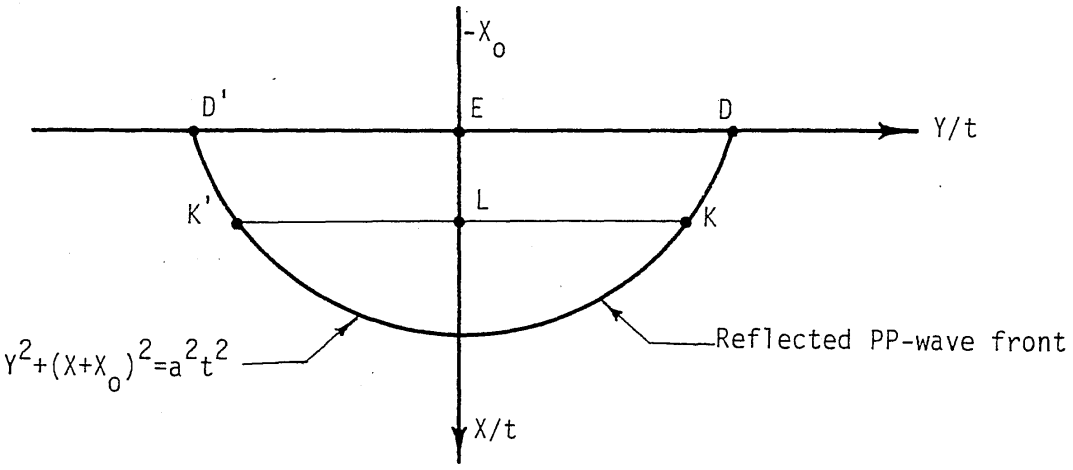

(a) Points in the (X/t, Y/t) plane

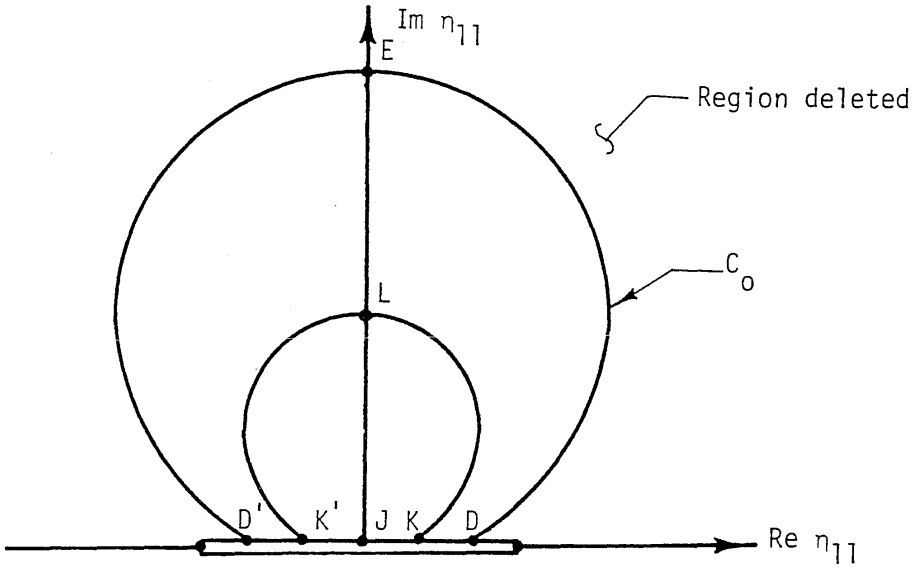

(b) Complex η_{11} plane

FIG. 11 MAPPING OF THE $X \geq 0$ HALF PLANE INTO THE COMPLEX η_{11} PLANE

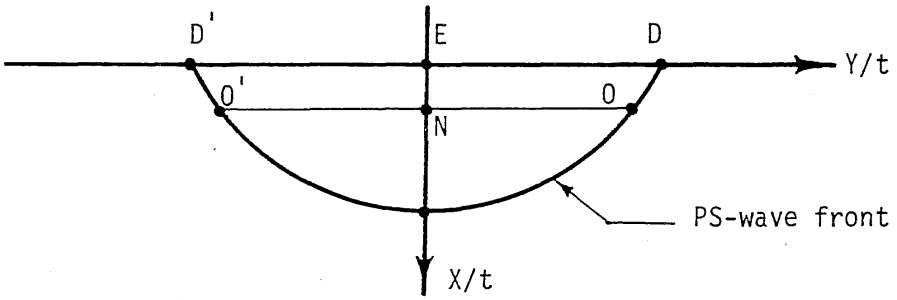

(a) Points in the (X/t, Y/t) plane

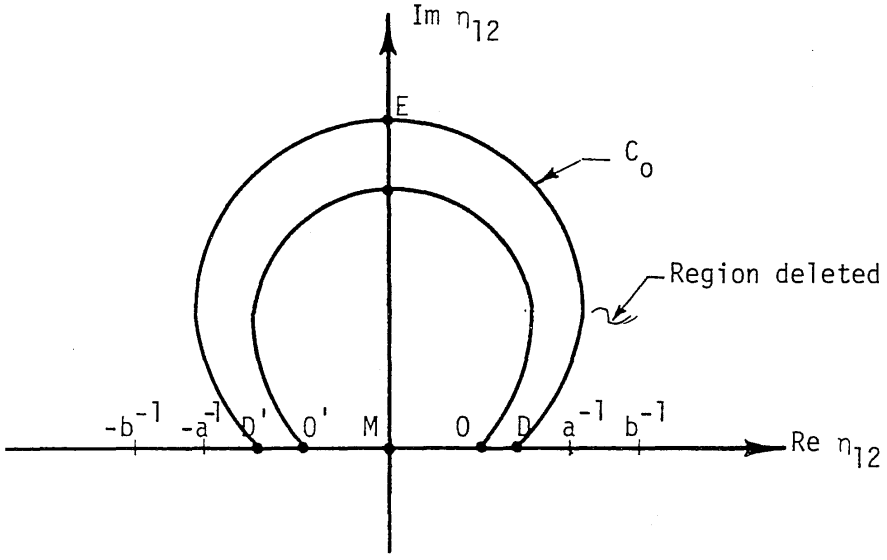

(b) Complex η_{12} plane

FIG. 12 MAPPING OF THE $X \geq 0$ HALF SPACE INTO THE COMPLEX η_{12} PLANE

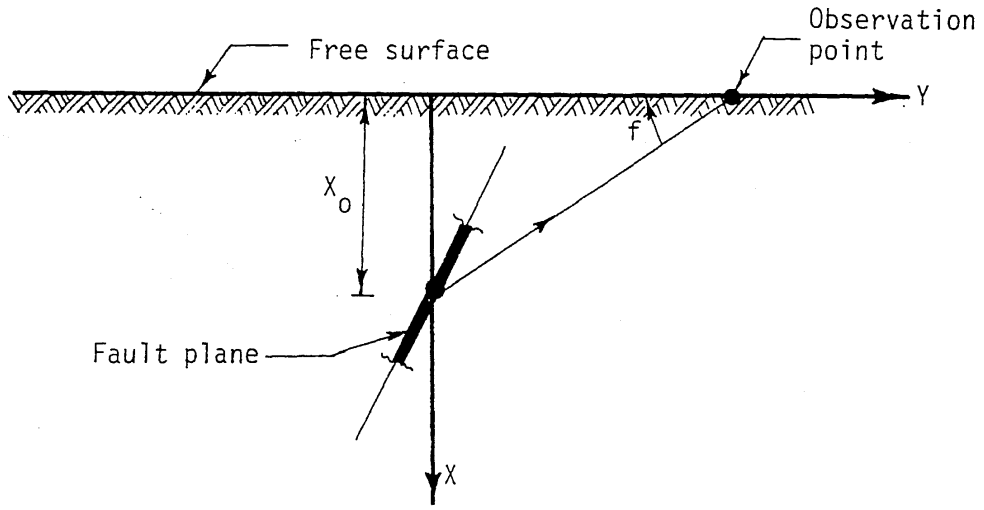

(a) Angle of incidence

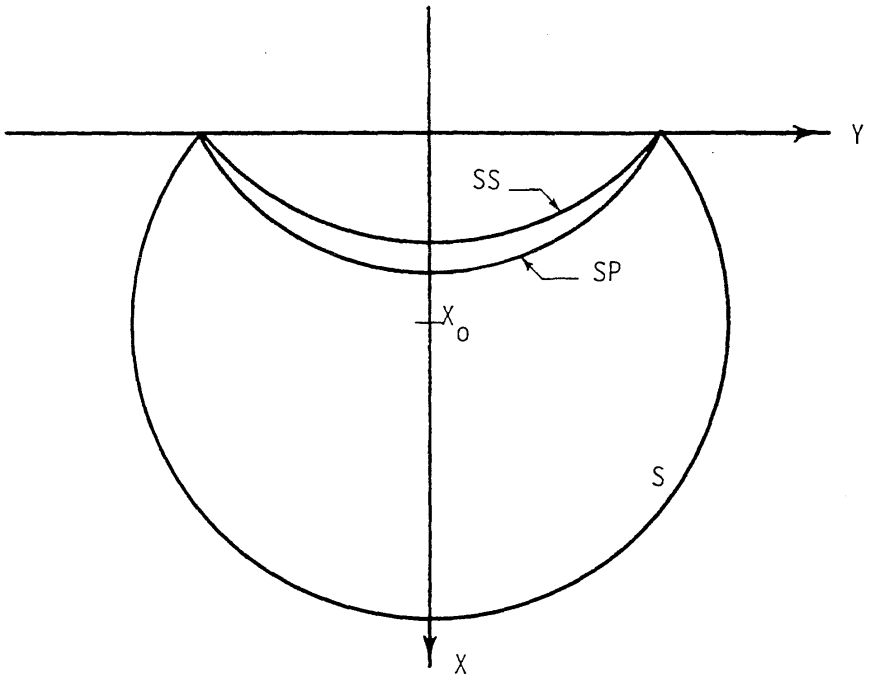

(b) Incident S and reflected SS and SP wave fronts

FIG. 13 TYPICAL WAVE FRONTS FOR THE S, SS, AND SP WAVES WHEN $f \geq \cos^{-1}(b/a)$

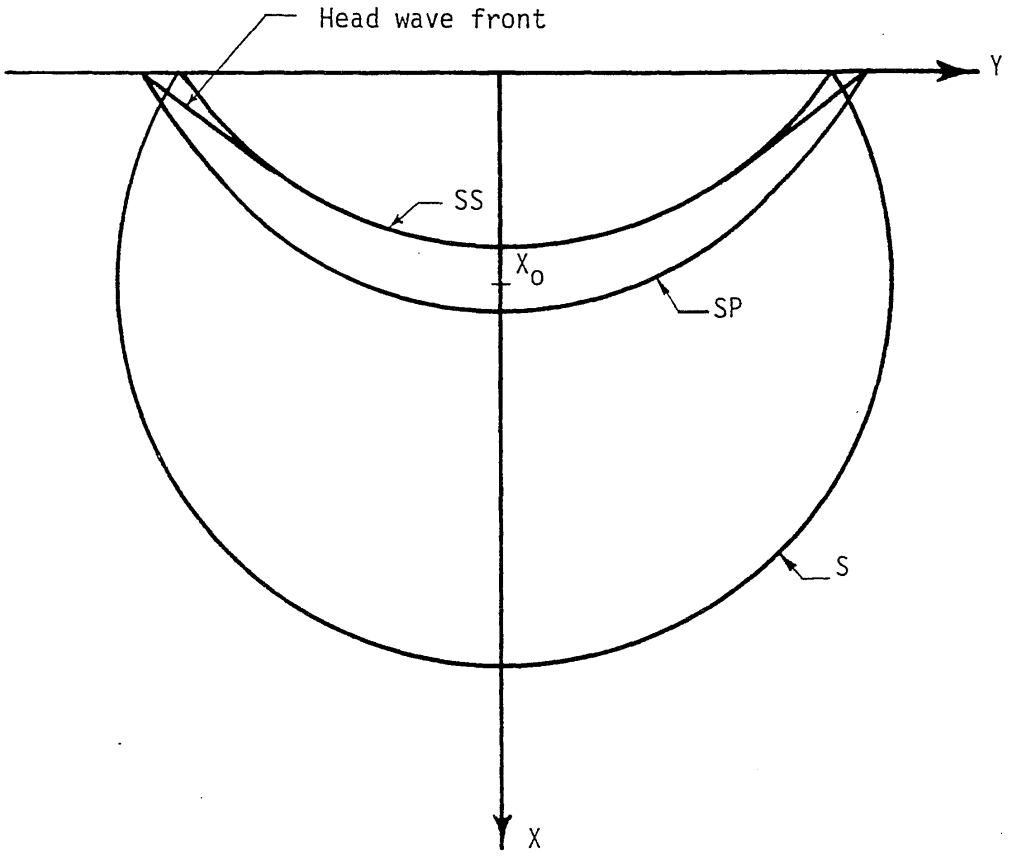

FIG. 14 TYPICAL WAVE FRONTS FOR THE S, SS, AND SP WAVES WHEN $f < \cos^{-1}(b/a)$

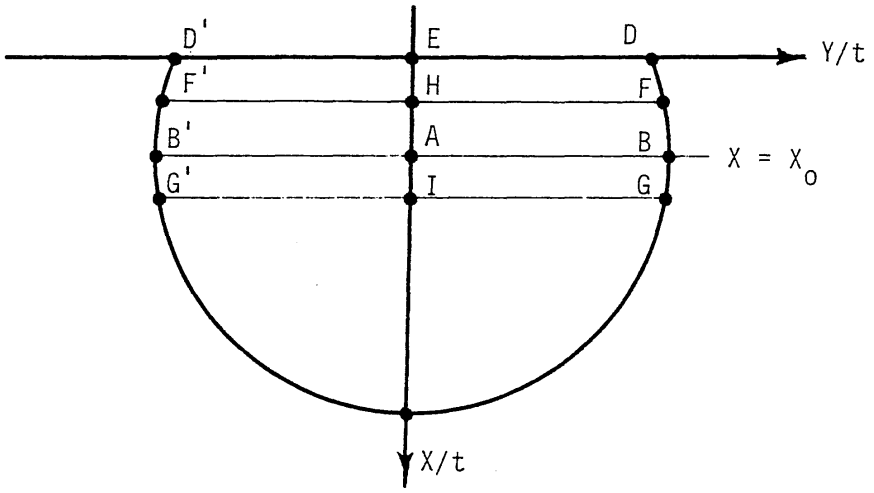

(a) Points in the (X/t, Y/t) plane

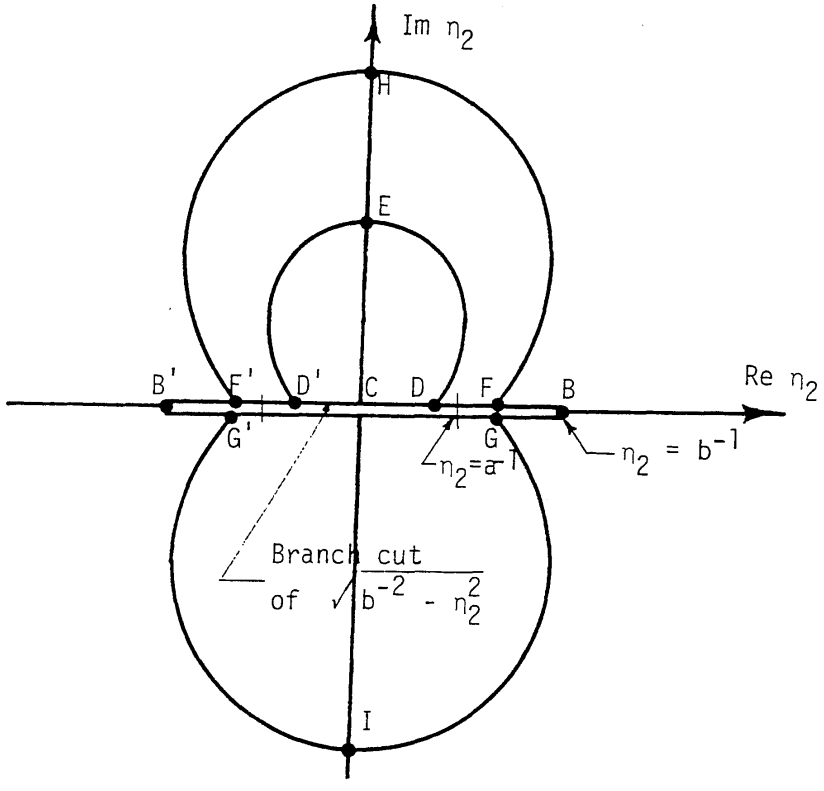

(b) Complex η_2 plane

FIG. 15 MAPPING OF THE $X \geq 0$ HALF SPACE INTO THE COMPLEX η_2 PLANE WHEN $f > \cos^{-1}(b/a)$

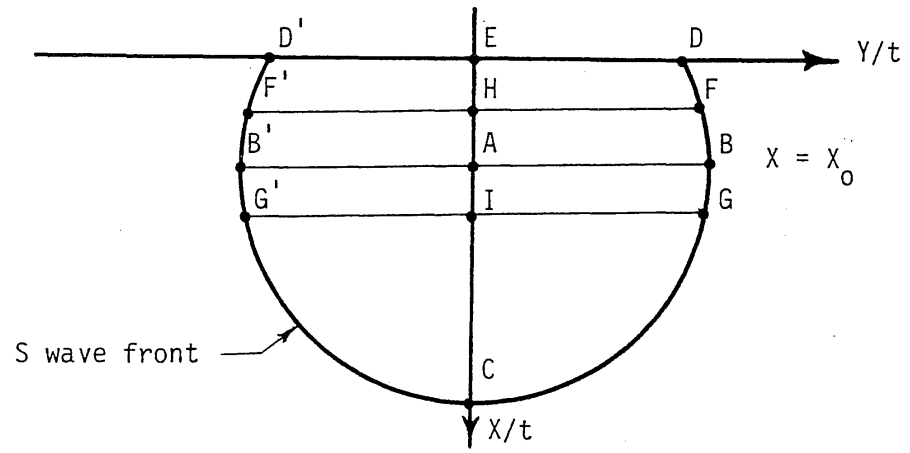

(a) Points in the (X/t, Y/t) plane

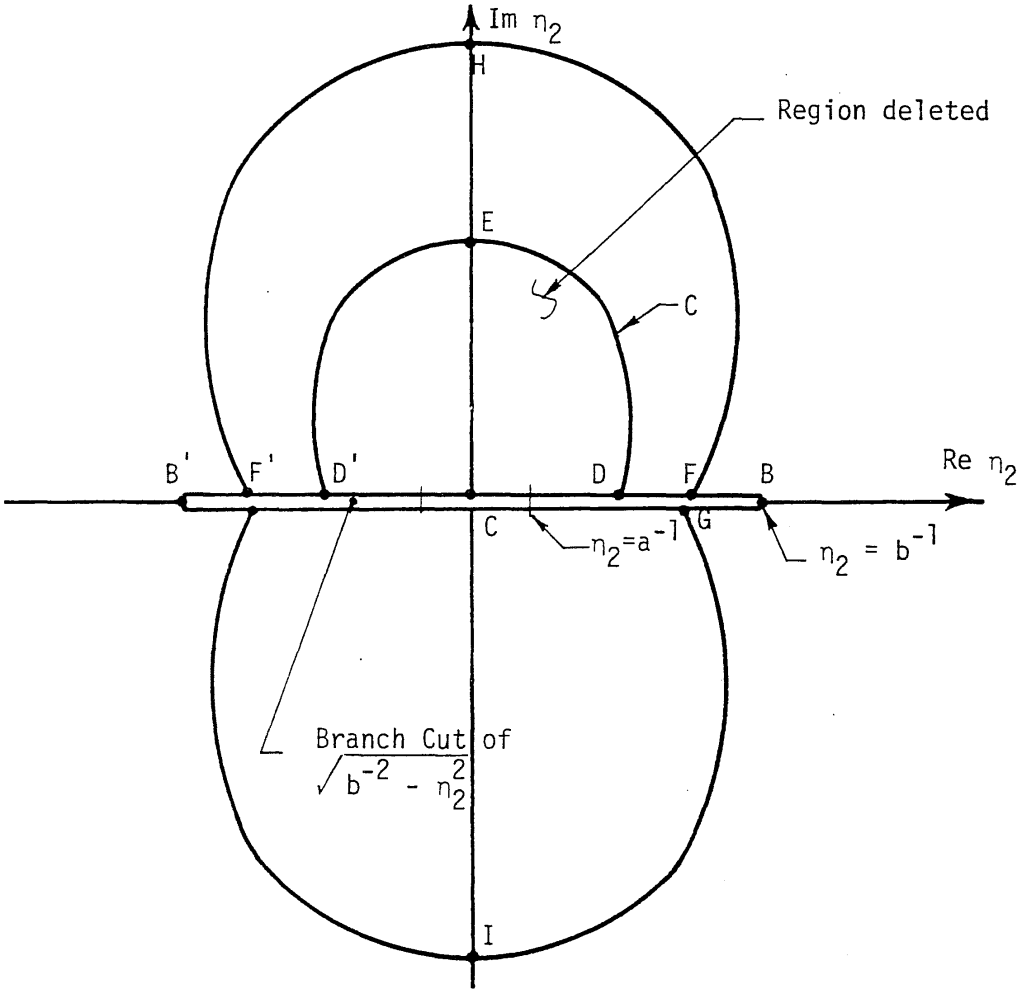

(b) Complex η_2 plane

FIG. 16 MAPPING OF THE $X \geq 0$ HALF SPACE INTO THE COMPLEX η_2 PLANE FOR $f < \cos^{-1}(b/a)$

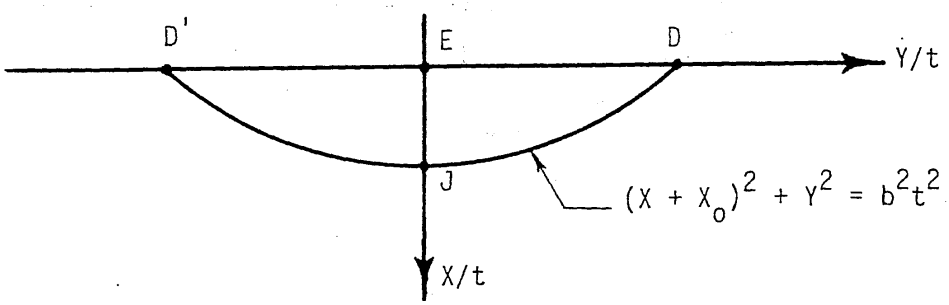

(a) Points in the (X/t, Y/t) plane

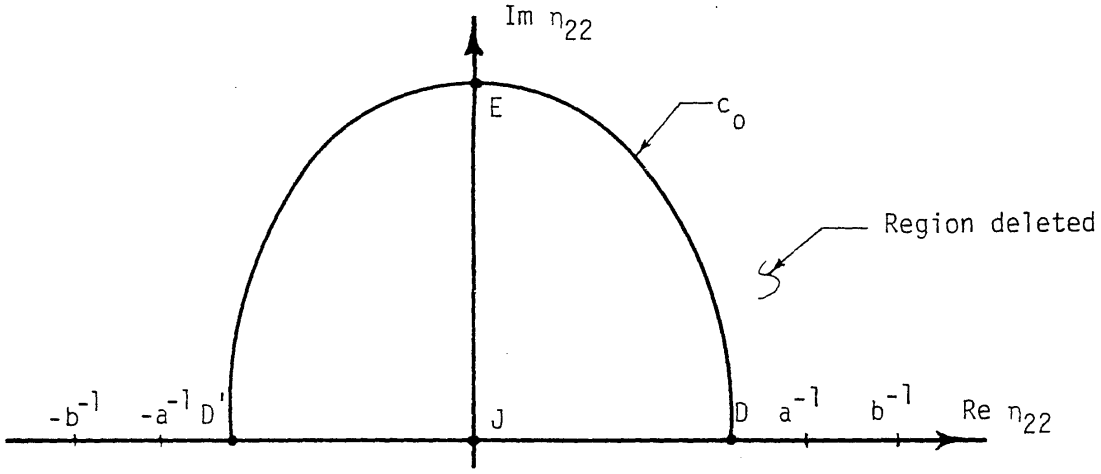

(b) Complex η_{22} plane

FIG. 17 MAPPING OF THE $X \geq 0$ HALF SPACE INTO THE COMPLEX η_{22} PLANE FOR $f > \cos^{-1}(b/a)$

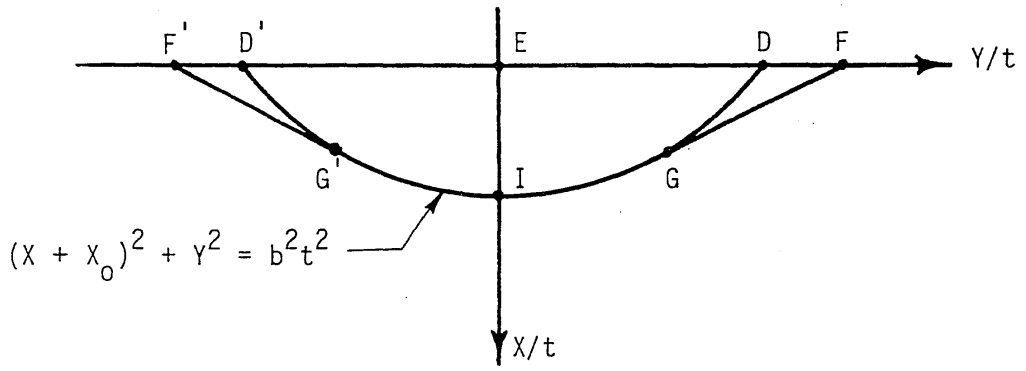

(a) Points in the (X/t, Y/t) plane

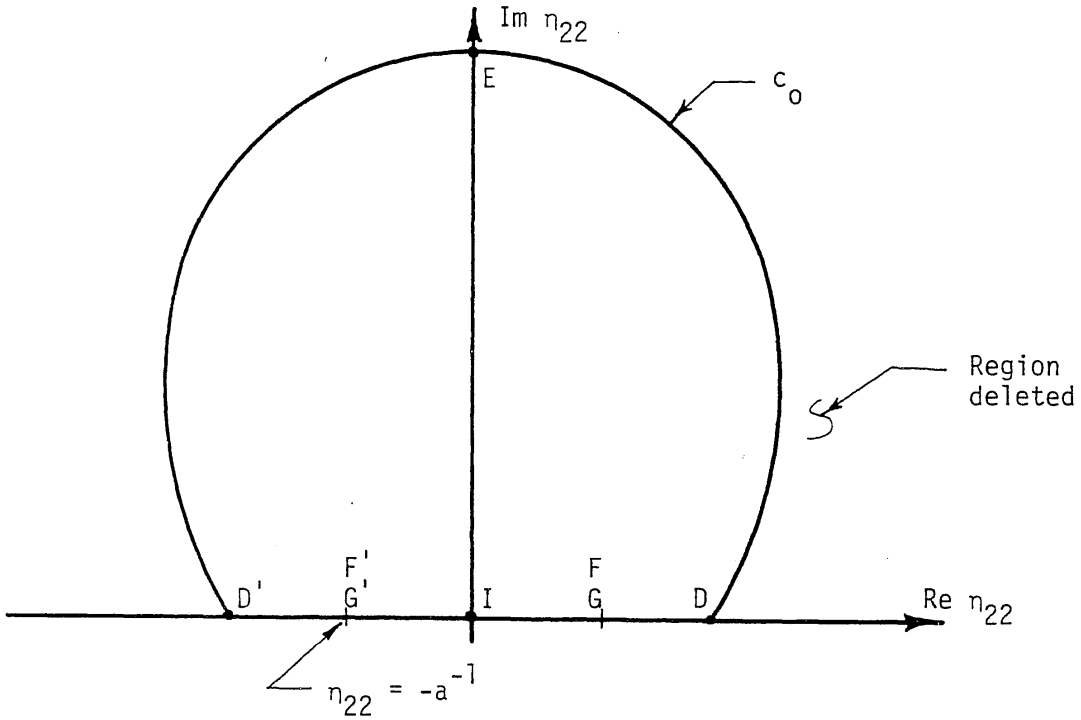

(b) Complex η_{22} plane

FIG. 18 MAPPING OF THE $X \geq 0$ HALF SPACE INTO THE COMPLEX η_{22} PLANE FOR $f < \cos^{-1}(b/a)$

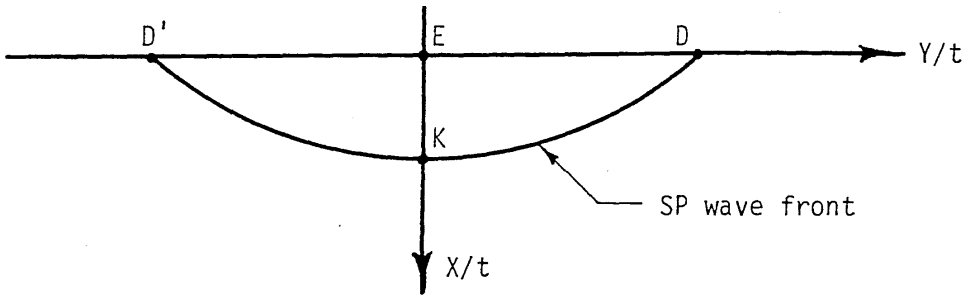

(a) Points in the (X/t, Y/t) plane

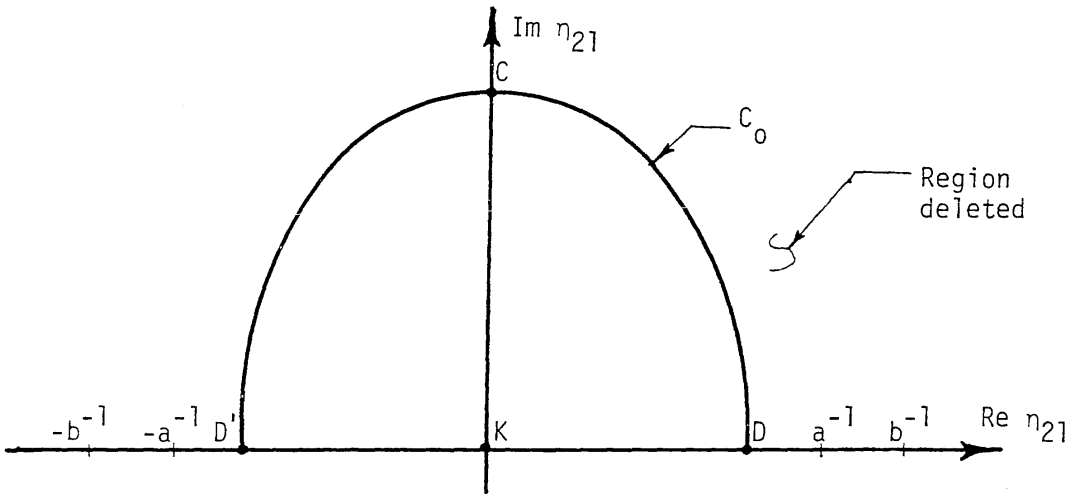

(b) Complex η_{21} plane

FIG. 19 MAPPING OF THE X > 0 HALF SPACE INTO THE COMPLEX η_{21} PLANE FOR $f > \cos^{-1}(b/a)$

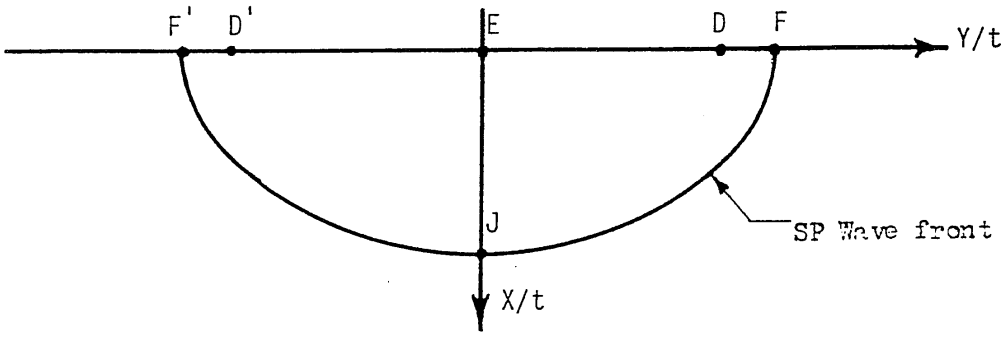

(a) Points in the (X/t, Y/t) plane

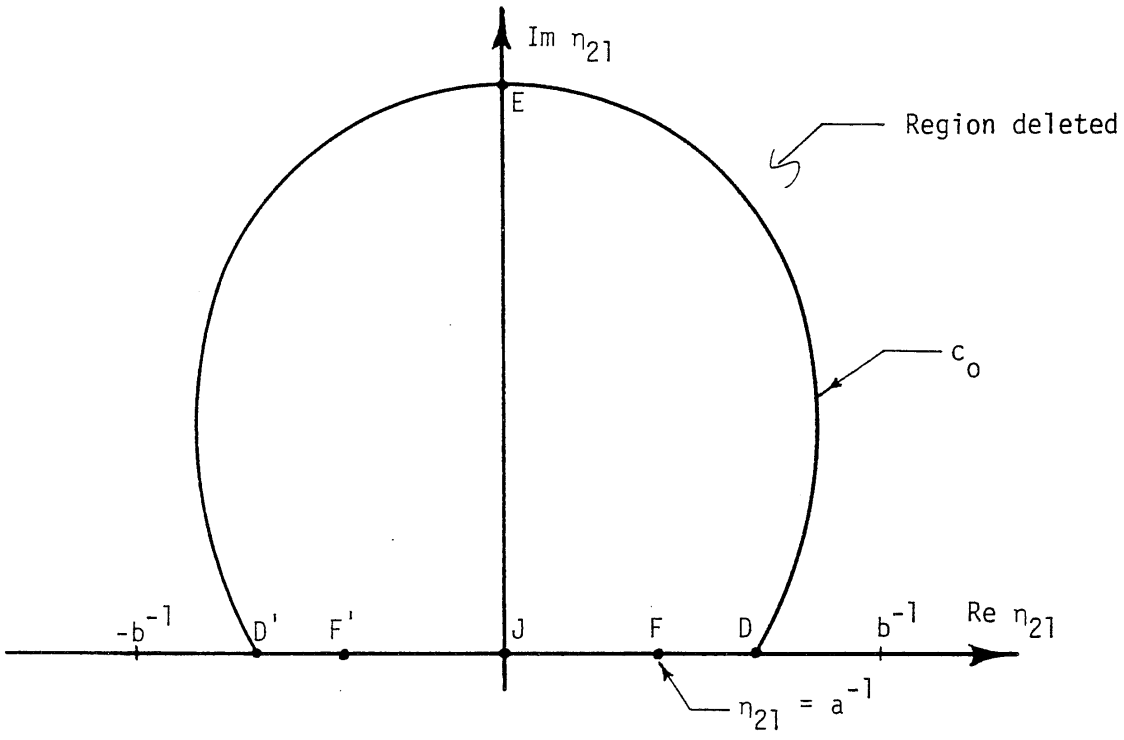

(b) Complex η_{21} plane

FIG. 20 MAPPING OF THE $X \geq 0$ HALF SPACE INTO THE COMPLEX η_{21} PLANE FOR $f < \cos^{-1}(b/a)$

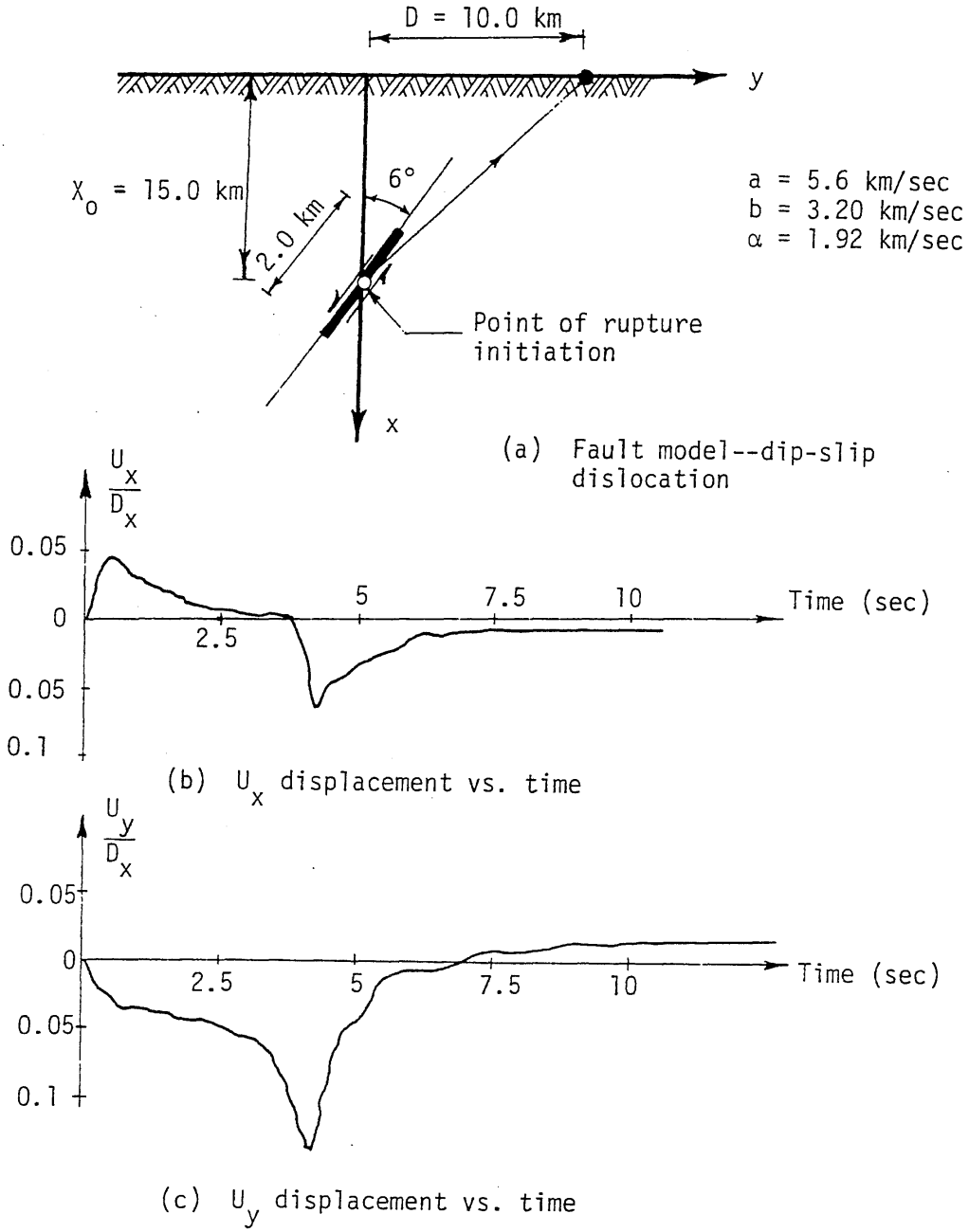

FIG. 21 TIME HISTORIES OF THE VERTICAL AND HORIZONTAL MOTION AT X = 0 AND Y = 10 KM

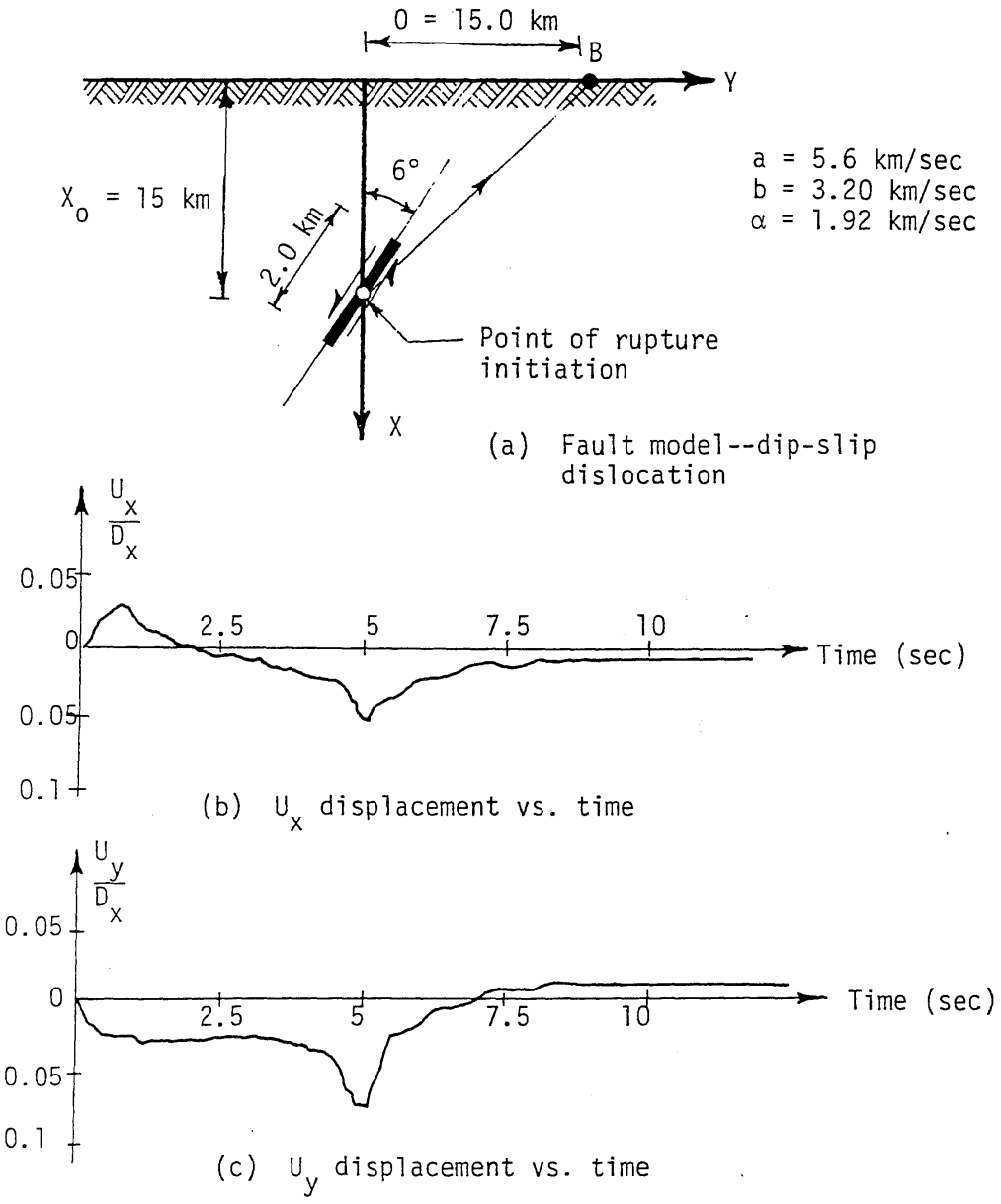

FIG. 22 TIME HISTORIES OF THE VERTICAL AND HORIZONTAL MOTION AT X = 0 AND Y = 15.0 KM

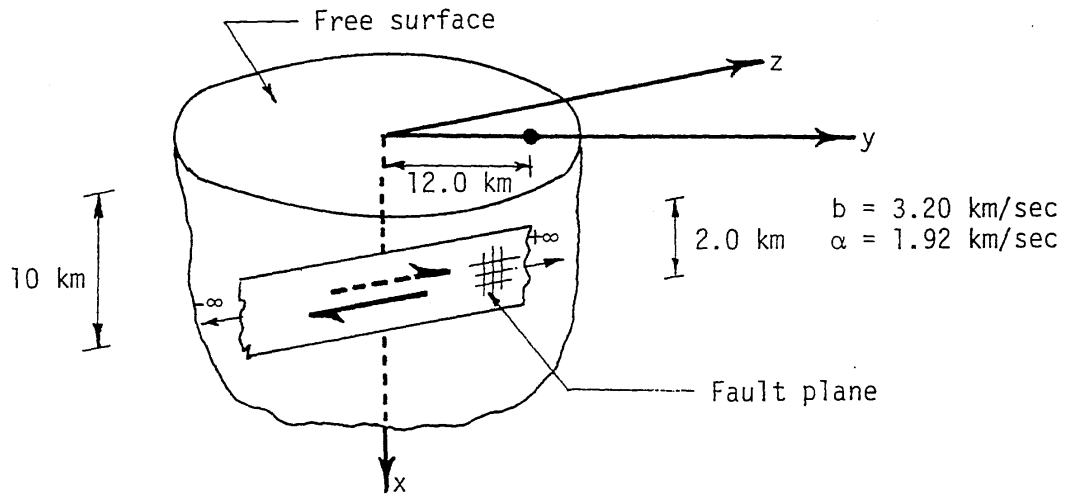

(a) Two-dimensional dislocation model (strike-slip faulting)

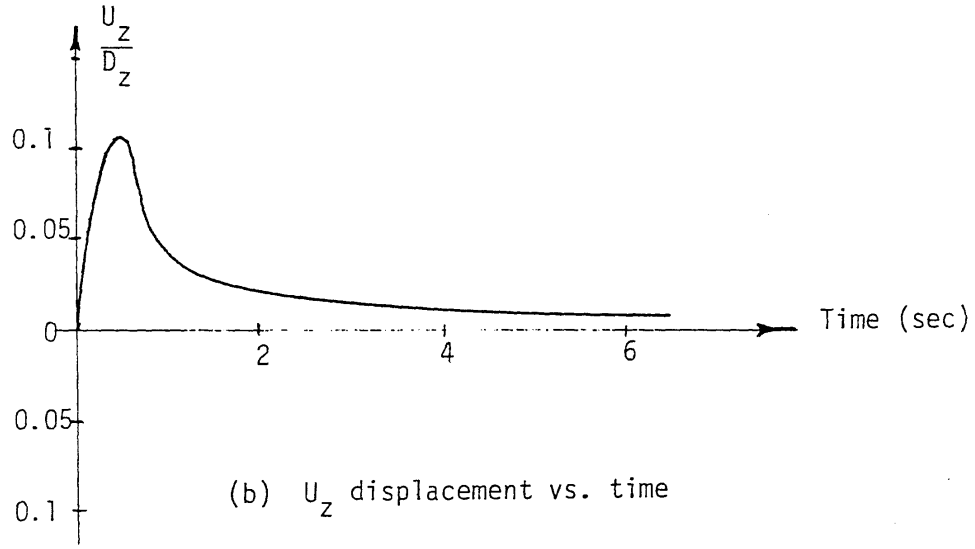

(b) U_z displacement vs. time

FIG. 23 SURFACE MOTION AT (X = 0, Y = 12 KM) DUE TO STRIKE-SLIP DISLOCATION

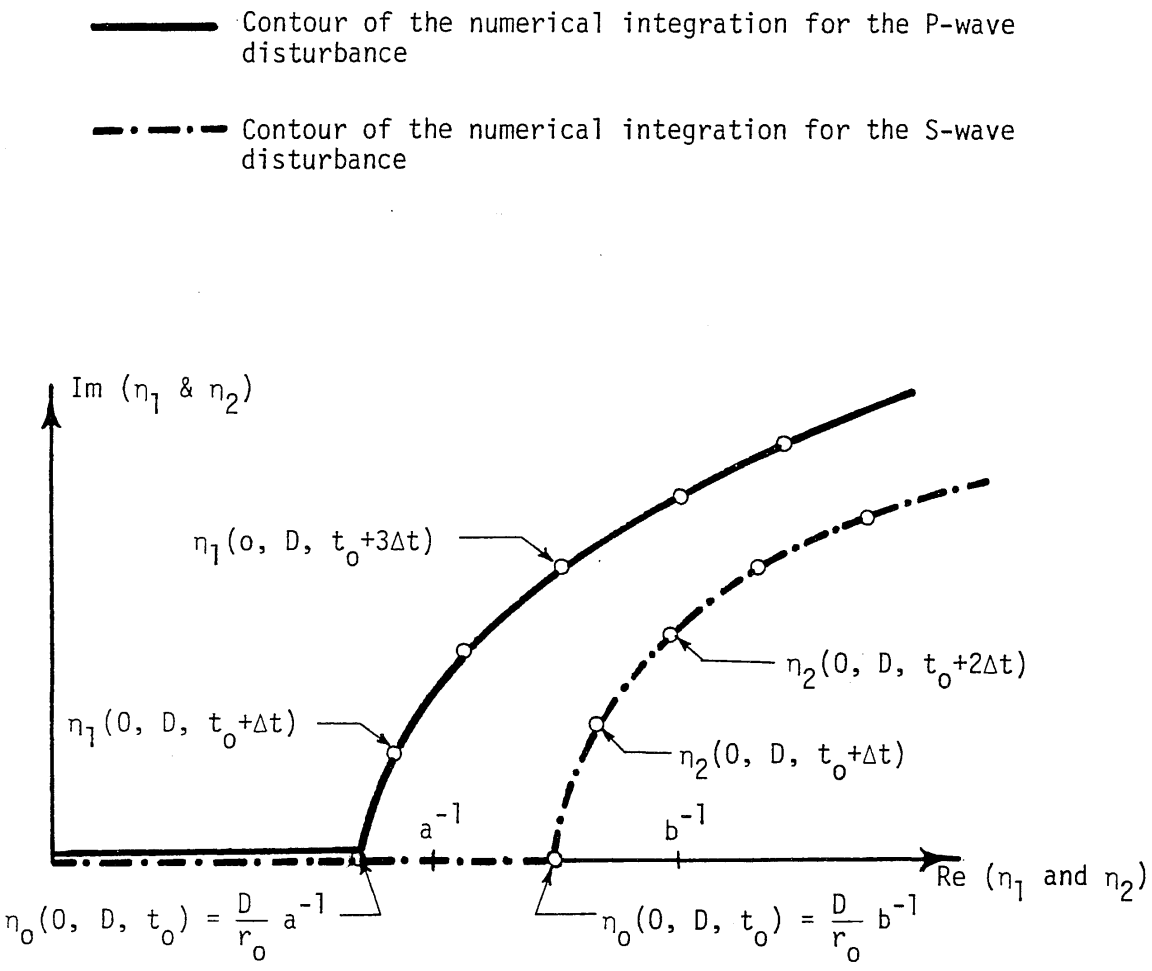

FIG. 24 TRACES OF $\eta_1(0, D, t)$ AND $\eta_2(0, D, t)$ IN THE COMPLEX η_1 AND η_2 PLANE

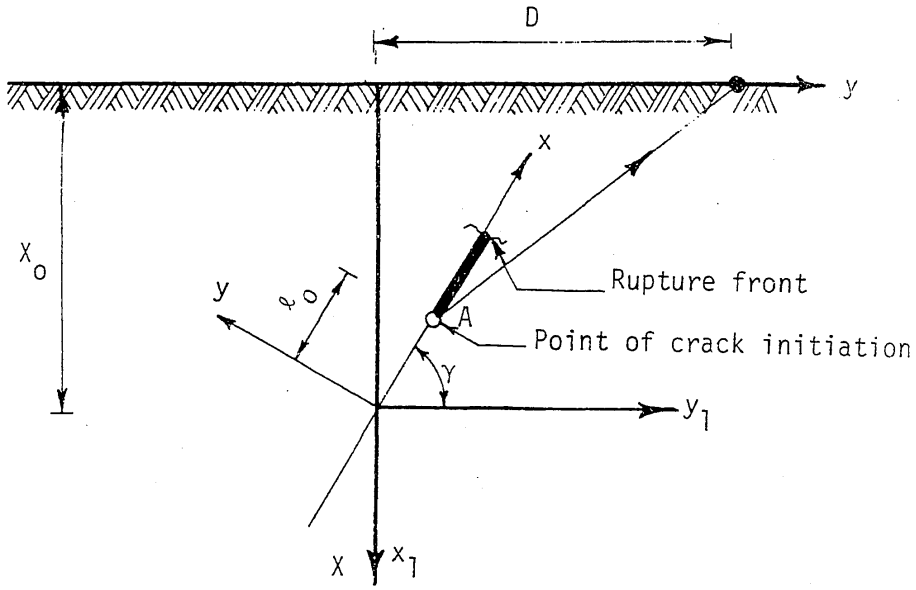

FIG. 25 UNILATERAL SHEAR FAULT PROPAGATING WITH VELOCITY α

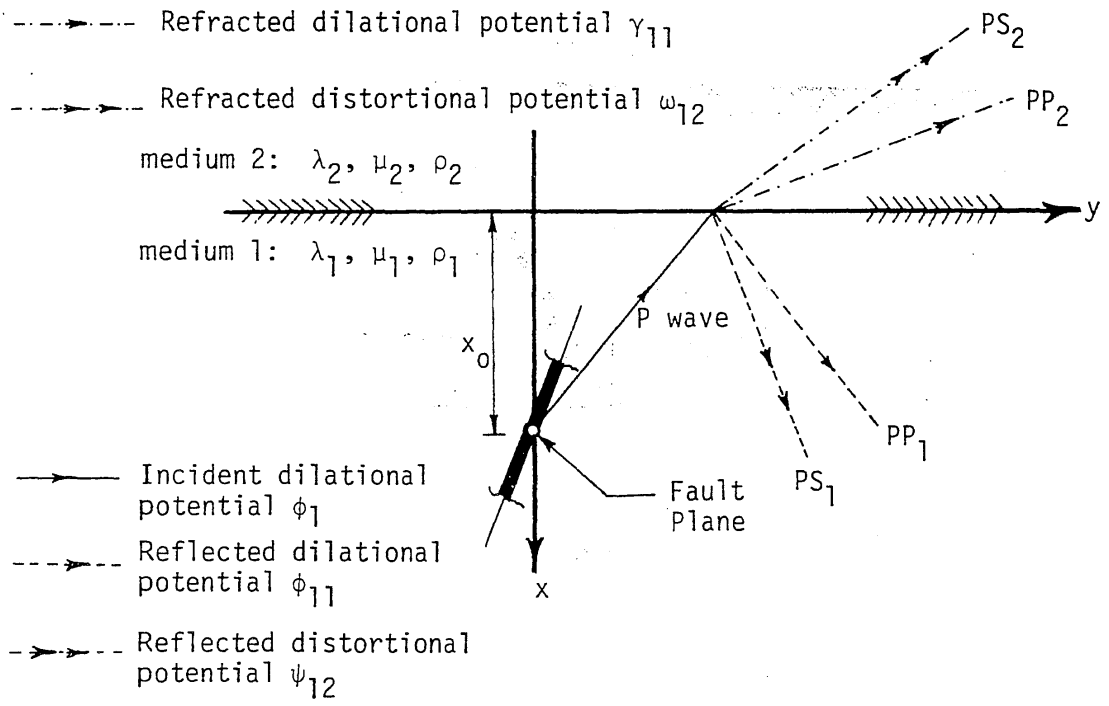

FIG. 26 REFLECTION AND REFRACTION OF P WAVE AT AN INTERFACE BETWEEN TWO ELASTIC SOLIDS

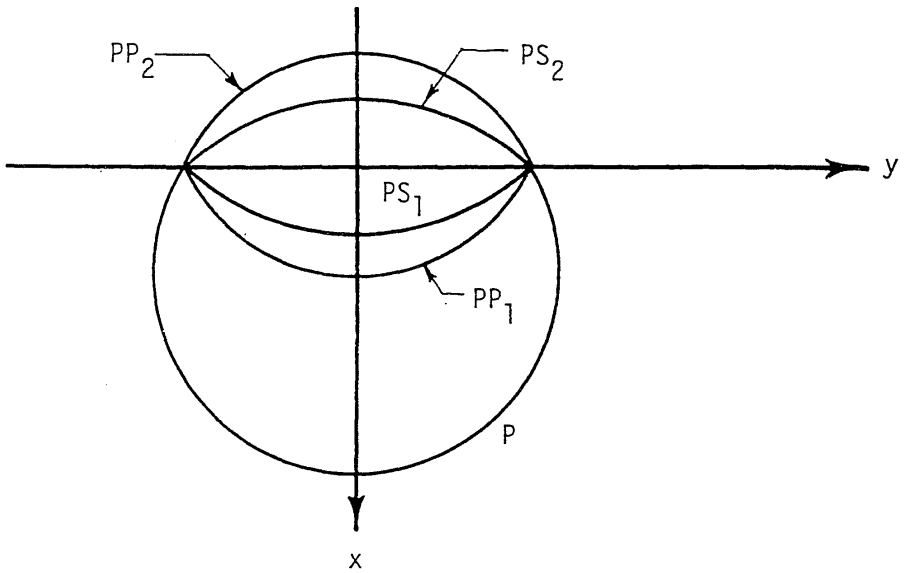

FIG. 27 WAVE FRONT PATTERN FOR AN INCIDENT P WAVE WITH $a_1 > b_1 > a_2 > b_2$

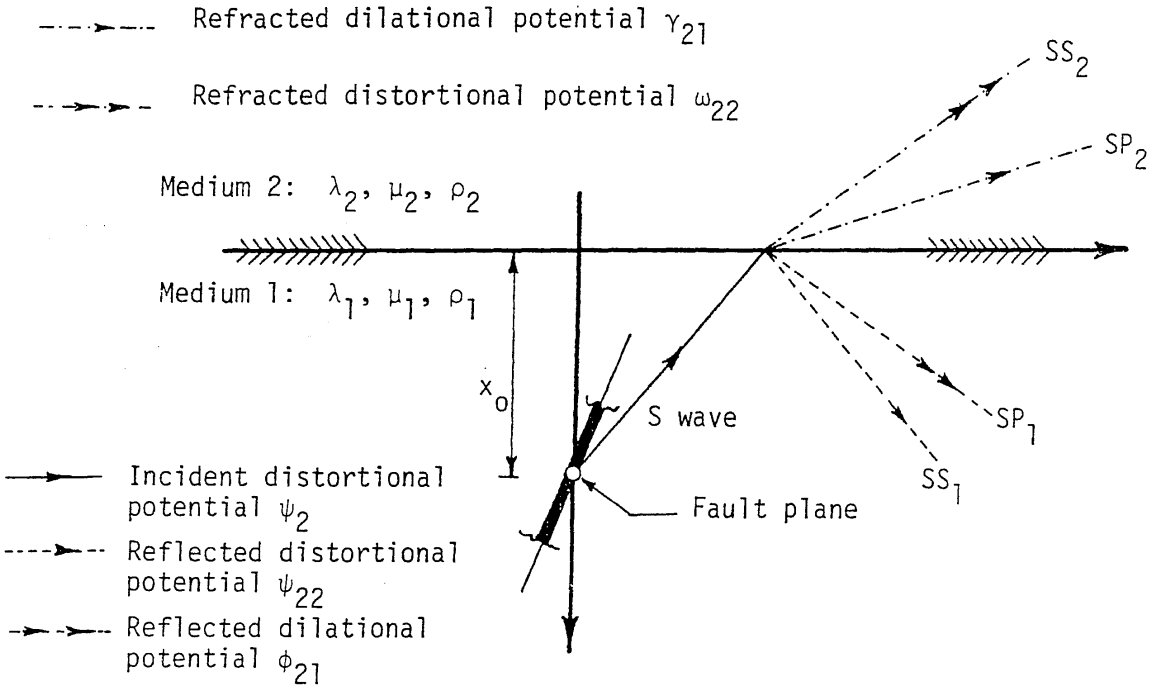

FIG. 28 REFLECTION AND REFRACTION OF S WAVE AT AN INTERFACE BETWEEN TWO ELASTIC SOLIDS

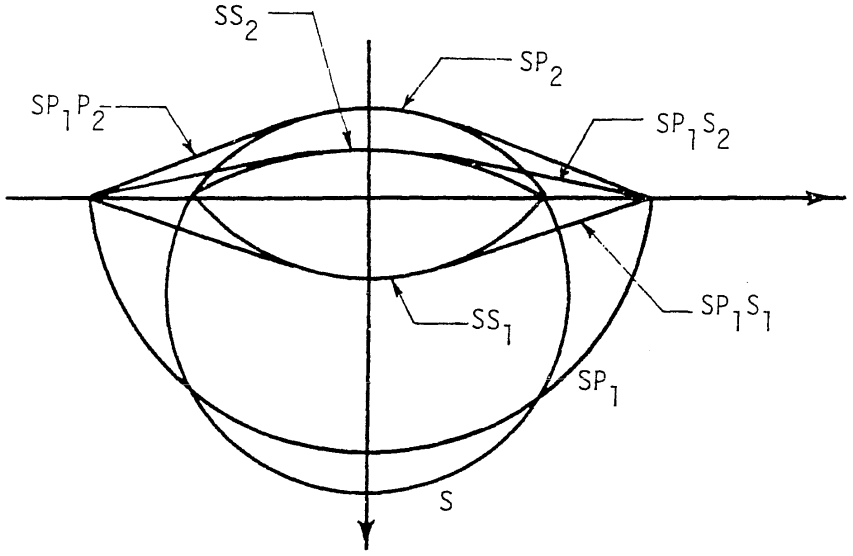

FIG. 29 WAVE FRONT PATTERN FOR AN INCIDENT S WAVE WITH $a_1 > b_1 > a_2 > b_2$

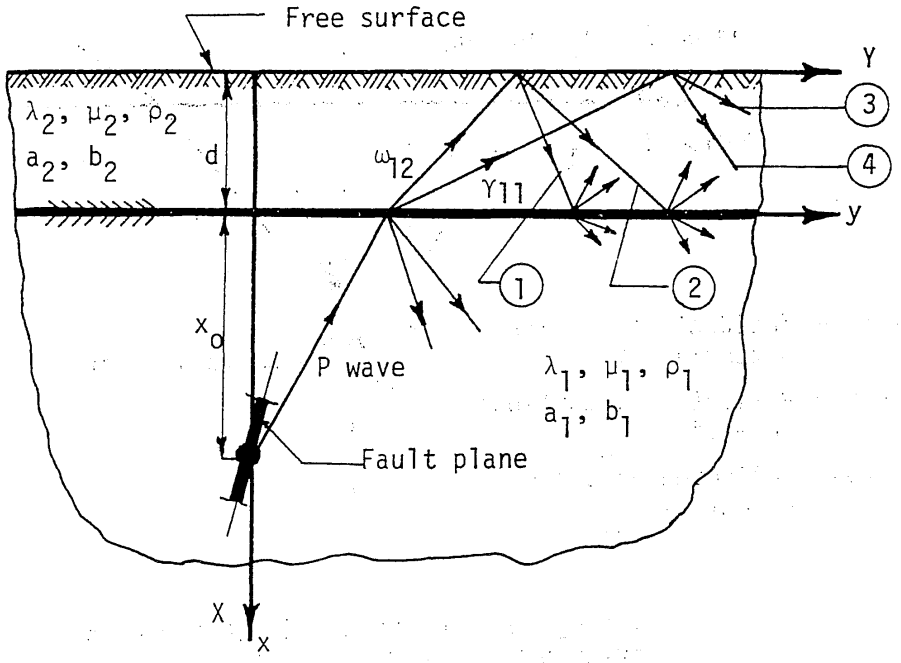

1. PS_2S_2-wave distortional potential ω_{122}
2. PS_2P_2-wave dilational potential γ_{121}
3. PP_2P_2-wave dilational potential γ_{111}
4. PP_2S_2-wave distortional potential ω_{112}

FIG. 30 PROPAGATING FAULT AS A SEISMIC SOURCE IN LAYERED HALF SPACE AND MULTIPLE REFLECTION AND REFRACTION OF THE ELASTIC WAVES AT THE SURFACES OF DISCONTINUITY

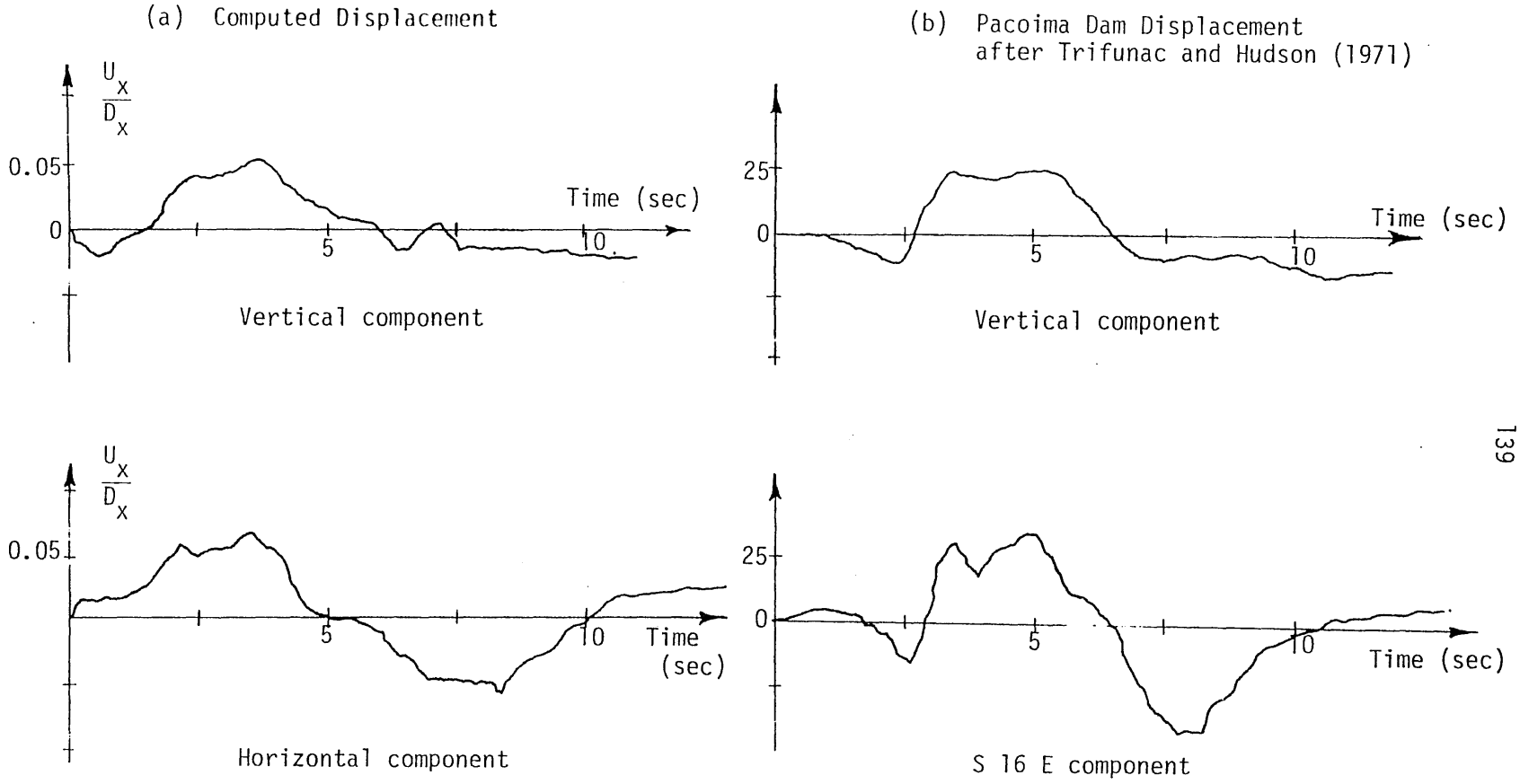

FIG. 31 (a) COMPUTED DISPLACEMENTS BASED ON THE TWO-DIMENSIONAL DISLOCATION MODEL (LAYERED HALF SPACE) AND (b) OBSERVED GROUND DISPLACEMENTS AT PACOIMA DAM DURING THE SAN FERNANDO EARTHQUAKE

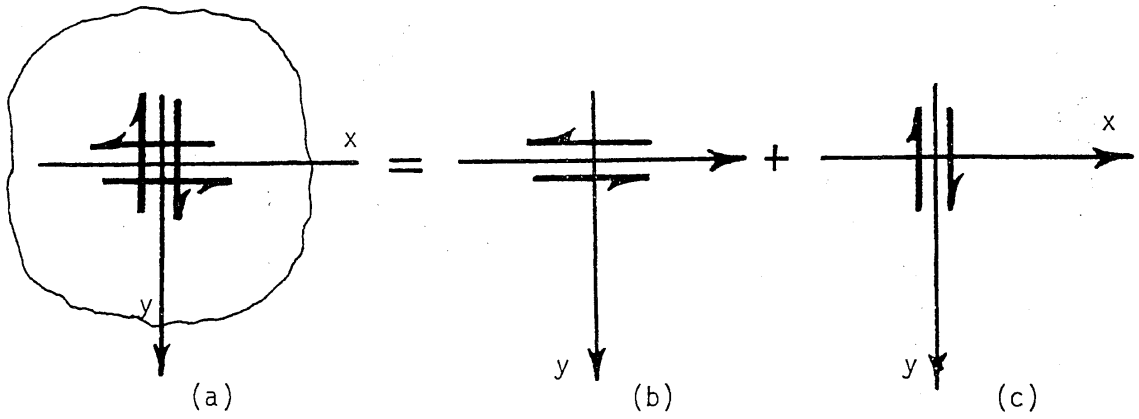

FIG 32 SUPERPOSITION OF TWO PERPENDICULAR DOUBLE-FORCE WITH MOMENTS OF OPPOSITE SIGNS

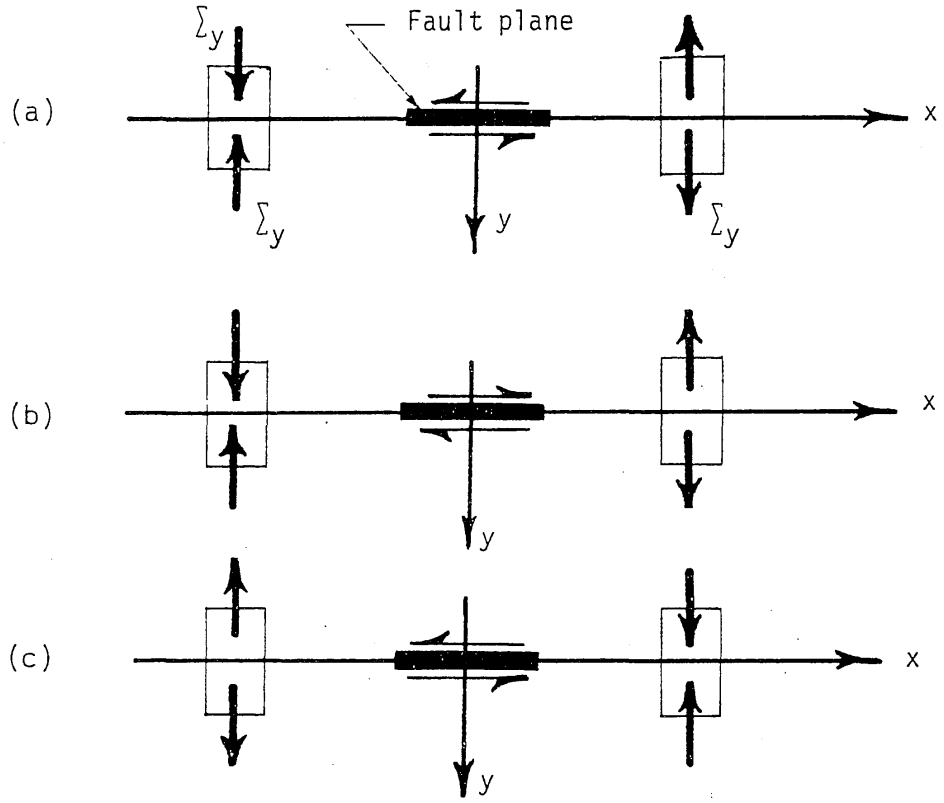

FIG. 33 NORMAL TRACTIONS AND DIRECTION OF FAULTING (a) IN THE ORIGINAL SYSTEM, (b) AFTER THE ENTIRE SYSTEM IS ROTATED ABOUT THE x-AXIS AND (c) WHEN THE SYSTEM IN (b) IS MULTIPLIED BY -1

APPENDIX A

EXPLANATION OF THE CONDITION $\sum_y$ =0 ON THE FAULT PLANE

The condition $\sum_y = 0$ (see Sec. 3.2.1), which may not be obvious at first glance, can be explained in the following manner. Consider a dislocation model confined to an elastic infinite medium such that two opposite sides of the fault plane acquire sudden displacement discontinuity along a segment of the fault. The direction of the relative movement and the axial stresses of two infinitesimal elements adjacent to the y = 0 surface are shown in Fig. 33a.

By rotating the entire system 180 degrees about the x-axis, the direction of the relative movement changes, whereas, the direction of the axial stresses remain unchanged (see Fig. 33b). When the field in Fig. 33b is multiplied by -1, the fault-slip on the y = 0 surface retains its original direction, however, the tensile stresses become compressional or vice-versa as illustrated in Fig. 33c. Since the rotation followed by multiplication by -1 must preserve the field, this change of the sign of the axial stresses cannot be possible unless $\sum_y = 0$.

APPENDIX B

DETERMINATION OF THE INCIDENT POTENTIALS RADIATED FROM A UNILATERALLY PROPAGATING FAULT IN AN INFINITE MEDIUM

The expressions for the incident potentials when the faulting starts at a point with coordinates ($x = +X_o^R$, $y = 0$) and propagates along the positive x-axis can be obtained in a manner similar to that of a bilateral faulting. For the case of dip-slip dislocation the conditions on the fault plane are:

$$R_{U_x} = D_x^R H(t - t_o)$$
$$R_{\Sigma_{yy}} = 0 \qquad \text{for } y = 0 \tag{B.1}$$

where $t_o = \frac{X_o^R}{\alpha}$ and α is the velocity of the crack propagation. Using the Cauchy integral theorem together with the Eqs. B.1, the complex displacement and axial traction are found to be

$$R_{U_x^*}(\bar{\theta}) = -\frac{1}{i\pi} \int_{-\infty}^{+\infty} \frac{U_x \, d\xi}{\xi - x} = \frac{-D_x^R}{2i\pi} \ln(1 - \alpha\theta) \tag{B.2}$$

and

$$R_{\Sigma_{yy}^*}(\bar{\theta}) = 0$$

where $\bar{\theta} = \frac{t}{x}$ on the $y = 0$ surface.

Following the procedure outlined at the end of Sec. 2.2.2, it can be easily verified that

$$\Phi'(\theta_1^R) = \frac{D_x^R \alpha b^2 \theta_1^R}{i\pi(1 - \alpha\theta_1^R)}$$

$$\Psi'(\theta_2^R) = \frac{D_x^R \alpha b^2 (b^{-2} - 2\theta_2^{R^2})}{(1 - \alpha\theta_2^R)\sqrt{b^{-2} - \theta_2^{R^2}}} \qquad \text{(B.3)}$$

The complex variable θ_i^R is defined by the equation

$$\theta_i^R = \frac{(t - t_o)(x - x_o^R) + iy\sqrt{(t - t_o)^2 - C_i^{-2}[(x - x_o)^2 + y^2]}}{(x - x_o)^2 + y^2} \qquad \text{(B.4)}$$

The problem of strike-slip faulting is determined in a manner analogue to that described above. The condition of zero tangential traction, when satisfied on the fault plane, results in an appropriate expression for the complex displacement function as follows:

$$W'(\theta_2^R) = \frac{D_z^R}{i\pi} \cdot \frac{\alpha}{1 - \alpha\theta_2^R} \qquad \text{(B.5)}$$

where, D_z^R is the amplitude of the strike-slip dislocation and θ_2^R is defined by Eq. B.4.

APPENDIX C

DETERMINATION OF THE DISPLACEMENT FIELDS CORRESPONDING TO TWO PERPENDICULAR DOUBLE FORCES WITH MOMENT

Solution for the problems involving a dynamic double force acting at a point beneath the surface of an elastic half space has been obtained by Farewell and Robinson and reported in Ref.[31]. The results of their study can be used to solve the problem under consideration in the following manner: Assume that two perpendicular double forces with moment act at a point inside an elastic full space as shown in Fig. 32a. The problem can be determined by decomposing it to two components each one of which is subjected to a double force with moment directed along the x and y-axis (see Figs. 32b and 32c). Solution for the first problem is found to be,

$$u_x^h = \mathrm{Re}\left\{ \frac{M_h b^2}{2i\pi\mu} \left[-\frac{\theta_1^2}{\delta_1'} - \frac{b^{-2} - \theta_2^2}{\delta_2'} \right] \right\}$$

$$u_y^h = \mathrm{Re}\left\{ \frac{M_h b^2}{2i\pi\mu} \left[-\frac{\theta_1\sqrt{a^{-2} - \theta_1^2}}{\delta_1'} + \frac{\theta_2\sqrt{b^{-2} - \theta_2^2}}{\delta_2'} \right] \right\} \qquad (C.1)$$

where u_x^h and u_y^h are the real parts of the displacements when a double-force with moment M_h acts horizontally.

Similar expressions can be obtained for the case in which a dynamic double force is directed vertically. The results are:

$$u_x^V = \mathrm{Re}\left\{ \frac{M_V b^2}{2i\pi\mu} \left[-\frac{\theta_1^2}{\delta_1'} + \frac{\theta_2^2}{\delta_2'} \right] \right\}$$

$$u_y^V = \mathrm{Re}\left\{ \frac{M_V b^2}{2i\pi\mu} \left[\frac{-\theta_1\sqrt{a^{-2} - \theta_1^2}}{\delta_1'} - \frac{\theta_2^3}{\delta_2'\sqrt{b^{-2} - \theta_2^2}} \right] \right. \qquad \text{(C.2)}$$

The moments M_h and M_V vary as step function in time. If we take $M_V = M_h = M$ and add Eqs. C.1 and C.2 together, the displacement fields for a point source consisting of two perpendicular double force with moment are as follows.

$$u_x = u_x^h + u_x^V = \mathrm{Re}\left\{ \frac{Mb^2}{i\pi\mu} \left[-\frac{\theta_1^2}{\delta_1'} + \frac{2\theta_2^2 - b^{-2}}{2\delta_2'} \right] \right\}$$

$$u_y = u_y^h + u_y^V = \mathrm{Re}\left\{ \frac{Mb^2}{i\pi\mu} \left[\frac{-\theta_1\sqrt{a^{-2} - \theta_1^2}}{\delta_1'} - \frac{\theta_2(2\theta_2^2 - b^{-2})}{\delta_2'\sqrt{b^{-2} - \theta_2^2}} \right] \right\} \qquad \text{(C.3)}$$

Equations C.3 are identical with the results of Sec. 3.6 indicating that a point dislocation is equivalent to two double force with moment.

APPENDIX D

COMPUTATION OF THE REFLECTED DISTURBANCES ARISING FROM THE INTERACTION OF THE PS_2S_2 AND PS_2P_2 WAVES WITH THE X=d SURFACE IN THE LAYERED HALF SPACE

The arrival of the dilational potential γ_{121} and distortional potential γ_{122} at the X = d surface gives rise to both reflected and refracted disturbances, as shown in Fig. 30. The reflected portion of these newly generated disturbances which contribute to the motion on the free surface are found to be:

i) Reflected dilational potential γ_{1211} due to PS_2P_s wave

$$\Gamma'_{1211}(\eta) = \frac{D_1(\eta)}{D(\eta)} \Gamma'_{121}(\eta) \tag{D.1}$$

where

$$\begin{aligned} D_1 = {} & K_2h_2(n_1 + 2\mu'\eta^2)^2 - K_1h_1(\mu'n_2 + 2\eta^2)^2 \\ & + \mu'(K_2h_1 - K_1h_2)(n_1 + 2\eta^2)(n_2 + 2\eta^2) \\ & + K_1K_2h_1h_2[4\eta^2(1 - \mu')^2] - \eta^2(n_1 - \mu'n_2)^2 \end{aligned} \tag{D.2}$$

$$\begin{aligned} D = {} & \eta^2(\mu'n_2 - n_1)^2 + K_2h_2(n_1 + 2\mu'\eta^2)^2 + K_1h_1(\mu'n_2 \\ & + 2\eta^2)^2 + K_1K_2h_1h_2[4\eta^2(1 - \mu)^2] \\ & + \mu'(K_1h_2 + K_2h_1)(n_2 + 2\eta^2)(n_1 + 2\eta^2) \end{aligned} \tag{D.3}$$

and

$$\Gamma'_{121}(\eta) = \frac{d\Gamma_{121}(\eta)}{d\eta} , \qquad \gamma_{121} = \text{Re } \Gamma_{121}$$

$$\gamma_{1211} = \text{Re } \Gamma_{1211} , \qquad \mu' = \frac{\mu_2}{\mu_1} \tag{D.4}$$

For a given point on the free surface, the complex parameter η is determined from the equation

$$\Delta_{1211} \equiv t - x\sqrt{a_2^{-2} - \eta^2} + 2d\sqrt{a_2^{-2} - \eta^2}$$

$$+ x_o\sqrt{a_1^{-2} - \eta^2} - y\eta = 0 \tag{D.5}$$

Other parameters are defined in Chapter 5;

ii) Reflected distortional potential γ_{1212} due to the PS_2P_2 wave

$$\Omega'_{1212} = \frac{D_2}{D} \Gamma'_{121} \tag{D.6}$$

where

$$D_2 = 2\eta K_2 [2K_1 h_1 (1 - \mu')(2\eta^2 + \mu' n_2)$$

$$+ (n_1 - \mu' n_2)(n_1 + 2\mu'\eta^2)] \tag{D.7}$$

The corresponding characteristic plane is defined by the equation

$$\Delta_{1212} \equiv t - x\sqrt{b_2^{-2} - \eta^2} + 2d\sqrt{b_2^{-2} - \eta^2}$$

$$+ d\sqrt{a_2^{-2} - \eta^2} + x_o\sqrt{a_1^{-2} - \eta^2} - y\eta = 0 \tag{D.8}$$

iii) Reflected dilational potential γ_{1221} due to the PS_2P_2 wave

$$\Gamma'_{1221} = \frac{D_3}{D} \Omega'_{122} \tag{D.9}$$

where

$$D_3 = -2\eta h_2[2K_1h_1(1 - \mu')(2\eta^2 + \mu' n_2) + (n_1 - \mu' n_2)(n_1 + 2\mu'\eta^2)] \tag{D.10}$$

and

$$\Delta_{1221} \quad t - x\sqrt{a_2^{-2} - \eta^2} + d\sqrt{a_2^{-2} - \eta^2} + 2d\sqrt{b_2^{-2} - \eta^2} + x_o\sqrt{a_1^{-2} - \eta^2} - y\eta = 0 \tag{D.11}$$

iv) Reflected distortional potential ω_{1222} due to the PS_2S_2 wave

$$\Omega'_{1222} = \frac{D_4}{D} \Omega'_{122} \tag{D.12}$$

where

$$D_4 = -\eta^2(n_1 - \mu' n_2)^2 - K_1h_1(2\eta^2 + \mu' n_2)^2 + K_2h_2(n_1 + 2\mu'\eta^2)^2 + K_1K_2h_1h_2[4\eta^2(1 - \mu')^2] - \mu'(K_2h_1 - K_1h_2)(n_1 + 2\eta^2)(n_2 + 2\eta^2) \tag{D.13}$$

and

$$\Delta_{1222} \equiv t - x\sqrt{b_2^{-2} - \eta^2} + 3d\sqrt{b_2^{-2} - \eta^2} + x_o\sqrt{a_1^{-2} - \eta^2} - y\eta = 0 \tag{D.14}$$

Calculation of the arrival time of these disturbances and the displacements corresponding to each one of them has been discussed in Chapter 5.

Similar expressions can be obtained when the potentials associated with the PP_2P_2 and PP_2S_2 waves are considered.

ONR DISTRIBUTION LIST

PART I - GOVERNMENT

Administrative & Liaison Activities

Chief of Naval Research
Department of the Navy
Arlington, Virginia 22217
Attn: Code 474 (2)
471
222

Director
ONR Branch Office
495 Summer Street
Boston, Massachusetts 02210

Director
ONR Branch Office
219 S. Dearborn Street
Chicago, Illinois 60604

Director
Naval Research Laboratory
Attn: Code 2629 (ONRL)
Washington, D.C. 20390 (6)

U.S. Naval Research Laboratory
Attn: Code 2627
Washington, D.C. 20390

Director
ONR - New York Area Office
715 Broadway - 5th Floor
New York, New York 10003

Director
ONR Branch Office
1030 E. Green Street
Pasadena, California 91101

Defense Documentation Center
Cameron Station
Alexandria, Virginia 22314

Army

Commanding Officer
U.S. Army Research Office Durham
Attn: Mr. J.J. Murray
CRD-AA-IP
Box CM, Duke Station
Durham, North Carolina 27706 (2)

Commanding Officer
AMXMR-ATL
Attn: Mr. R. Shea
U.S. Army Materials Res. Agency
Watertown, Massachusetts 02172

Watervliet Arsenal
MAGGS Research Center
Watervliet, New York 12189
Attn: Director of Research

Technical Library

Redstone Scientific Info. Center
Chief, Document Section
U.S. Army Missile Command
Redstone Arsenal, Alabama 35809

Army R & D Center
Fort Belvoir, Virginia 22060

Navy

Commanding Officer and Director
Naval Ship Research & Development Center
Bethesda, Maryland 20034
Attn: Code 042 (Tech. Lib. Br.)
17 (Struc. Mech. Lab.)
172
172
174
177
1800 (Appl. Math. Lab.)
5412S (Dr. W.D. Sette)
19 (Dr. M.M. Sevik)
1901 (Dr. M. Strassberg)
1945
196 (Dr. D. Feit)
1962

Naval Weapons Laboratory
Dahlgren, Virginia 22448

Naval Research Laboratory
Washington, D.C. 20375
Attn: Code 8400
8410
8430
8440
6300
6390
6380

Undersea Explosion Research Div.
Naval Ship R & D Center
Norfolk Naval Shipyard
Portsmouth, Virginia 23709
Attn: Dr. E. Palmer
Code 780

Naval Ship Research & Development Center
Annapolis Division
Annapolis, Maryland 21402
Attn: Code 2740 - Dr. Y.F. Wang
28 - Mr. R.J. Wolfe
281 - Mr. R.B. Niederberger
2814 - Dr. H. Vanderveldt

Technical Library
Naval Underwater Weapons Center
Pasadena Annex
3202 E. Foothill Blvd.
Pasadena, California 91107

U.S. Naval Weapons Center
China Lake, California 93557
Attn: Code 4062 - Mr. W. Werback
4520 - Mr. Ken Bischel

Commanding Officer
U.S. Naval Civil Engr. Lab.
Code L31
Port Hueneme, California 93041

Technical Director
U.S. Naval Ordnance Laboratory
White Oak
Silver Spring, Maryland 20910

Technical Director
Naval Undersea R & D Center
San Diego, California 92132

Supervisor of Shipbuilding
U.S. Navy
Newport News, Virginia 23607

Technical Director
Mare Island Naval Shipyard
Vallejo, California 94592

U.S. Navy Underwater Sound Ref. Lab.
Office of Naval Research
P.O. Box 8337
Orlando, Florida 32806

Chief of Naval Operations
Dept. of the Navy
Washington, D.C. 20350
Attn: Code Op07T

Strategic Systems Project Office
Department of the Navy
Washington, D.C. 20390
Attn: NSP-001 Chief Scientist

Deep Submergence Systems
Naval Ship Systems Command
Code 39522
Department of the Navy
Washington, D.C. 20360

Engineering Dept.
U.S. Naval Academy
Annapolis, Maryland 21402

Naval Air Systems Command
Dept. of the Navy
Washington, D.C. 20360
Attn: NAVAIR 5302 Aero & Structures
5308 Structures
52031F Materials
604 Tech. Library
320B Structures

Director, Aero Mechanics
Naval Air Development Center
Johnsville
Warminster, Pennsylvania 18974

Technical Director
U.S. Naval Undersea R & D Center
San Diego, California 92132

Engineering Department
U.S. Naval Academy
Annapolis, Maryland 21402

Naval Facilities Engineering Command
Dept. of the Navy
Washington, D.C. 20360
Attn: NAVFAC 03 Research & Development
04 Research & Development
14114 Tech. Library

Naval Sea Systems Command
Dept. of the Navy
Washington, D.C. 20360
Attn: NAVSHIP 03 Res. & Technology
031 Ch. Scientist for R & D
03412 Hydromechanics
037 Ship Silencing Div.
035 Weapons Dynamics

Naval Ship Engineering Center
Prince George's Plaza
Hyattsville, Maryland 20782
Attn: NAVSEC 6100 Ship Sys Engr & Des Dep
6102C Computer-Aided Ship Des
6105G
6110 Ship Concept Design
6120 Hull Div.
6120D Hull Div.
6128 Surface Ship Struct.
6129 Submarine Struct.

Air Force

Commander WADD
Wright-Patterson Air Force Base
Dayton, Ohio 45433
Attn: Code WWRMDD
AFFDL (FDDS)
Structures Division
AFLC (MCEEA)

Chief, Applied Mechanics Group
U.S. Air Force Inst. of Tech.
Wright-Patterson Air Force Base
Dayton, Ohio 45433

Chief, Civil Engineering Branch
WLRC, Research Division
Air Force Weapons Laboratory
Kirtland AFB, New Mexico 87117

Air Force Office of Scientific Research
1400 Wilson Blvd.
Arlington, Virginia 22209
Attn: Machanics Div.

NASA

Structures Research Division
National Aeronautics & Space Admin.
Langley Research Center
Langley Station
Hampton, Virginia 23365

National Aeronautical & Space Admin.
Associate Administrator for Advanced
Research & Technology
Washington, D.C. 02546

Scientific & Tech. Info. Facility
NASA Representative (S-AK/DL)
P.O. Box 5700
Bethesda, Maryland 20014

Other Government Activities

Commandant
Chief, Testing & Development Div.
U.S. Coast Guard
1300 E. Street, N.W.
Washington, D.C. 20226

Technical Director
Marine Corps Dev. & Educ. Command
Quantico, Virginia 22134

Director
National Bureau of Standards
Washington, D.C. 20234
Attn: Mr. B.L. Wilson, EM 219

Dr. M. Gaus
National Science Foundation
Engineering Division
Washington, D.C. 20550

Science & Tech. Division
Library of Congress
Washington, D.C. 20540

Director
Defense Nuclear Agency
Washington, D.C. 20305
Attn: SPSS

Commander Field Command
Defense Nuclear Agency
Sandia Base
Albuquerque, New Mexico 87115

Director Defense Research & Engrg
Technical Library
Room 3C-128
The Pentagon
Washington, D.C. 20301

Chief, Airframe & Equipment Branch
FS-120
Office of Flight Standards
Federal Aviation Agency
Washington, D.C. 20553

Chief, Reserach and Development
Maritime Administration
Washington, D.C. 20235

Deputy Chief, Office of Ship Constr.
Maritime Administration
Washington, D.C. 20235
Attn: Mr. U.L. Russo

Atomic Energy Commission
Div. of Reactor Devel. & Tech.
Germantown, Maryland 20767

Ship Hull Research Committee
National Research Council
National Academy of Sciences
2101 Constitution Avenue
Washington, D.C. 20418
Attn: Mr. A.R. Lytle

PART 2 - CONTRACTORS AND OTHER TECHNICAL COLLABORATORS

Universities

Dr. J. Tinsley Oden
University of Texas at Austin
345 Eng. Science Bldg.
Austin, Texas 78712

Prof. Julius Miklowitz
California Institute of Technology
Div. of Engineering & Applied Sciences
Pasadena, California 91109

Dr. Harold Liebowitz, Dean
School of Engr. & Applied Science
George Washington University
725 - 23rd St., N.W.
Washington, D.C. 20006

Prof. Eli Sternberg
California Institute of Technology
Div. of Engr. & Applied Sciences
Pasadena, California 91109

Prof. Paul M. Naghdi
University of California
Div. of Applied Mechanics
Etcheverry Hall
Berkeley, California 94720

Professor P.S. Symonds
Brown University
Division of Engineering
Providence, Rhode Island 02912

Prof. A.J. Durelli
The Catholic University of America
Civil/Mechanical Engineering
Washington, D.C. 20017

Prof. R.B. Testa
Columbia University
Dept. of Civil Engineering
S.W. Mudd Bldg.
New York, New York 10027

Prof. H.H. Bleich
Columbia University
Dept. of Civil Engineering
Amsterdam & 120th Streets
New York, New York 10027

Prof. F.L. DiMaggio
Columbia University
Dept. of Civil Engineering
616 Mudd Building
New York, New York 10027

Prof. A.M. Freudenthal
George Washington University
School of Engineering &
Applied Science
Washington, D.C. 20006

D.C. Evans
University of Utah
Computer Science Division
Salt Lake City, Utah 84112

Prof. Norman Jones
Massachusetts Inst. of Technology
Dept. of Naval Architecture &
Marine Engrng
Cambridge, Massachusetts 02139

Professor Albert I. King
Biomechanics Research Center
Wayne State University
Detroit, Michigan 48202

Dr. V.R. Hodgson
Wayne State University
School of Medicine
Detroit, Michigan 48202

Dean B.A. Boley
Northwestern University
Technological Institute
2145 Sheridan Road
Evanston, Illinois 60201

Prof. P.G. Hodge, Jr.
University of Minnesota
Dept. of Aerospace Engng & Mechanics
Minneapolis, Minnesota 55455

Dr. D.C. Drucker
University of Illinois
Dean of Engineering
Urbana, Illinois 61801

Prof. N.M. Newmark
University of Illinois
Dept. of Civil Engineering
Urbana, Illinois 61801

Prof. E. Reissner
University of California, San Diego
Dept. of Applied Mechanics
La Jolla, California 92037

Prof. William A. Nash
University of Massachusetts
Dept. of Mechanics & Aerospace Engng.
Amherst, Massachusetts 01002

Library (Code 0384)
U.S. Naval Postgraduate School
Monterey, California 93940

Prof. Arnold Allentuch
Newark College of Engineering
Dept. of Mechanical Engineering
323 High Street
Newark, New Jersey 07102

Dr. George Herrmann
Stanford University
Dept. of Applied Mechanics
Stanford, California 94305

Prof. J. D. Achenbach
Northwestern University
Dept. of Civil Engineering
Evanston, Illinois 60201

Director, Applied Research Lab.
Pennsylvania State University
P.O. Box 30
State College, Pennsylvania 16801

Prof. Eugen J. Skudrzyk
Pennsylvania State University
Applied Research Laboratory
Dept. of Physics - P.O. Box 30
State College, Pennsylvania 16801

Prof. J. Kempner
Polytechnic Institute of Brooklyn
Dept. of Aero. Engrg. & Applied Mech.
333 Jay Street
Brooklyn, New York 11201

Prof. J. Klosner
Polytechnic Institute of Brooklyn
Dept. of Aerospace & Appl. Mech.
333 Jay Street
Brooklyn, New York 11201

Prof. R.A. Schapery
Texas A & M University
Dept. of Civil Engineering
College Station, Texas 77840

Prof. W.D. Pilkey
University of Virginia
Dept. of Aerospace Engineering
Charlottesville, Virginia 22903

Dr. K.D. Schaeffer
University of Maryland
Aerospace Engineering Dept.
College Park, Maryland 20742

Prof. K.D. Willmert
Clarkson College of Technology
Dept. of Mechanical Engineering
Potsdam, New York 13676

Dr. J.A. Stricklin
Texas A & M University
Aerospace Engineering Dept.
College Station, Texas 77843

Dr. L.A. Schmit
University of California, LA
School of Engineering & Applied Science
Los Angeles, California 90024

Dr. H.A. Kamel
The University of Arizona
Aerospace & Mech. Engineering Dept.
Tucson, Arizona 85721

Dr. B.S. Berger
University of Maryland
Dept. of Mechanical Engineering
College Park, Maryland 20742

Prof. G.R. Irwin
Dept. of Mechanical Engineering
University of Maryland
College Park, Maryland 20742

Dr. S.J. Fenves
Carnegie-Mellon University
Dept. of Civil Engineering
Schenley Park
Pittsburgh, Pennsylvania 15213

Dr. Ronald L. Huston
Dept. of Engineering Analysis
Mail Box 112
University of Cincinnati
Cincinnati, Ohio 45221

Prof. George Sih
Dept. of Mechanics
Lehigh University
Bethlehem, Pennsylvania 18015

Prof. A.S. Kobayashi
University of Washington
Dept. of Mechanical Engineering
Seattle, Washington 98105

Librarian
Webb Institute of Naval Architecture
Cresent Beach Road
Glen Cove, New York 11542

Prof. Daniel Frederick
Virginia Polytechnic Institute
Dept. of Engineering Mechanics
Blacksburg, Virginia 24061

Prof. A.C. Eringen
Dept. of Aerospace & Mech. Sciences
Princeton University
Princeton, New Jersey 08540

Dr. S.L.Koh
School of Aero., Astro. & Engr. Sc.
Purdue University
Lafayette, Indiana 47907

Prof. E.H. Lee
Div. of Engrg. Mechanics
Stanford University
Stanford, California 94305

Prof. R.D. Mindlin
Dept. of Civil Engrg.
Columbia University
S.W. Mudd Building
New York, New York 10027

Prof. S.B. Dong
University of California
Dept. of Mechanics
Los Angeles, California 90024

Prof. Burt Paul
University of Pennsylvania
Towne School of Civil & Mech. Engrg.
Rm. 113 - Towne Building
220 S. 33rd Street
Philadelphia, Pennsylvania 19104

Prof. H.W. Liu
Dept. of Chemical Engr. & Metal.
Syracuse University
Syracuse, New York 13210

Prof. S. Bodner
Technion R & D Foundation
Haifa, ISRAEL

Prof. R.J.H. Bollard
Chairman, Aeronautical Engr. Dept.
207 Guggenheim Hall
University of Washington
Seattle, Washington 98105

Prof. G.S. Heller
Division of Engineering
Brown University
Providence, Rhode Island 02912

Prof. Werner Goldsmith
Dept. of Mechanical Engineering
Div. of Applied Mechanics
University of California
Berkeley, California 94720

Prof. J.R. Rice
Division of Engineering
Brown University
Providence, Rhode Island 02912

Prof. R.S. Rivlin
Center for the Application of Mathematics
Lehigh University
Bethlehem, Pennsylvania 18105

Library (Code 0384)
U.S. Naval Postgraduate School
Monterey, California 93940

Dr. Francis Cozzarelli
Div. of Interdisciplinary Studies/Research
School of Engineering
State University of New York
Buffalo, New York 14214

Industry and Research Institutes

Library Services Department
Report Section Bldg. 14-14
Argonne National Laboratory
9700 S. Cass Avenue
Argonne, Illinois 60440

Dr. M.C. Junger
Cambridge Acoustical Associates
129 Mount Auburn St.
Cambridge, Massachusetts 02138

Dr. L.H. Chen
General Dynamics Corporation
Electric Boat Division
Groton, Connecticut 06340

Dr. J.E. Greenspon
J.G. Engineering Research Associates
3831 Menlo Drive
Baltimore, Maryland 21215

Dr. S. Batdorf
The Aerospace Corporation
P.O. Box 92957
Los Angeles, California 90009

Dr. K.C. Park
Lockheed Palo Alto Research Laboratory
Dept. 5233, Bldg. 205
3251 Hanover Street
Palo Alto, California 94304

Library Newport News Shipbuilding and
Dry Dock Company
Newport News, Virginia 23607

Dr. W.F. Bozich
McDonnell Douglas Corporation
5301 Bolsa Avenue
Huntington Beach, California 92647

Dr. H.N. Abramson
Southwest Research Institute
Technical Vice President
Mechanical Sciences
P.O. Drawer 28510
San Antonio, Texas 78284

Dr. R.C. DeHart
Southwest Research Institute
Dept. of Structural Research
P.O. Box 28510
San Antonio, Texas 78284

Dr. M.L. Baron
Weidlinger Associates
Consulting Engineers
110 East 59th Street
New York, New York 10022

Dr. W.A. von Riesemann
Sandia Laboratories
Sandia Base
Albuquerque, New Mexico 87115

Dr. T.L. Geers
Lockheed Missiles & Space Co.
Palo Alto Research Laboratory
3251 Hanover Street
Palo Alto, California 94304

Dr. J.L. Tocher
Boeing Computer Services, Inc.
P.O. Box 24346
Seattle, Washington 98124

Mr. William Caywood
Code BBE, Applied Physics Laboratory
8621 Georgia Avenue
Silver Spring, Maryland 20034

Mr. P.C. Durup
Lockheed-California Company
Aeromechanics Dept., 74-43
Burbank, California 91503

UNCLASSIFIED

SECURITY CLASSIFICATION OF THIS PAGE (When Data Entered)

REPORT DOCUMENTATION PAGE		READ INSTRUCTIONS BEFORE COMPLETING FORM
1. REPORT NUMBER UILU-ENG-75-2025	2. GOVT ACCESSION NO.	3. RECIPIENT'S CATALOG NUMBER
4. TITLE (and Subtitle) MOTION ON THE SURFACE OF A LAYERED ELASTIC HALF SPACE PRODUCED BY A BURIED DISLOCATION PULSE		5. TYPE OF REPORT & PERIOD COVERED Technical Report 6. PERFORMING ORG. REPORT NUMBER SRS No. 421
7. AUTHOR(s) Mirhamid Seyyedian-Choobi Arthur R. Robinson		8. CONTRACT OR GRANT NUMBER(s) N00014-75-C-0164
9. PERFORMING ORGANIZATION NAME AND ADDRESS Department of Civil Engineering University of Illinois at Urbana-Champaign Urbana, Illinois 61801		10. PROGRAM ELEMENT, PROJECT, TASK AREA & WORK UNIT NUMBERS Project No. NR 064-183
11. CONTROLLING OFFICE NAME AND ADDRESS Office of Naval Research, CODE N00014 Department of the Navy Arlington, Virginia 22217		12. REPORT DATE November, 1975 13. NUMBER OF PAGES 149
14. MONITORING AGENCY NAME & ADDRESS(if different from Controlling Office) Material Science Division Structural Mechanics Division (CODE 474) Office of Naval Research (800 Quincy Street) Arlington, Virginia 22217		15. SECURITY CLASS. (of this report) UNCLASSIFIED 15a. DECLASSIFICATION/DOWNGRADING SCHEDULE

16. DISTRIBUTION STATEMENT (of this Report)

Approved for Public Release: Distribution Unlimited

17. DISTRIBUTION STATEMENT (of the abstract entered in Block 20, if different from Report)

18. SUPPLEMENTARY NOTES

19. KEY WORDS (Continue on reverse side if necessary and identify by block number)

elastic wave propagation; earthquake source mechanisms; layered half space

20. ABSTRACT (Continue on reverse side if necessary and identify by block number)

In this work solutions are developed for the motions generated in an elastic half space or a half space with a softer layer above it by propagating dislocations on an inclined fault plane. Both dip-slip and strike-slip relative motions have been considered. The dislocations are two-dimensional motions originating in the lower layer. The area over which dislocations are present spreads from a line source as the front of the dislocation propagates on the fault plane. The propagating fault can be stopped suddenly on both sides or on just one side.

DD FORM 1 JAN 73 1473 EDITION OF 1 NOV 65 IS OBSOLETE

UNCLASSIFIED

SECURITY CLASSIFICATION OF THIS PAGE (When Data Entered)

20.

Surface motions are computed using an extension of the Smirnov-Sobolev method for self-similar solutions. The extension is needed to take care of non-parallel boundaries arising from the inclination of the fault plane to the horizontal.

The effect of layering is shown to be extremely important in providing motions at the surface which have the type of "rebound" that is noted in displacements inferred from strong-motion records of earthquakes. The motions obtained for a single spreading dislocation which suddenly starts and stops is compared with the displacement found from the Pacoima Dam records in the 1971 San Fernando earthquake. The general shape of the motion is seen to correspond well to the results for a single pulse in a layered solid, whereas the case of no layering cannot produce a similar motion.